جمهورية العراق
وزارة التعليم العـــالي والبحث العلـمي
جامـــعة بابـــل / كليـــة العلوم
قســـم الفيزيـــاء

تقييم الغطاء النباتي الارضي لمحافظة بابل باستخدام تقنيات الاستشعار عن بعد ونظم المعلومات الجغرافية

رسالة

مقدمة إلى قسم الفيزياء، كلية العلوم، جامعة بابل جزءا" من متطلبات نيل شهادة الماجستير في العلوم/ الفيزياء

قدمتها

زهراء علي نايف حمزه

(بكالوريوس علوم فيزياء، ٢٠١٨)

بإشراف

أ. م. د
أميره ابو السود حمادي السعدوني

أ. د.
ابتسام فاضل خنجر

٢٠٢١ م

١٤٤٣ هـ

Republic of Iraq

Ministry of Higher Education and Scientific Research

University of Babylon, College of Science

Department of Physics

Assessment the Land Vegetation Cover for Babylon Government by Using Remote Sensing and GIS Techniques

A Thesis

Submitted to the Council of the Department of Physics, College of Science, University of Babylon

In Partial Fulfillment of the Requirements for the Degree of Master of Science in Physics

By

Zahraa Ali Naife Hamza

(B. Sc. in Physics, 2018)

Supervised by

Asst. Prof. Dr.

Ameerah Ab. Al-Sadooni

Prof. Dr.

Ebtesam F. Khanjer

2021 A.D **1443 A.H**

بسم الله الرحمن الرحيم

وَالتِّينِ وَالزَّيْتُونِ (١) وَطُورِ سِينِينَ (٢)

وَهَذَا الْبَلَدِ الْأَمِينِ (٣)

صدق الله العظيم

سورة التين آية (١ - ٣)

Acknowledgements

*All praise to **ALLAH** for giving me the inner strength and good health for completing this thesis. I would like to express my sincere gratitude and appreciation to my supervisors Assist. Prof. Dr. **Ameerah Ab. Al-Sadooni** and Prof. Dr. **Ebtesam F.Khanjer** for putting in this research plan and their valuable guidance and help throughout the course of this study. In addition, I would especially like to express my deep appreciation to them for their kindness, patience and understanding through difficult times that I went through during the study period.*

Furthermore, I would like to give my indebtedness to my wonderful family: My father, mother, sisters and brother for their patience, support and enthusiastic encouragement during this research.

Last but not least, I would like to express my thanks to all my friends, Huda, Noor Al huda and Walaa colleagues who helped me in one way or another in the fulfillment of this work, to those who indirectly contributed in this research, your kindness means a lot to me. Thank you very much.

Zahraa

Dedications

To the great teacher and leader, our messenger Mohammed, and his family that Allah prefers and introduces among all human beings

To my deceased father, may God have mercy on him

To my second father and my bond in life, who did not make me need something that may prolong his life and preserve it

to my dear mother, and may God prolong her life and preserve it

to my brothers, God made their days happy

to friends and companions in my path, may God bless them in their lives

to everyone Stand with me and support me I give you this work

Zahraa

Summary

The normalized difference vegetation index (NDVI) represents an effective graphical parameter to analyze remote sensing data that are collected by a space platform, in order to investigate the trend of the live green vegetation in the observed target. In this research, the change detection of vegetation in Babylon Governorate was done by tracing the NDVI and NDWI factors for temporal Landsat satellite images. These images were used and utilized in two different terms: in March 19 th in 2001 and March 5th in 2019. The Arc-GIS ver. 10.3 program was adopted to analyze the collected data.

The final results indicate a spatial variation in the NDVI, where it increases from 192191310 m^2 in 2001 to 216833220 m^2 in 2019 between the two observed periods. About 25 X 10^6 m^2 as a new area that is covered with vegetation between the two observed periods (2001 and 2019). Where the increased trends can be explained by the evolution of agricultural styles that used by farmers.

The normalized difference water index (NDWI) value for the same period, shows that the water area increased from 46802700 m^2 in 2001 to 123406200 m^2 in 2019.

In order to compare the results of the NDVI indices with the field results from the ground, the agricultural data were obtained from the Babylon Agricultural Directorate for the period from 2009 to 2019, these data cover a wide range of information about agricultural production such as, number of trees (fag, palm, citrus (oranges, grapes, and pomegranates)) and cultivated areas for grain crop (wheat

and yellow corn) for different districts into Babylon Governorate, and the results were nearly identical to those of the NDVI measurements.

الخلاصة

مؤشر الغطاء النباتي للفرق الطبيعي (NDVI) هو مؤشر رسومي فعال يمكن استخدامه لتحليل قياسات الاستشعار عن بعد باستخدام منصة فضائية، من أجل التحقيق فيما اذا كان الهدف يحتوي على نباتات خضراء حية ام لا. في هذا البحث، تم الكشف عن تغيير الغطاء النباتي ومحتوى الماء في محافظة بابل من خلال تتبع المعاملين NDWI و NDVI لصور القمر الصناعي Temporal Landsat. حيث تم استخدامها في فترتين مختلفتين: في ١٩ مارس ٢٠٠١ و ٥ مارس في ٢٠١٩. و تم الاعتماد على برنامج Arc-GIS. ver 10.3 لتحليل البيانات التي تم جمعها.

تشير النتائج النهائية إلى وجود تباين مكاني في مؤشر ال NDVI حيث يرتفع من ١٩٢١٩١٣١٠ م^{٢} إلى ٢١٦٨٣٣٢٢٠ م^{٢} بين الفترتين المرصودة. حوالي ٢٥ × ١٠^{٦} م^{٢} كمنطقة جديدة مغطاة بالنباتات بين الفترتين المرصودة (٢٠٠١ و ٢٠١٩). حيث يمكن تفسير الاتجاهات المتزايدة من خلال تطور الأساليب الزراعية التي يستخدمها المزارعون.

اما فيما يخص مؤشر المياه للفرق الطبيعي ل NDWI لنفس الفترة الزمنية، حيث تزداد مساحة المحتوى المائي من ٤٦٨٠٢٧٠٠ م^{٢} في ٢٠٠١ إلى ١٢٣٤٠٦٢٠٠ م^{٢} في ٢٠١٩.

من أجل مقارنة نتائج مؤشرات ال NDVI مع النتائج الميدانية من الأرض، تم الحصول على البيانات الزراعية من مديرية زراعة بابل للفترة من ٢٠٠٩ إلى ٢٠١٩، وتغطي هذه البيانات مجموعة واسعة من المعلومات حول الإنتاج الزراعي مثل عدد الأشجار (التين والنخيل والحمضيات (البرتقال والعنب والرمان)) والمساحات المزروعة لمحصول الحبوب (القمح والذرة الصفراء) لمناطق مختلفة في محافظة بابل، وكانت النتائج متطابقة تقريبا مع نتائج قياس ال NDVI.

Chapter Two

Theoretical Concept

2.1 Introduction

The RS with the GIS are the modern sciences discipline for modeling, acquisition integrating, management and analysis of data that spatially referenced. The process of remote sensing is initiated with electromagnetic radiations from the satellite itself (active RS) or from the Sun (passive RS). The incident radiations are reflected, absorbed and transmitted while interacting with the Earth's surface. The satellite sensor measures these reflected radiations, which contain information about the terrestrial processes taking place during the overpass of the satellite at a location. The terrestrial processes include the components of the hydrological cycle, vegetation processes, interactions with water bodies, topography, and geomorphology topography. Each of the terrestrial processes could be sensitive to measurements in only specific wavelengths/frequencies. So, it is essential to identify the satellite sensors that are appropriate for the purpose. Furthermore, the satellite measurements are also influenced by spatial, temporal, radiometric resolutions and spectral resolutions, which are associated with sensor configuration [37].

The development and modern technologies of geographic systems including the GIS and the RS are mission, powerful and effective tools in degradation assessment and monitoring land changes. Satellites of (RS) like Landsat-5 thematic mapper (TM) and Landsat-8 operational land image (OLI) collect data with various; resolutions, spectrum, and periods of time, which provide a valuable information to understand the

process of land loss [38]. Some indices are capable to reflect environmental changes, and could be adopted to monitor and assess degradation trends, such as the NDVI, which is used in knowing and achieving vegetation on a large scale, and the NDWI, which is used as a complementary index to the NDVI [39].

In 2013, Landsat-8 was launched, including an enhanced TIRS camera with two bands (Band 10 and Band 11) covering the thermal spectrum within (10.6 - 12.51) μm and intended to improve the atmospheric correction and that by means of a split-window technique [40].

With the launch of Landsat 1, the one originally named –ERTS1 for Earth Resources Technology Satellite, it was finally renamed to Landsat. The improvement and development of Landsat 8 was the result of communion between the US space agency (NASA) and the US Geological Survey (USGS). One of the most important strengths aspect of Landsat, in general, its ability to re-inspect every spot on earth every 16 days, and has the long-term data archive so the images that captured by it can be compared from the time 1982, and also has relatively the rich spectral information [41].

The newest satellite in the Landsat croup is Landsat-8 of Earth remote sensing missions dating back to 1972. These satellites have collected and archived moderate resolution data of the entire Earth's land surface long enough to be useful for monitoring trends and evaluating how land use has changed. Applications of Landsat data include agriculture, land mapping and change detection to uses in fresh and coastal waters and ice and snow [42].

2.2 The Remote Sensing

The term "remote sensing" generally refers to the use of satellite- or aircraft- based sensor technologies to detect and classify objects on Earth, including the surface and in the atmosphere and oceans, based on propagated signals (e.g. electromagnetic radiation), figure (2-1) shows the type of RS. It may be split into [43]:

a) Active- remote sensing : when a signal is emitted by a satellite or aircraft and its reflection by the object is detected by the sensor, or from the object which irradiated artificially- producing energy source.

b) Passive- remote sensing: when the reflection of sunlight is detected by the sensor or emitted electromagnetic radiation from natural sources.

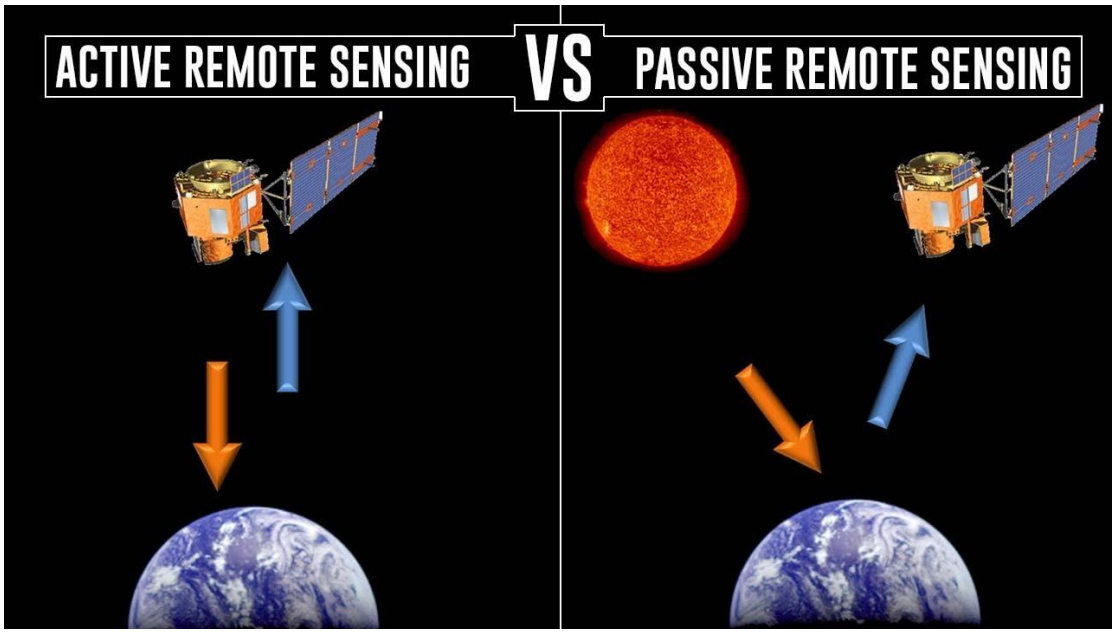

Figure (2 - 1): Active and passive remote sensing [44].

The remote sensing is the process of detecting and monitoring the physical characteristics of an area by measuring its reflected and emitted

radiation at a distance (typically from aircraft or satellite). Special cameras collect remotely sensed images, which help researchers "sense" things about the Earth. Some examples are:

1. Cameras on satellites and airplanes take images of large areas on the Earth's surface, allowing us to see much more than we can see when standing on the ground.
2. Sonar systems can be used on ships to obtain images of the ocean floor without needing to travel to the bottom of the ocean.
3. Cameras on satellites can be used to make images of temperature changes in the oceans.

Include some specific uses of remotely sensed images of the Earth include:

1. Large forest fires can be mapped from space, allowing rangers to see a much larger area than from the ground.
2. Tracking clouds to help predict the weather or watching erupting volcanoes, and help watching for dust storms.
3. Tracking the growth of a cities and changes in farmland or forests over several years or decades.
4. Discovery and mapping of the rugged topography of the ocean floor (e.g., large mountain ranges, deep canyons, and the “magnetic striping” on the ocean floor) [45].

2.2.1 Landsat

The Landsat program is a large project of a series of Earth monitoring and imaging satellite, managed to operate satellite images of the Earth, by NASA and United States Geological Survey (USGS). The satellite was launched on 23rd of July 1972, for land resources

technology. It has been the only satellite system that designed and operated in order to repeatedly observes the global land surface with moderate resolution. The first satellite that was launched was the Earth Resources Technology Satellite (ERTS-1), which was later renamed (Landsat 1), and the latest model Landsat 8 was launched on the 11th of February 2013. These images are stored in the United States and at Landsat receiving stations around the world, which are a unique and important resource for researches and applications of a global change in geology, agriculture, cartography, surveillance, regional planning, forestry, and education [41].

The increasingly long baseline of Landsat data are geo- and radiometrically consistent and calibrated has led to the generation of new information, through modern algorithm and processing methods. Cloud-based high-performance computing allows for bringing algorithms to data, empowering scientists and practitioners to generate new insights and robust information products over broad areas. As captured in data downloads of Landsat data, where at the present time there are more than 1 million images per month, a large and sophisticated user base is implementing integrated analyses and often unprecedented scales. Landsat sensors are used to see everything that the human eye can not see. The earth's orbit is about 705 km (438 miles). In addition, the sensors record a light reflected and emitted from the surface of the Earth with wavelengths defined by infrared and visible waves [46].

2.2.2 Landsat 5

Landsat-5 carried both the Thematic Mapper (TM) and Multispectral Scanner (MSS) sensors, where MSS data acquisitions over the United States in 1992, and the global acquisitions was ended in 1999. After the fail of TM sensor in November 2011, the MSS instrument was putted

back again online, where over 15,000 (MSS) scenes were gathered from the period between June 2012, until January 2013. Thematic Mapper (TM) include 7 bands [47]:

1. Band (1) Visible (0.45 to 0.52 µm) (30 m).
2. Band (2) Visible (0.52 to 0.60 µm) (30 m).
3. Band (3) Visible (0.63 to 0.69 µm) (30 m).
4. Band (4) Near-Infrared (0.76 to 0.90 µm) (30 m).
5. Band (5) Near-Infrared (1.55 to 1.75 µm) (30 m).
6. Band (6) Thermal (10.40 to 12.50 µm) (120 m).
7. Band (7) Mid-Infrared (2.08 to 2.35 µm) (30 m).

2.2.3 Landsat 8

Landsat 8, was launched on 11 February 2013. on-board there are the following tools :

1) The Operational Land Imager (OLI) with nine spectral bands in the visual (VIS), near infrared (NIR), and the shortwave infrared (SWIR) spectral regions, figure (2-2) shows the structure of OLI.

2) The Thermal Infrared Sensor (TIRS) with two spectral bands in the LWIR, figure (2-3) shows the TIRS sensor [48].

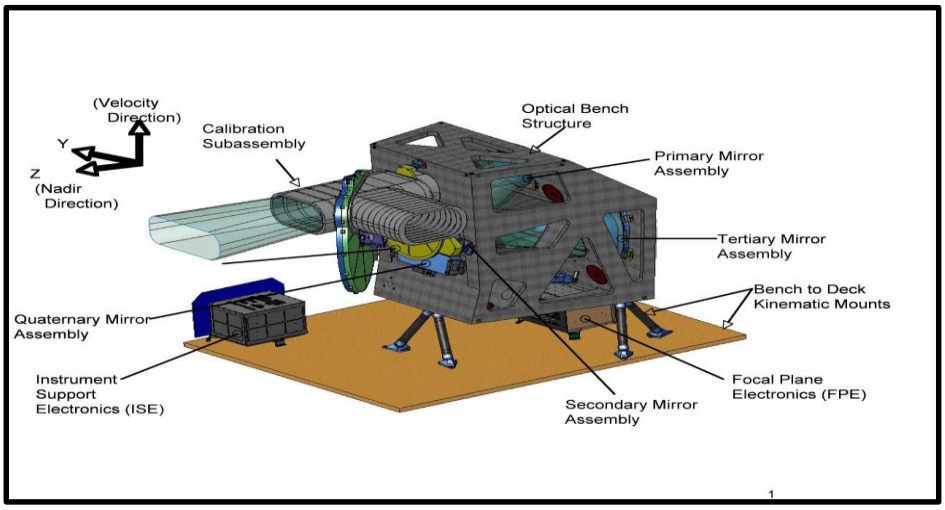

Figure (2 - 2): OLI structure [49].

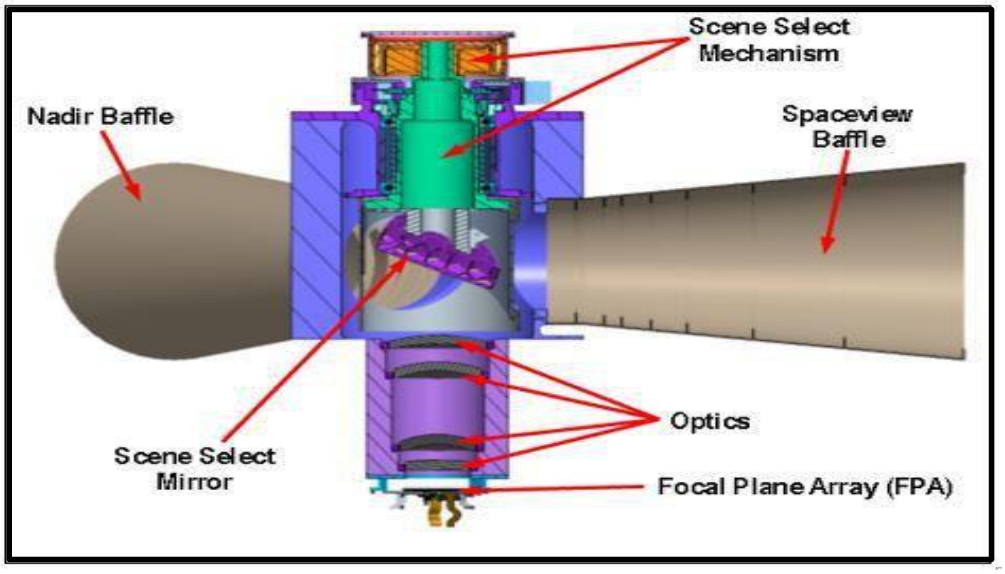

Figure (2 - 3): Thermal infrared sensor [50].

Where the OLI sensor provides nine spectral bands (1- 9) and TIRS provides two spectral bands (10 - 11). Seven bands from band (2) to band (8) of OLI which are consistent with the TM and ETM+ sensors. The new two spectral bands, band (1) and band (9) allow measuring water resources and coastal region realization and improving the detection of cirrus clouds. TIRS behaves thermal imaging can be applicable to evapotranspiration rate measure for water management, figure (2-4) shows the component of Landsat 8 [51].

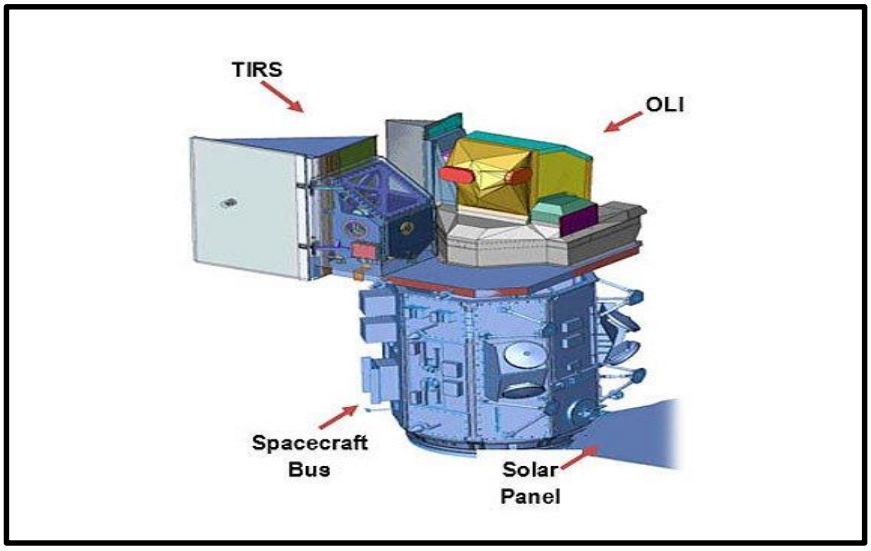

Figure (2 - 4): Landsat 8: satellite imagery overview [52].

Table (2 - 1): The characteristic of bands which observed by the sensors [53].

Band	Resolution (m)	Wavelength (µm)	Description	Sensor
1	30	0.43 - 0.45	Coastal/Aerosol	Operational Land Imager (OLI)
2	30	0.45 - 0.51	Blue	OLI
3	30	0.53 - 0.59	Green	OLI
4	30	0.64 - 0.67	Red	OLI
5	30	0.85 - 0.88	Near Infrared	OLI
6	60	1.57 - 1.65	Short wave Infrared	OLI
7	30	2.11 - 2.29	Short-wave Infrared	OLI
8	15	0.50 - 0.68	Panchromatic	OLI
9	30	1.36 - 1.38	Cirrus	OLI
10	100	10.6 - 11.19	Thermal Infrared	Thermal Infrared Sensor (TIRS)
11	100	11.50 - 12.51	Thermal Infrared	TIRS

2.2.4 Types of band for Landsat 8

1- Band (1):

A blue band (band 1) uses to detect ocean color near coastal regions. This new band will help scientists to measure chlorophyll focus (i.e., ocean color) in coastal regions. Most of the chlorophyll comes from phytoplankton, tiny plant-like organisms that live in surface waters. This analysis is important by using remote sensing to check water quality. This band is called (Coastal /Aerosol), and has a wavelength of (0.433 - 0.453) µm, and resolution 30 m [54].

2- Bands (2, 3, 4):

Bands (2, 3, 4) they are blue, green and red. These bands are called (Visible). These bands are of wavelengths (0.45 - 0.515, 0.525 - 0.600

and 0.630 - 0.680) μm respectively, the resolution for these bands is 30 m [55].

3- Band (5):

The Near Infrared (NIR), this part of the spectrum is special and important for studying ecology because the water of the healthy plants in their leaves scatters the wavelengths back into the sky. By comparing the NIR with another bands, values of the NDVI reflects the plants health more precisely than the visible greenness of the plants. The wavelength for band (5) is between (0.845 - 0.885) μm, and the resolution is 30 m [55].

4- Bands (6, 7):

Bands (6 and 7) cover various slices of the Short Wavelength Infrared (SWIR). They are especially useful to distinguish and study the soil from dry soil, and for geology (rocks and soils that look similar in other bands often have powerful contrasts in (SWIR). These bands span wavelengths (1.560 - 1.660, 2.100 - 2.300) μm respectively, and the resolution for these bands is 30 m [55].

2- Band (8):

Panchromatic band is black and white band which compile energy from visible spectrum combined. As collated assists in more collection of light, the images are sharp, which is actually 15 m resolution. These are used in pan sharpening the regular lower resolution images, and the rang of wavelength for this band is (0.500 - 0.680) μm [56].

3- Band (9):

Thin high clouds are hard to spot in satellite images. Both the clouds and their shadows can interfere with measurements. OLI's new shortwave-infrared band (band 9) will be capable to detect these clouds better than previous Landsat sensors, because it measures light in a short-wave infrared band especially is sensitive to the presence of cirrus clouds,

the wavelength for this band is (1.360 - 1.390) μm, and the resolution is 30 m [54].

4- Band (10, 11):

Thermal Infrared (TIR) bands measure the temperature on the ground itself. Analyzing these bands, heat islands can be identified in urban areas. Both of the bands show stripping effect but band (11) shows more instability in values than band (10), these bands are of wavelengths (10.30 - 11.30, 11.50 - 12.50) μm respectively, and the resolution is 100 m for both bands [56].

2.2.5 Satellite Sensors

Each satellite carries sensors that senses the electromagnetic spectrum as follows:

1. **Landsat 1-5 Multispectral Scanner** (MSS) images consist of four spectral bands with 60 m spatial resolution. Approximate scene size is 170 km north-south by 185 km east-west (106 miles by 115 miles). Specific band designations differ from Landsat 1 - 3 to Landsat 4 - 5.

Table (2 - 2): The characteristic of bands observed by the sensor of Landsat (1 - 5) [53].

Landsat 1 - 5 Multispectral Scanner (MSS)			
Landsat 1 – 3	**Landsat 4 – 5**	**Wavelength (μm)**	**Resolution (m)**
Band 4	Band 1	0.5 - 0.6	60
Band 5	Band 2	0.6 - 0.7	60
Band 6	Band 3	0.7 - 0.8	60
Band 7	Band 4	0.8 - 1.1	60

2. **Landsat 4-5 Thematic Mappe**r (TM) images consist of seven spectral bands with a spatial resolution of 30 m for Bands 1 to 5 and 7. Spatial resolution for Band 6 (thermal infrared) is 120 m, but is resampled to 30 m pixels. Approximate scene size is 170 km north-south by 183 km east-west (106 miles by 114 miles).

Table (2 - 3): The characteristic of bands observed by the sensor of Landsat (4 - 5) [53].

Landsat 4 - 5 Thematic Mapper (TM)		
Landsat 4 – 5	**Wavelength (μm)**	**Resolution (m)**
Band 1	0.45 - 0.52	30
Band 2	0.52 - 0.60	30
Band 3	0.63 - 0.69	30
Band 4	0.76 - 0.90	30
Band 5	1.55 - 1.75	30
Band 6	10.40 - 12.50	30
Band 7	2.08 - 2.35	30

3. **Landsat 7 Enhanced Thematic Mapper Plus** (ETM+) images consist of eight spectral bands with a spatial resolution of 30 m for Bands 1 to 7. The resolution for Band 8 (panchromatic) is 15 m. All bands can collect one of two gain settings (high or low) for increased radiometric sensitivity and dynamic range, while Band 6 collects both high and low gain

for all scenes. Approximate scene size is 170 km north-south by 183 km east-west (106 miles by 114 miles).

Table (2 - 4): The characteristic of bands observed by the sensor of Landsat 7 [53].

Landsat 7 Enhanced Thematic Mapper Plus (ETM+)		
Landsat 7	**Wavelength (μm)**	**Resolution (m)**
Band 1	0.45 - 0.52	30
Band 2	0.52 - 0.60	30
Band 3	0.63 - 0.69	30
Band 4	0.77 - 0.90	30
Band 5	1.55 - 1.75	30
Band 6	10.40 - 12.50	30
Band 7	2.09 - 2.35	30
Band 8	0.52 - 0.90	15

4. **Landsat 8 Operational Land Imager** (OLI) **and Thermal Infrared Sensor** (TIRS) images consist of nine spectral bands with a spatial resolution of 30 m for Bands 1 to 7 and 9. New band 1 (ultra-blue) is useful for coastal and aerosol studies. New band 9 is useful for cirrus cloud detection. The resolution for Band 8 (panchromatic) is 15 m. Thermal bands 10 and 11 are useful in providing more accurate surface temperatures and are collected at 100 m. Approximate scene size is 170 km north-south by 183 km east-west (106 miles by 114 miles). The instruments on Landsat 9 are being designed as improved copies of Landsat 8, figure (2-5) shows the different bands of electromagnetic range [21].

Table (2 - 5): The characteristic of bands observed by the sensor of Landsat (8 - 9) [57].

Landsat 8 - 9 Operational Land Imager (OLI) and Thermal Infrared Sensor (TIRS)		
Bands	**Wavelength (µm)**	**Resolution (m)**
Band 1 - Coastal aerosol	0.43 - 0.45	30
Band 2 – Blue	0.45 - 0.51	30
Band 3 – Green	0.53 - 0.59	30
Band 4 – Red	0.64 - 0.67	30
Band 5 - Near Infrared (NIR)	0.85 - 0.88	30
Band 6 - SWIR 1	1.57 - 1.65	30
Band 7 - SWIR 2	2.11 - 2.29	30
Band 8 – Panchromatic	0.50 - 0.68	15
Band 9 – Cirrus	1.36 - 1.38	30
Band 10 - Thermal Infrared (TIRS) 1	10.6 - 11.19	100
Band 11 - Thermal Infrared (TIRS) 2	11.50 - 12.51	100

Figure (2 - 5) : Different bands of frequencies along the electromagnetic range [53].

2.2.6 The Acquisition Schedules for the Landsat Satellites

The Landsat 7 and Landsat 8 satellites orbit the Earth at an altitude of 705 km (438 miles) in a 185 km (115 miles) south, moving from north to south over the sunlit side of the Earth in a sun synchronous orbit, following the World Reference System (WRS-2). Each satellite makes a complete orbit every 99 minutes, completes about 14 full orbits in one day, and crosses every point on Earth once every 16 days.

The satellite's orbits are offset to allow 8 day repeat coverage of any Landsat scene area on the globe. Between the two satellites, more than 1,500 scenes are added to the USGS archive every day.

Traveling on the descending (daytime) node from the north to the south, the satellites cross the equator on each pass at a time that provides the maximum illumination with minimum water vapor (haze and cloud build-up). Landsat 7 and Landsat 8 crosses the equator at 10:00 a.m. +/- 15 minutes (mean local time).

The Landsat 7 and Landsat 8 satellites each acquire data in accordance with their respective Long Term Acquisition Plan (LTAP) using parameters such as seasonality, land definition, historical cloud cover, gain settings, and sun angle [58].

2.2.7 Representation of Different Colors in Infrared Color Aerial Photograph

The color-infrared (CIR) aerial photography often calles "false color" photography because it renders the scene in colors not normally seen by the human eye-is widely used for interpretation of natural resources. Atmospheric haze does not interfere with the acquisition of the image, figure (2-6) shows example for false colors.

1. Live vegetation is almost associated with red tones. Very intense reds indicate dense, vigorously growing vegetation. As plant vigor decreases, the vegetation appears as lighter shades of red and pink, various shades of greens, and possibly tans.
2. Bare soils appear as shades of white, blue, or green in most agricultural regions. In general, darker shades of each color indicate moister soil.
3. Man-made features appear in tones that relate to the materials with which they are made. Asphalt roads, for example, are dark blue or black; gravel or dirt roads are lighter colors depending on their composition; and clean concrete roads are light in tone. The colors of buildings are similarly dependent on the materials used to create them.
4. Water appears as shades of blue, varying from nearly black (clean water) to very pale blue (increasing amounts of sediment). The color of very shallow water is often determined by the material present at the bottom of the water. For example, a very shallow stream with a sandy bottom will appear white due to the high level of sand reflection [59].

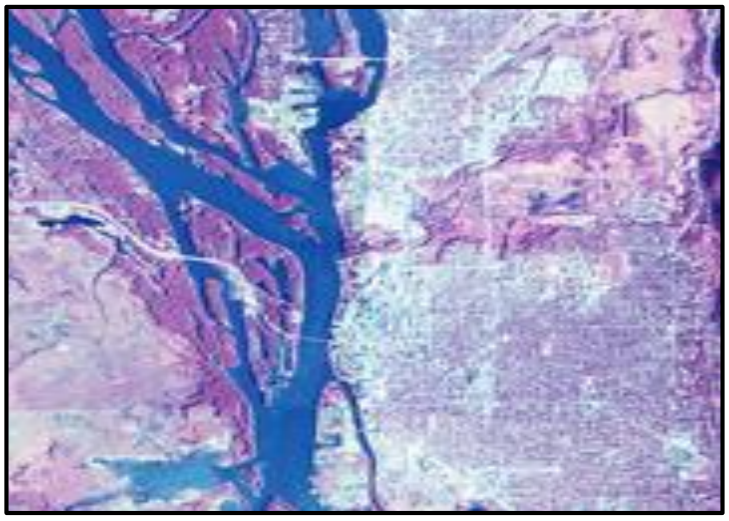

Figure (2 - 6): Photography (false colors) [58].

2.2.8 Types of Resolution

Four types of resolution define the RS imagery: spatial, spectral (optical RS), radiometric, and temporal [60].

1. Spatial resolution

Spatial resolution refers to the size of one pixel on the ground. For example 15 m means that one pixel on the image corresponds to a square of 15 by 15 m on the ground. This sometimes referred to as Ground Sample Distance (GSD). Temporal resolution refers to how often data of the same area is collected. This is typically referred to as Revisit Time. Sensors can trade spatial resolution for temporal resolution, but it is difficult to maximum both. Sensors have a high spatial resolution cover a smaller area then a sensor with the same number of pixels but with a lower spatial resolution. With a smaller field of view it takes longer to cover the same area, thus as spatial resolution increases, temporal resolution decreases, figure (2-7) illustrates the meaning of spatial resolution.

Freely available imagery (e.g., Landsat, Sentinel, MODIS) tends to either have a revisit time measured in days (1 - 4) days with resolution in the hundreds of meters (300 - 500) m, or a revisit time measured in weeks (10 - 20) days with resolutions in the tens of meters (10 - 30) m.

The high resolution commercial imagery is available up to 3 m resolution, with revisit times varying quite a bit. Some sensors are tasked, or pointed to collect specific areas rather than always just collecting the area directly below. As a result, some areas may not be covered at all by tasked satellites. While there is still a premium for the highest resolution imagery (< 0.50 m), medium to low resolution is

suitable for many applications, and increasingly affordable or available at no cost [60].

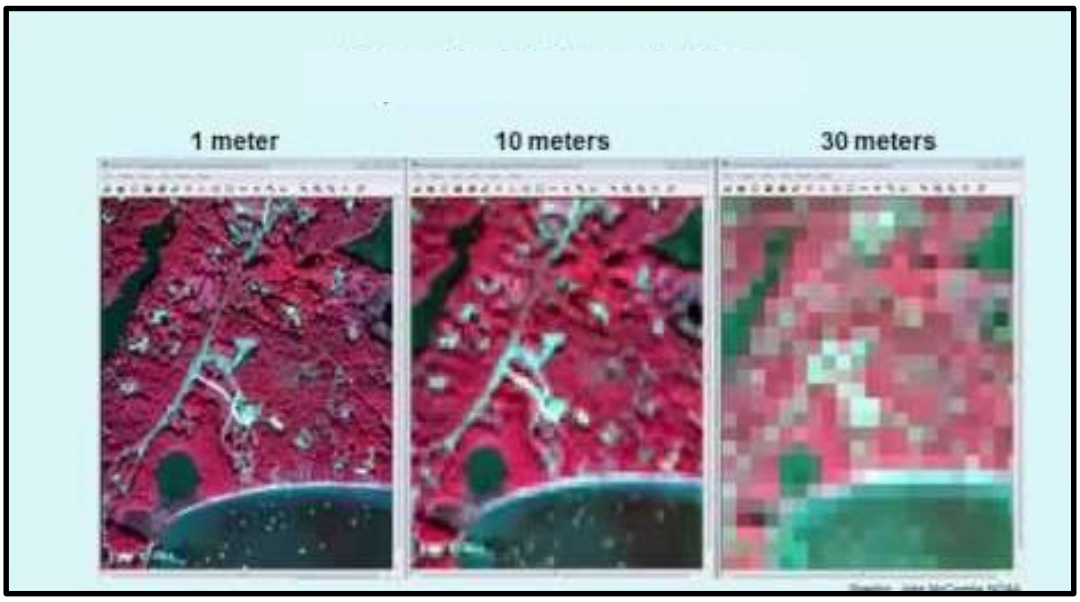

Figure (2 - 7): Spatial resolution [61].

2. Spectral (optical RS) resolution

The spectral resolution describes the ability of a sensor to define fine wavelength intervals. The finer the spectral resolution, the narrower the wavelength range for a particular channel or band. Black and white film records wavelengths extending over much, or all of the visible portion of the electromagnetic spectrum. Figure (2-8) illustrates the meaning of spectral resolution, the various wavelengths of the visible spectrum are not individually distinguished. The overall reflectance in the entire visible portion is recorded. Colour film is also sensitive to the reflected energy over the visible portion of the spectrum, but has higher spectral resolution, as it is individually sensitive to the reflected energy at the blue, green, and red wavelengths of the spectrum. Thus, it can represent features of various colors based on their reflectance in each of these distinct wavelength ranges [62].

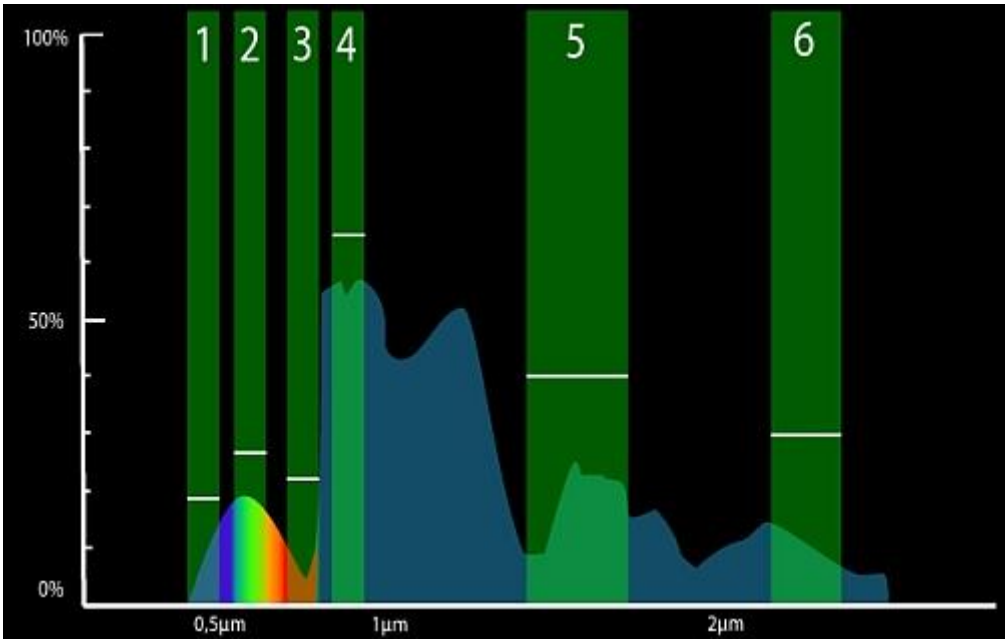

Figure (2 - 8): Bands of a characteristic multispectral sensor. Here, the blue, red, and green light as well as the near and normal infrared range were recorded [50].

3. Radiometric resolution

The radiometric resolution of an imaging system describes its ability to discriminate very slight differences in energy the finer the radiometric resolution of a sensor, the more sensitive it is to detecting small differences in reflected or emitted energy.

Imagery data are represented by positive digital numbers which vary from 0 to (one less than) a selected power of 2. This range corresponds to the number of bits used for coding numbers in binary format. Each bit records an exponent of power 2 (e.g. 1 bit = 2^1 = 2). The maximum number of brightness levels available depends on the number of bits used in representing the energy recorded. Thus, if a sensor used 8 bits to record the data, there would be 2^8 = 256 digital values available, ranging from 0 to 255. However, if only 4 bits were used, then only 2^4 = 16 values ranging from 0 to 15 would be available. Thus, the

radiometric resolution would be much less. Image data are generally displayed in a range of grey tones, with black representing a digital number of 0 and white representing the maximum value (for example, 255 in 8-bit data), figure (2-9) illustrates the meaning of radiometric resolution, By comparing a 2-bit image with an 8-bit image, we can see that there is a large difference in the level of detail discernible depending on their radiometric resolutions [60, 63].

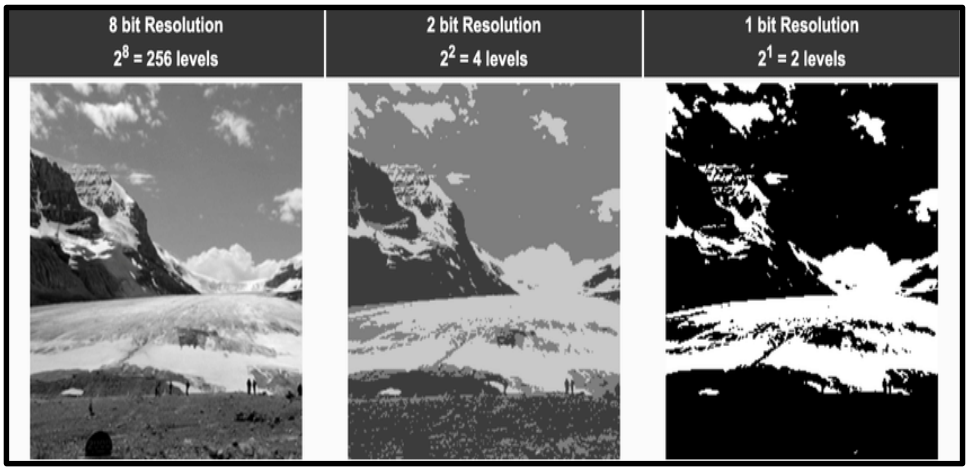

Figure (2 - 9): From left to right, 8 bit, 2 bit and 1 bit radiometric resolutions are shown [64].

4. Temporal resolution

The temporal resolution describes how often a scene is imaged as determined by the platform and its operation. The temporal resolution of satellite imagery is determined by the satellite's revisit time. Landsat missions have a 16 day temporal resolution while the commercial Planet Scope satellite constellation achieves daily revisits, figure (2-10) illustrates the meaning of temporal resolution [65].

The ability to collect imagery of the same area of the Earth's surface at different periods of time is one of the most important elements for applying remote sensing data. Spectral characteristics of features may

change over time and these changes can be detected by collecting and comparing multi-temporal imagery. For example, during the growing season, most species of vegetation are in a continual state of change and our ability to monitor those subtle changes using remote sensing is dependent on when and how frequently we collect imagery. By imaging on a continuing basis at different times we are able to monitor the changes that take place on the Earth's surface, whether they are naturally occurring (such as changes in natural vegetation cover or flooding) or induced by humans (such as deforestation or urban development) [66].

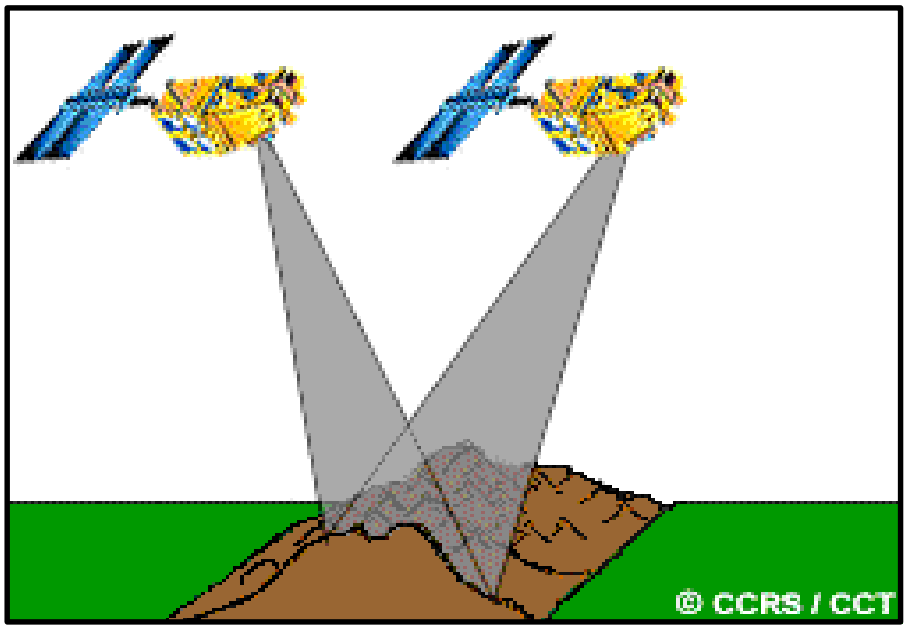

Figure (2 - 10): Temporal resolution [66].

2.3 The Geographic Information System (GIS)

The GIS can provide four sets of capabilities in order to deal with georeferenced data, which are [67]:

1. Data capture and preparation.
2. Data management includes storage and maintenance.
3. Data manipulation and analysis.
4. Data presentation.

2.3.1 Data Types Used in the GIS

The GIS system use twofold categories of datasets: Spatial data and non-spatial data:

(a) Spatial data: is the datasets (vector and raster) that have been prepared through field surveys or remote sensed data that is referenced on the earth's surface. The composition of these datasets include satellite images, coordinates among others that are interpreted to produce thematic maps which can aid agricultural planning towards to the sustainable use of limited resources, figure (2-11) shows the different between vector and raster data [67].

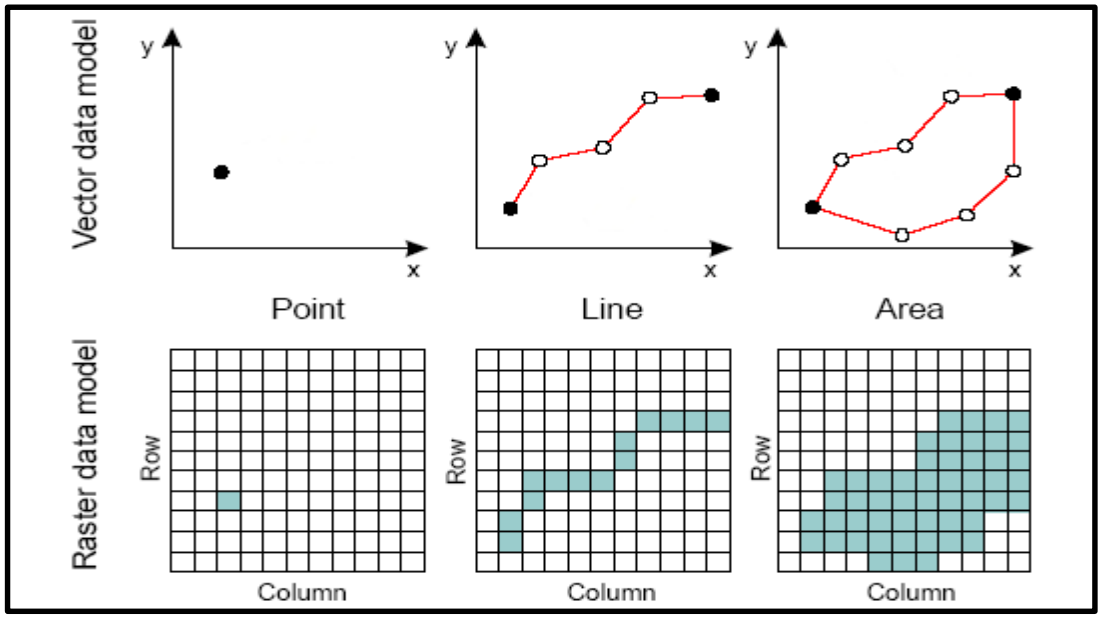

Figure (2 - 11): The GIS data (Raster and Vector data model) [68].

The geospatial data is represented in a form of co-ordinates. In vector data, the basic units of spatial information are points, polygons and lines (arcs). Each of these units is composed simply as a series of one or more co-ordinate points, for example, a polygon is a collection of related lines and a line is a collection of related points. Figure (2-12) shows the various types of layers that can be used in the GIS.

1. Co- ordinate

Pairs of numbers expressing horizontal distances along orthogonal axes, or triplets of numbers measuring horizontal and vertical distances, or n-numbers along n-axes expressing a precise location in n-dimensional space. Co-ordinates generally represent locations on the earth's surface relative to other locations.

2. Point

A zero-dimensional abstraction of an object represented by a single X, Y co-ordinate. A point normally represents a geographic feature too small to be displayed as a line or area, for example, the location of a building location on a small-scale map, or tower.

3. Line

A set of ordered co-ordinates that represent the shape of geographic features too narrow to be displayed as an area at the given scale (streams contours, street centerlines, or contours), or linear features with no area (county boundary lines). A lines is synonymous with an arc.

4. Polygon

A feature used to represent areas. A polygon is defined by the lines that make up its boundary and a point inside its boundary for identification. Polygons have attributes that describe the geographic feature they represent such as forest, district [69].

(b) Non- spatial data : The non- spatial data are attributes as complimentary to the spatial data and describe what is at a point, along a line or in a polygon and as socio-economic characteristics from other sources. The attributes of a soil category could be the depth of soil, texture, drainage, erosion [67].

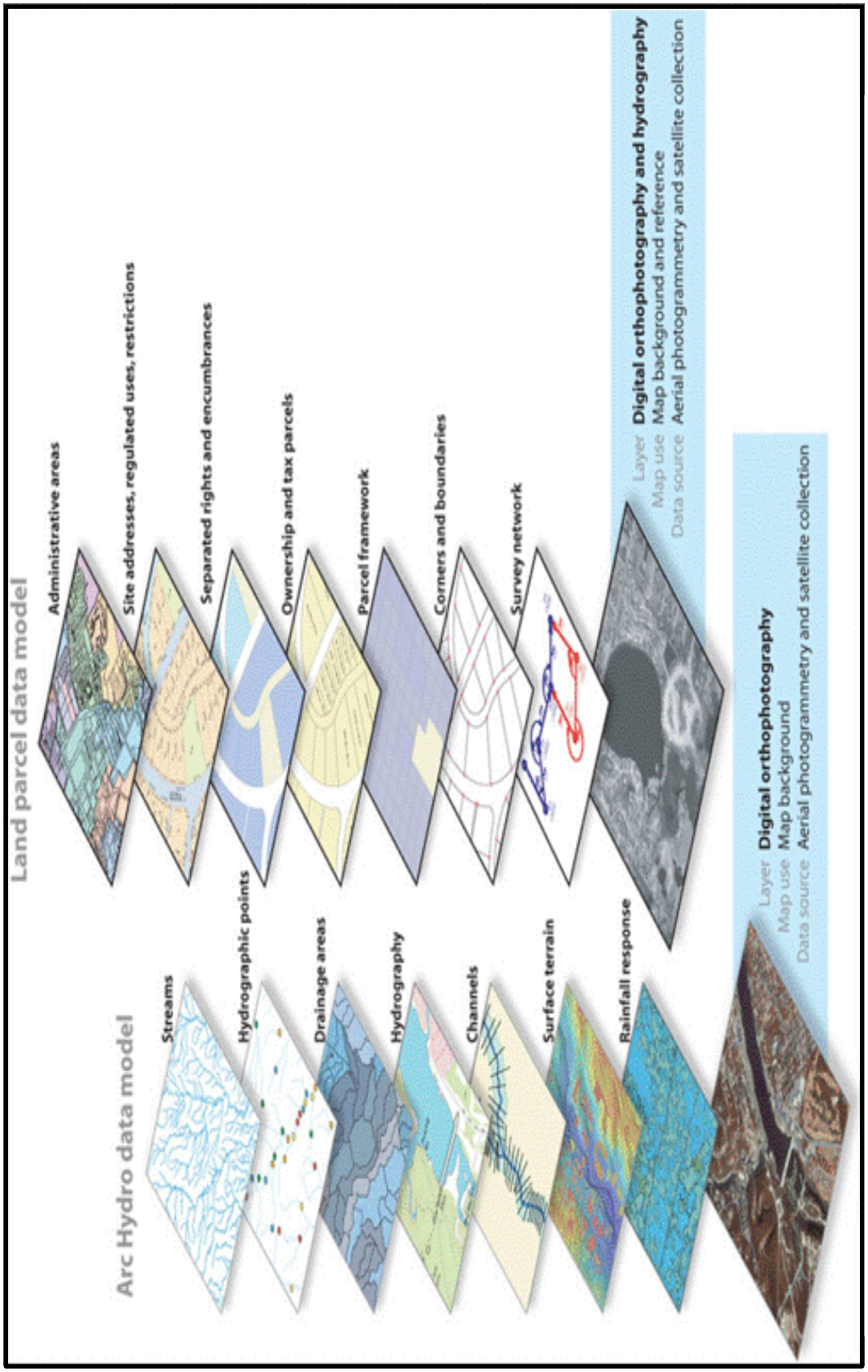

Figure (2 - 12): This is a schematic of the various types of layers that can be used in the GIS [68].

2.3.2 Components of the GIS

The GIS has mainly 5 components: Hardware, Software, Data, People, and Methods, shows that in figure (2-13).

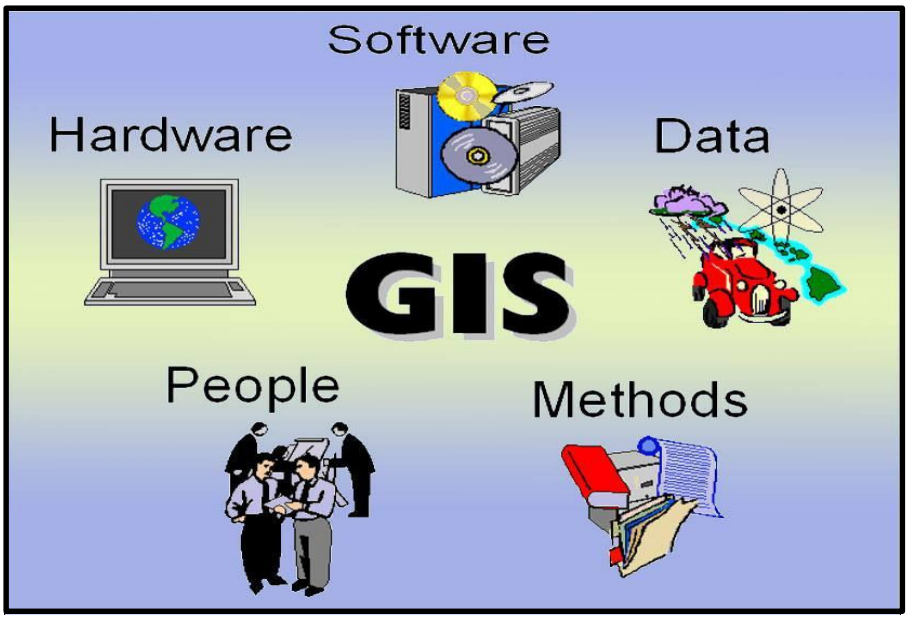

Figure (2 - 13): Components of the GIS [70].

1. **Hardware:** Hardware is the computer on which a GIS operates; the GIS software runs on a wide range of hardware types, from centralized computer server to desktop computers and in networked configurations or stand-alone. Hardware relates to device used by end users such as graphic devices or scanners and plotters. Data storage and manipulation is done using a range of processor. The choice of hardware system range from 300 MHz Personal Computers to Super Computers having capability in Tera FLOPS. The computer forms the backbone of the GIS hardware, which gets its input through the Scanner or a digitizer board. Scanner converts a picture into a digital image for further processing. The output of scanner can be stored in many formats

for example JPG, TIFF, BMP, etc. plotters and Printers are the most common output devices for a GIS hardware setup [71, 72].

2. **The Software :** GIS software provides the functions and tools needed to store, analyze, and display geographic information. The key components in a GIS software are [73] :

1. Tools for the input and manipulation of geographic information.
2. A database management system (DBMS).
3. Tools that support geographic query, visualization and analysis.
4. A graphical user interface (GUI) for easy access to tools.

3. **Data:** Possibly the most important component of the GIS is the data. Geographic data and related tabular data can be collected in-house or purchased from a commercial data provider. The GIS will integrate spatial data with other data resources and can even use a DBMS, used by most organizations to organize and maintain their data. Data is one of the most important, they are often very expensive, components of the GIS. All data in the GIS are either spatial data or attribute data. Spatial data tells us where something occurs. Attribute data tells what occurs; it tells us the nature or characteristics of the spatial data. Geographic data, which is comprised of geographic features and their corresponding attribute information, is entered into the GIS using a technique called (digitizing). This process involves digitally encoding geographic features, such as roads, buildings or county boundaries. Digitizing is done by tracing the location, path or boundary of geographic features either on a computer screen using a scanned map in the background, or a paper map that is attached to a digitizing tablet. The digitizing process can be very tedious and

time consuming, especially when capturing large datasets such as soil polygons, streams or topographic contours [72].

4. **People:** The GIS technology has a limited value and ineffective without the people who manage the system and develop plans for applying it to real-world problems. The GIS users range from technical specialists who design and maintain the system to those who use it to help them perform their everyday work [74].

5. **Methods** : A successful GIS operates according to a well-designed plan and business rules, which are the models and operating practices unique to each organization. Geographic Information System- The organized activity by which people [74]:

1. Measure aspects of geographic phenomena and processes.
2. Represent these measurements, usually in the form of a computer database, to emphasize spatial themes, entities and relationships.
3. Operate upon these representations to produce more measurements and to discover new relationships by integrating disparate sources.
4. Transform these representations to conform to other frameworks of entities and relationships.

2.3.3 Functions of the GIS Softwares

1. Data Capture: It helps in geographic and tabular (attribute) data input in layers.
2. Storage: The two basic data models for geographic data storage are raster and vector.
3. Querying: It helps in finding specific features based on the location or attribute value.

4. Analysis: It is useful in understanding the interaction of spatial relationship between multiple datasets.
5. Display: It helps in visualizing the geographic features using a variety of symbology.
6. Output: It displays results in a variety of formats, such as maps, reports and graphs for better interpretation and access to appropriate solution [73].

2.4 Vegetation Indices

The solar radiation reflected by plants depends on the morphological and chemical characteristics of the plant. The plant type, water content, and canopy characteristics affect the light reflected in each spectral band differently. The used of reflected light measured in ultraviolet, visible (blue, green, red), and near- and mid-infrared portions of the spectrum has commonly been used to develop various vegetation indices that provide useful information on plant conditions and structure. Vegetation indices are mathematical expressions that combine measured reflectance in many spectral bands to produce a value that helps assess crop growth, vigor, and several other vegetation properties such as chlorophyll content and biomass. Mapping of these indices can help understand spatial-temporal variability in crop conditions, figure (2-14) shows the spectral reflectance curve [75].

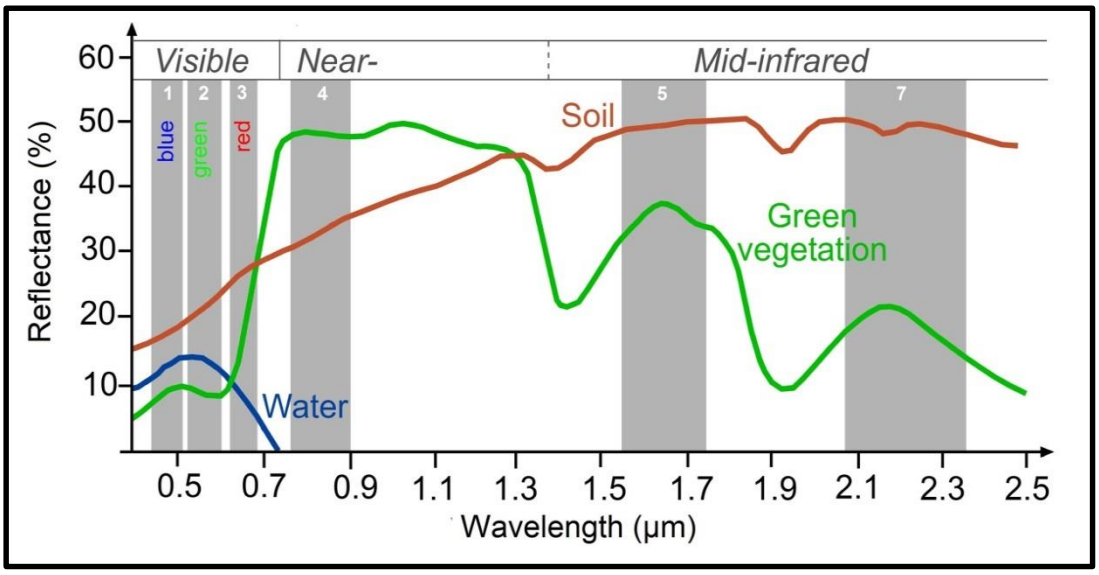

Figure (2 - 14): The spectral reflectance curve [76].

2.4.1 The Normalized Difference Vegetation Index (NDVI)

The NDVI is an effective graphical indicator that can be used to analyze remote sensing measurements using a space platform, in order to investigate the trend of the live green vegetation in the observed target. The NDVI is an important technique for identifying the various features displayed in the 3-band satellite image (Green, Red and NIR). As this indicator is a simple and important digital signal that can be used to analyze the RS measurements, from a remote platform and assess whether the target or object being observed contains live green vegetation or not [77]. The most accurate digital processing method for satellite images in the presentation of vegetation cover. Where it is based on the fact that the plants exhibit high reflectivity in the wavelength range Near infrared and low reflectivity wavelength range red.

The NDVI has been commonly used for remote sensing of vegetation at last decades. It depends on the reflectance or radiances that were recorded by the red channel (≈ 0.66 μm) and the near-IR channel (≈ 0.86 μm). It is a calculation that is used to identify the vegetation

condition and health through the levels of chlorophyll that is detected in the leaves. The red channel can trace the strong chlorophyll absorption region, and the near-IR channel can record the high reflectance plateau of the vegetation.

In order to calculate the NDVI the following formula is applied [77]:

$$NDVI = \frac{(NIR - R\ Visible)}{(NIR + R\ Visible)} \quad (1)$$

Where:

NDVI = Normalized difference vegetation index.

NIR = The near infrared band.

Red = The red band.

$$In\ Landsat\ 4-7, \qquad NDVI = \frac{(Band\ 4 - Band\ 3)}{(Band\ 4 + Band\ 3)} \quad (2)$$

$$In\ Landsat\ 8, \qquad NDVI = \frac{(Band\ 5 - Band\ 4)}{(Band\ 5 + Band\ 4)} \quad (3)$$

The NDVI values have ranged from (+1 to -1), in general, where a positive value indicates the presence of vegetation cover and the higher the resulting positive value, the greater the vegetation, and density of the plants and have healthier and the opposite is true with regard to the negative values that indicate non- vegetation, figure (2-15) shows the NDVI values [78].

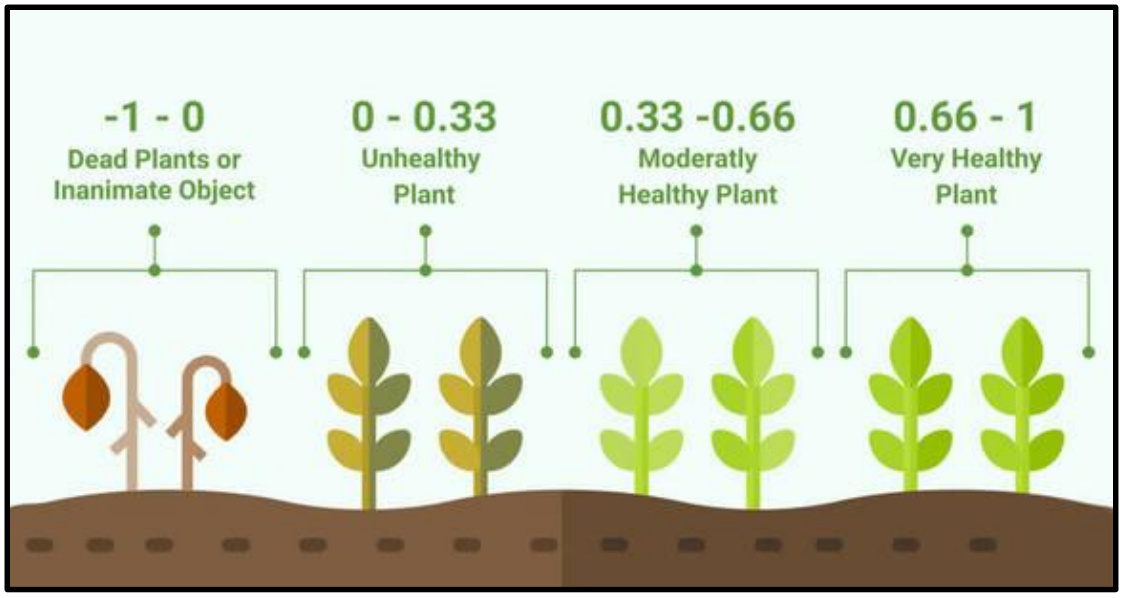

Figure (2 - 15): The NDVI values represent the healthy of the plant [79].

2.4.2 The Normalized Difference Water Index (NDWI):

The NDWI is use for the water bodies analysis. The NDWI can enhance water information efficiently in most cases. It is sensitive to build-up land and result in over-estimated water bodies. The NDWI products can be used in conjunction with the NDVI change products to assess context of apparent change areas.

Water bodies have low reflectance. It only reflects within visible portion of the electromagnetic spectrum. Water bodies in their liquid state are generally high reflectance on Blue (0.4 - 0.5) µm spectrum than Green (0.5 - 0.6) µm and Red (0.6 - 0.7) µm spectrum. Clear water having greatest reflectance in the blue portion of the visible spectrum. So, water appear blue. Turbid water has higher reflectance in visible spectrum. There is no reflection in Near Infrared (NIR) and beyond. The NDWI is developed by Gao (1996) to enhance the water related features of the landscapes. This index uses the near infrared (NIR) and the Short-Wave infrared (SWIR) bands. The NDWI can be calculated by following formula [76]:

$$NDWI = \frac{(NIR-SWIR)}{(NIR+SWIR)} \quad (4)$$

Where:

NDWI = Normalized Difference Water Index.

NIR = Near Infra-Red Band.

SWIR = Short Wave Infrared Band.

For Landsat 4-7, $NDWI = \frac{(Band4-Band5)}{(Band4+Band5)}$ (5)

For Landsat 8, $NDWI = \frac{(Band5-Band6)}{(Band5+Band6)}$ (6)

This index was proposed to discover surface water in wetland environments and to allow the measurement of surface water extent [80]. Based on the fact that water has strongest absorption while vegetation has strongest reflectivity at near infra-red, Mcfeeters S.K. (1996) proposed the method of NDWI to highlight water body. NDWI proved to work well in separating water body and vegetation but has limitations when it comes to soil and built up area, figure (2-16) shows the three different versions of the NDWI [45].

Similarly, the NDWI value lies between -1 to 1. Generally, water bodies the NDWI value is greater than 0.5. Vegetation has much smaller values which distinguishing vegetation from water bodies easily. Build-up features having positive values lies between 0 to 0.2 [76].

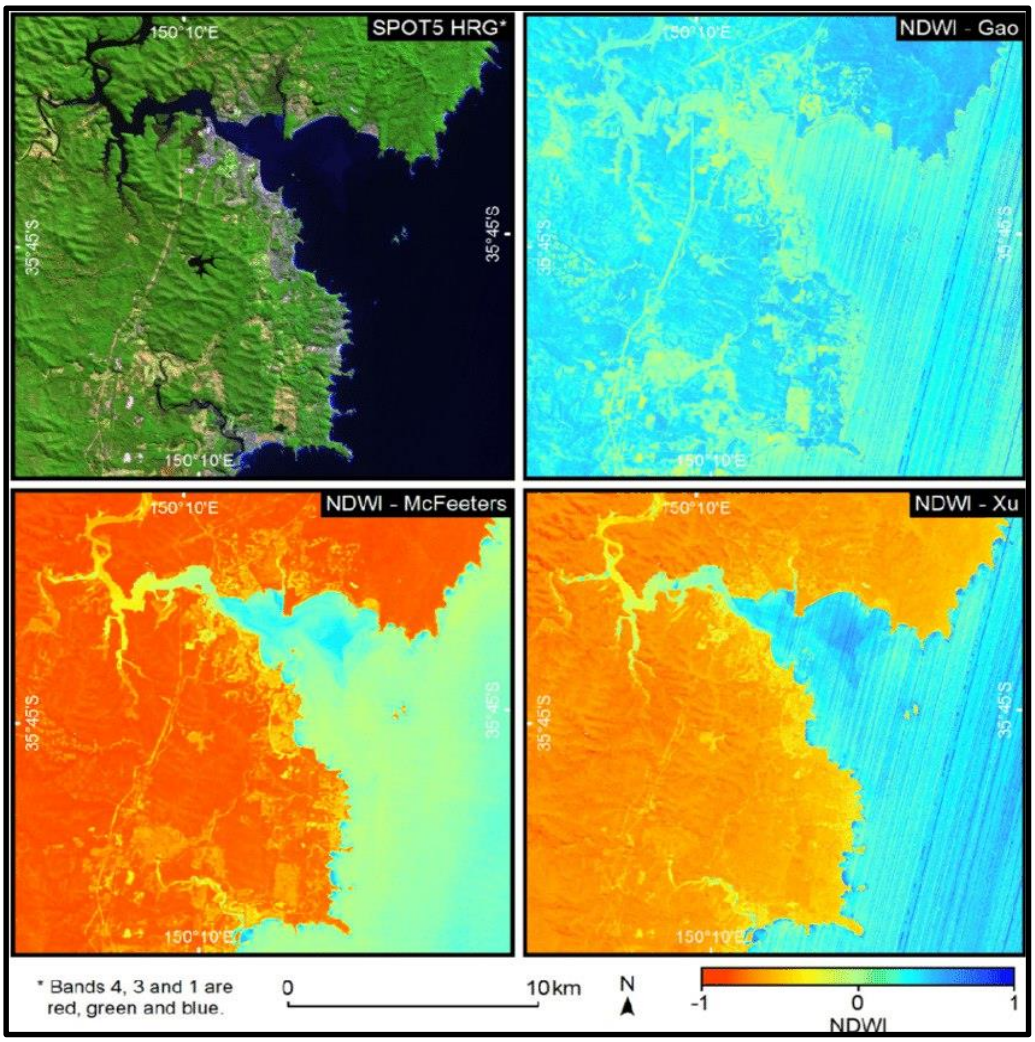

Figure (2 - 16): Three different versions of the normalized difference water index (NDWI) for a subset of a SPOT5 HRG image [84].

2.4.3 The Soil Adjusted Vegetation Index (SAVI)

The SAVI equation introduces a soil-brightness-dependent correction factor, L, soil conditioning index compensates for the difference in soil background conditions. NIR is the reflectance from the near-infrared band, and R is the reflectance from the red visible band. Applying a correction for the soil provides more accurate information on the condition of the vegetation itself [83].

The SAVI includes a soil calibration factor (L) to minimize the soil background influences:

$$SAVI = \frac{(Band_{NIR} - Band_{Red})(1+L)}{(Band_{NIR} + Band_{Red} + L)} \quad (7)$$

Where :

Band $_{NIR}$ = The reflectance at NIR.

Band $_{Red}$ = The reflectance at Red.

L = The soil conditioning index varying between 0 and 1.

The value of L close to 1 representing a high degree of vegetation coverage and thus soil background has no effect on the retrieval of vegetation information. A value of L equal to 0.5 is considered for the most common environmental conditions and was found to minimize the effects of soil brightness variation and eliminate the need for calibration under different soil conditions, figure (2-17) shows the SAVI for growth stages [84].

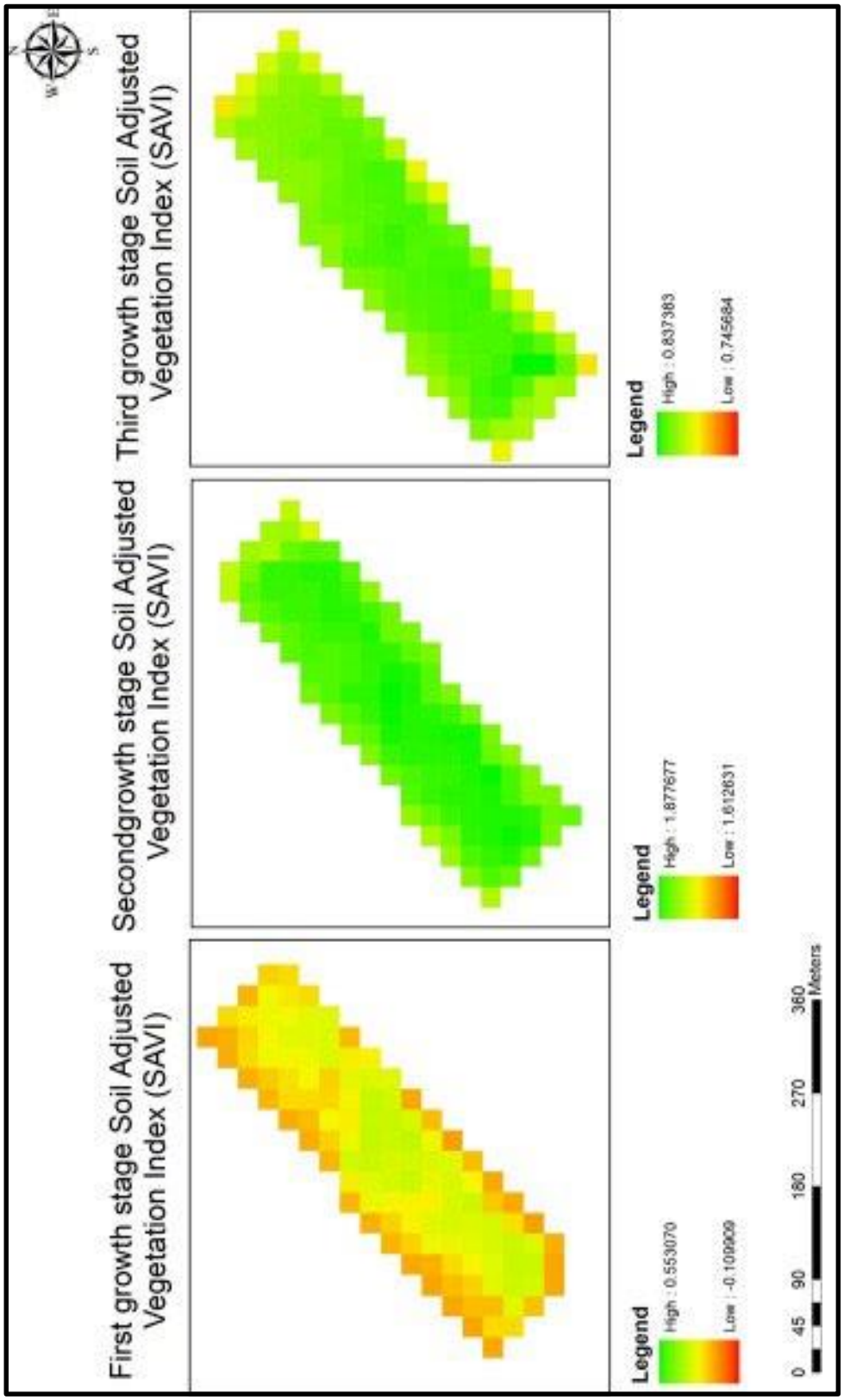

Figure (2 - 17): The Soil-Adjusted Vegetation Index (SAVI) for growth stages [85].

2.4.4 The Enhanced Vegetation Index (EVI)

The EVI was developed to improve the NDVI by optimizing the vegetation signal by using the blue reflectance to correct for soil background signals and reduce atmospheric influences, including aerosol scattering. The EVI is similar to the NDVI and can be used to quantify vegetation greenness. However, the EVI corrects for some atmospheric conditions and canopy background noise and is more sensitive in areas with dense vegetation. figure (2-18) shows the meaning of the EVI. The EVI is defined by the following equation:

$$EVI = 2.5 * \frac{(Band_{NIR} - Band_{RED})}{(Band_{NIR} + 6 * Band_{RED} - 7.5 * Band_{BLUE} + 1)} \quad (8)$$

Where:

$Band_{NIR}$ = Surface reflectance at 800 nm.

$Band_{RED}$ = Surface reflactance at 680 nm.

$Band_{BLUE}$ = Surface reflactance at 450 nm.

In Landsat 4-7, $EVI = 2.5 * \frac{(Band4 - Band3)}{(Band4 + 6 * Band3 - 7.5 * Band1 + 1)}$ (9)

In Landsat 8, $EVI = 2.5 * \frac{(Band5 - Band4)}{(Band5 + 6 * Band4 - 7.5 * Band2 + 1)}$ (10)

The value of this index ranges from -1 to 1. The common range for green vegetation is 0.2 to 0.8 [59].

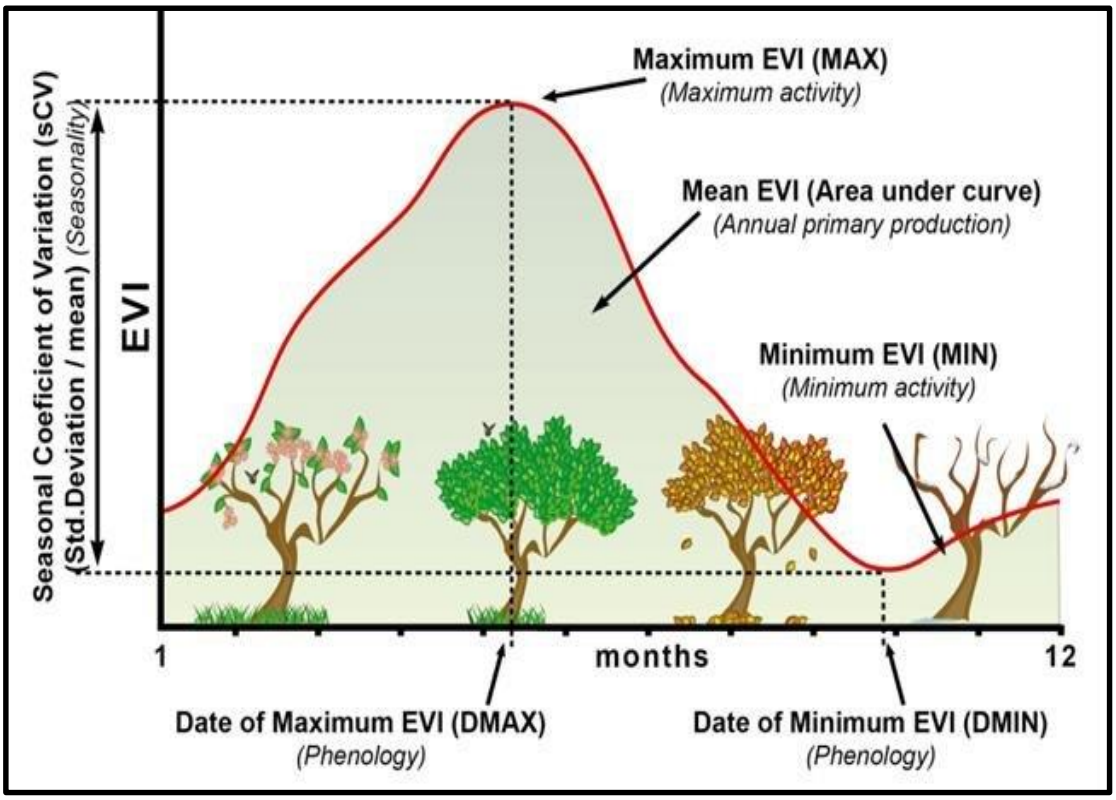

Figure (2 - 18): The Enhanced Vegetation Index (EVI) annual curve and attributes used in the functional characterization of the Pas (EVI_Mean, EVI_sCV, EVI_Max, EVI_Min, DMax and DMin) [86].

2.5 Classification

Image classification can be defined as the process that is done to categorize all the pixels in an image or raw that remotely sensed satellite data, to obtain the given set of the labels or land cover features. The aim of the classification process is to group all pixels in a digital image into one of the different land cover themes\classes.

Methods belonging to pixel-based classification approaches perform classification by assigning each pixel to the target features of the land cover. This can be accomplished using the two types of classification are as follows [87, 88]:

1. **Supervised Classification**

Supervised classifiers utilize samples of known features of each land cover class, known as "training sites" to classify pixels of unknown characteristics of digital images. parametric pixel-based classifiers. There are image classification methods to separate green and non-green pixels in DCI, some supervised methods such as the maximum likelihood (ML), the minimum distance (MD), the Mahalanobis distance (MH).

2. **Unsupervised Classification**

Unsupervised classifiers aggregate pixels with comparative spectral values into unique groups in accordance with predefined statistical criteria where by the classifier joins and reassigns spectral groups into more informative feature classes. for example the paralle-lepiped (PA), as unsupervised method, such as the K-means algorithm.

2.5.1 Maximum likelihood (ML) classifiers

maximum likelihood (ML) classifiers require prior knowledge and learning about cover features with respect to the statistical distribution of the information to be characterized for the distinctive classes utilized, information that is frequently hard to come [88].

The land use classification is based on multispectral supervised classification approach using (ML) classifier. The first step in the process of supervised classification is to locate the representative training sites for each land-cover type that can be identified in the image. There are many categories of land use, the main ones: agriculture, aquatic

vegetation, barren/open land, high-density urban area, low-density urban area, other vegetation (forest, parks, etc.) and water [89].

2.6 Climate and Weather

The weather in Babylon Governorate can be divided into the following four seasons [90] :

1. **Spring season:** starts from the beginning of March and extends to the end of May. The maximum temperature ranges between 14 - 30 °C, while the minimum temperature ranges between 4 - 17 °C
2. **Summer:** starts from the beginning of June and continues until the end of August. The maximum temperature that starts from 30 °C, and rises to reach its peak in mid-July to reach 40 °C, and drops again to reach at the end of the summer to 35 °C.
3. **Autumn:** The autumn season extends from the first of September, and extends until it reaches the end of November, and the maximum temperature in it starts from 30 °C, and decreases to the end of the season 18 °C, while the lowest temperature begins It has a temperature of 21 °C, and continues to drop until the weather starts to cool down, and the temperature becomes 5 °C.
4. **Winter:** The winter season extends from the beginning of December and continues until the end of February, and the maximum temperature in it starts from 13 °C, and decreases until the temperature at the coldest time becomes 8 °C, then temperatures start to rise until that It reaches 15 °C, while the lowest temperature starts from 3 Celsius, and decreases to reach 2 below zero, to be the lowest temperature during the year, and then rise again to reach at the end of winter to 5 °C [90].

Given the importance of climate and its impact on agricultural production, so we review some of its elements as follows [91]:

1. **Temperature**: Each plant has thermal limits called basic temperature limits for growth. Agricultural crops represented by minimum temperatures are known as zero growth, which is the degree at which the crop begins to grow, and the plant's growth may stop and be subjected to combustion or the occurrence of severe damages such as vegetative drought and wilting of the plant when the temperature rises.
2. **Rains**: Each plant or crop needs a specific amount of water necessary for its growth, for example barley needs (500 - 700) mm and corn (60 - 1100) mm.
3. **Wind** : The wind has a clear importance in transporting grain and the pollination process. It is also the plant exposed to damage and sabotage when the wind speed exceeds 25 km / hour.
4. **Sunlight**: Sunlight decomposes into a number of rays, and red light is the most important light belt in the formation of carbohydrates. When the intensity of light increases, the amount of organic matter increases and doubles the amount of organic matter within the process of photosynthesis and crops differ in their need for light. The number of light hours for plants is between (5 - 10) hours / day [90 , 91].

Chapter Three

Results and Experimental Work

3.1 Introduction

This chapter will show the methodology that was used to determine the change detection in vegetation and water covers of Babylon Governorate. In addition, the estimation of land cover of the study area was investigated by using the supervised classification technique. The related data to this project were obtained, through data processing by using the specialized software Arc- GIS Ver.10.3.

3.2 The Strategy of Work

The following flowchart (Figure (3 - 1)) explains the strategy of the work to calculate the change detection of Babylon Governorate between (2001, 2019) by using the Remote sensing and the GIS.

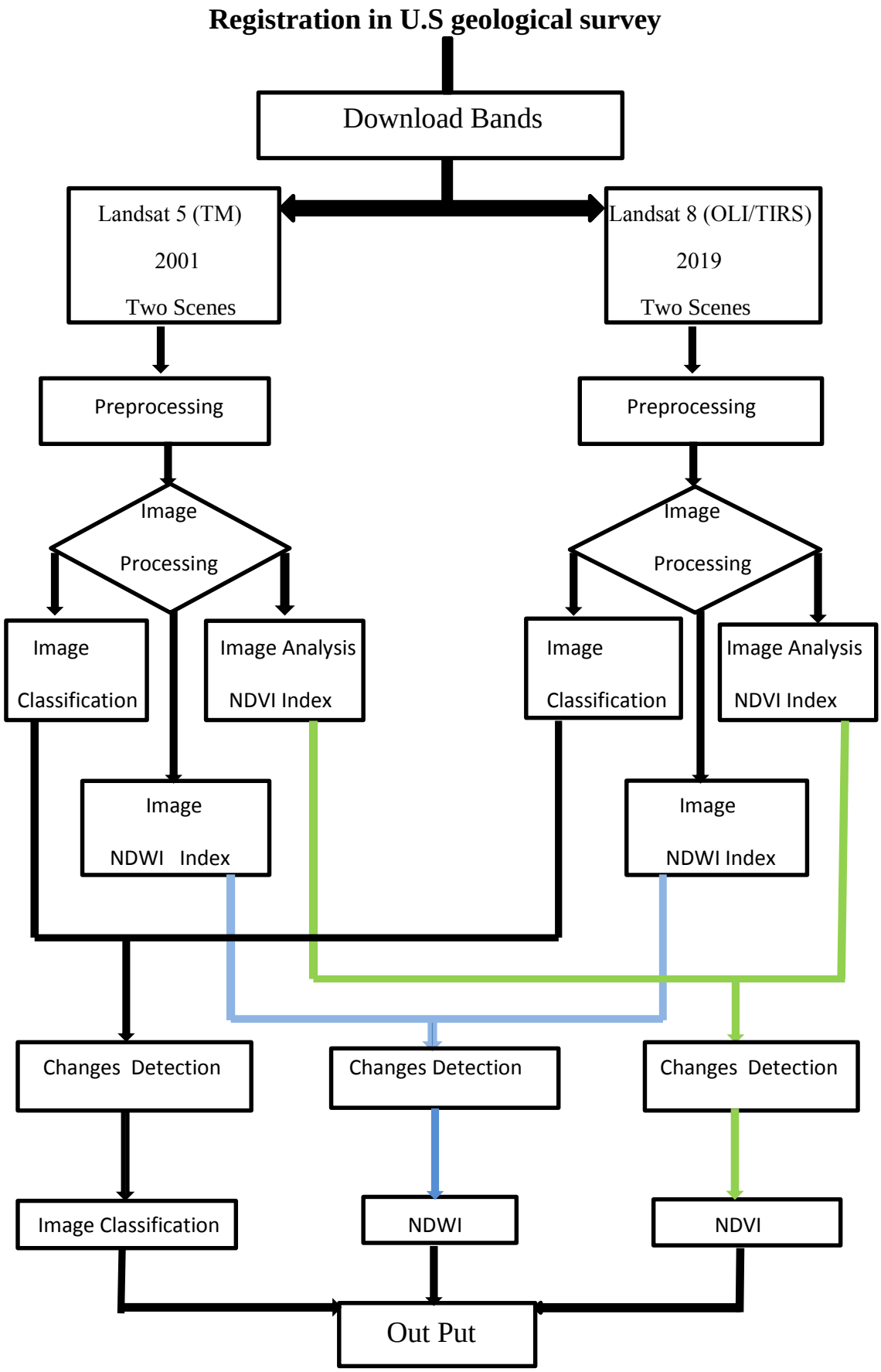

Figure (3 - 1): The mechanism of action that was used by the author (Source: Researcher work).

3.3 The Download of Images from Landsat 5 and Landsat 8

Two images were downloaded by using two satellites of Landsat satellites series, the first one was on March 19th 2001 by using Landsat 5, the second was on March 5th 2019 by using Landsat 8. Two satellites were used because the period of study that started before the lunching of Landsat 8 that was covered a study duration about 19 years. As shown in the following images, some of the Landsat 5 and Landsat 8 images were very cloudy, so it was difficult to monitor the vegetation growth. Thus, it is important to choose conditions with the lowest amounts of clouds and dusty particles to the download images good quality. The downloading of Landsat 8 images depends on the website (USGS).

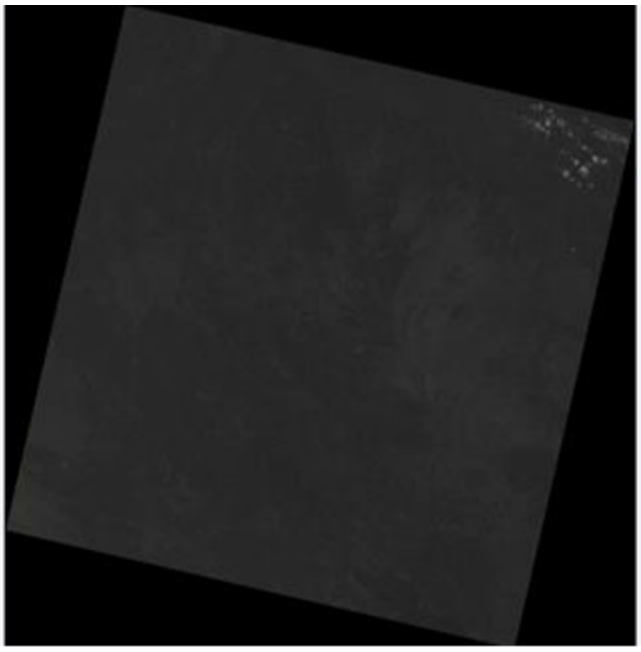

Figure (3 - 2): The B1 for Landsat 8 Row 37 Path 168 5/3/2019.

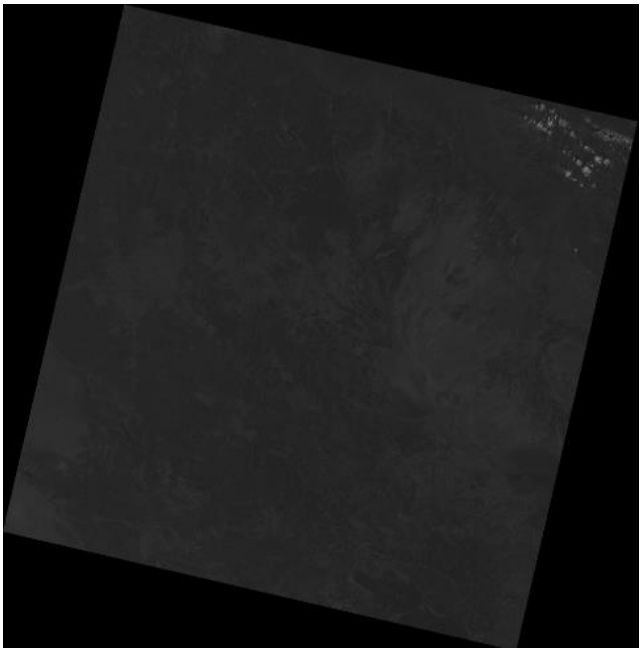

Figure (3 - 3): The B2 for Landsat 8 Row 37 Path 168 5/3/2019.

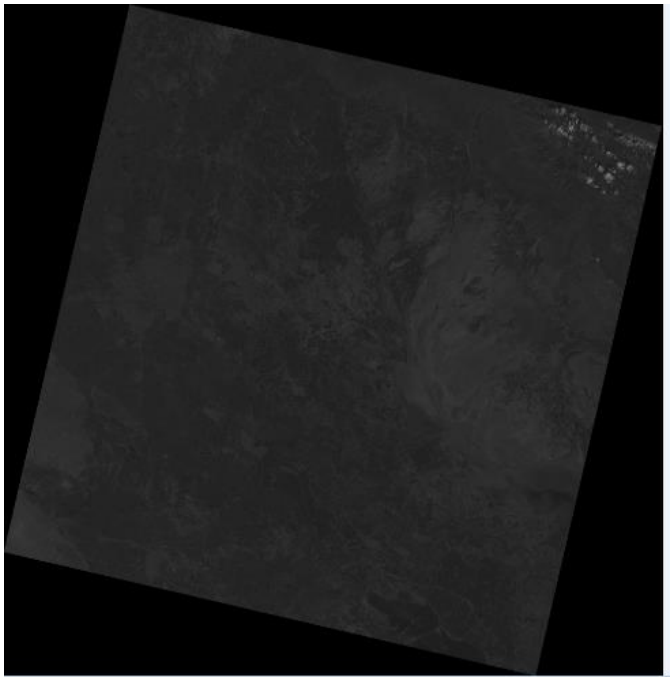

Figure (3 - 4): The B3 for the Landsat 8 Row 37 Path 168 5/3/2019.

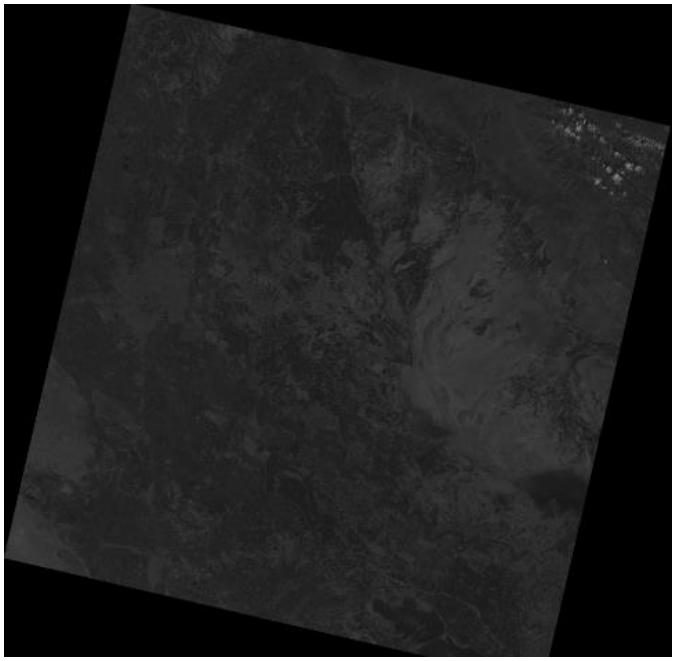

Figure (3 - 5): The B4 for Landsat 8 Row 37 Path 168 5/3/2019.

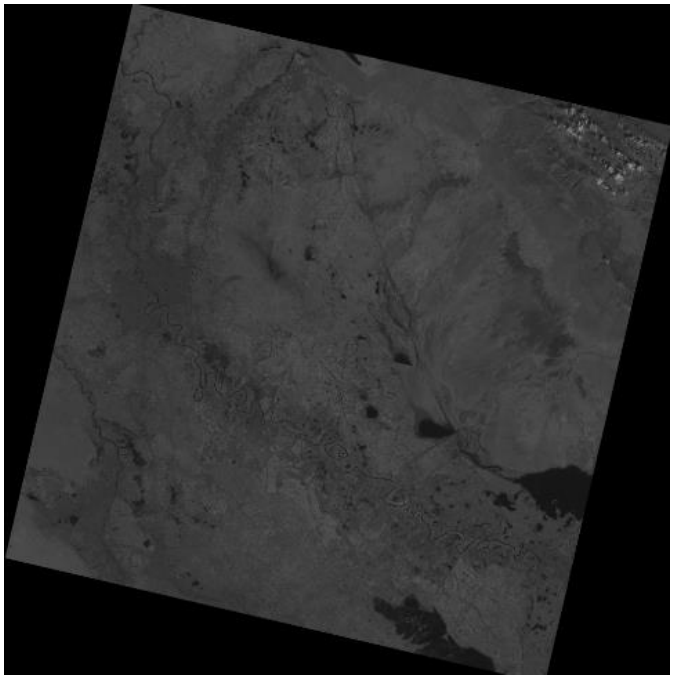

Figure (3 - 6): The B5 for Landsat 8 Row 37 Path 168 5/3/2019.

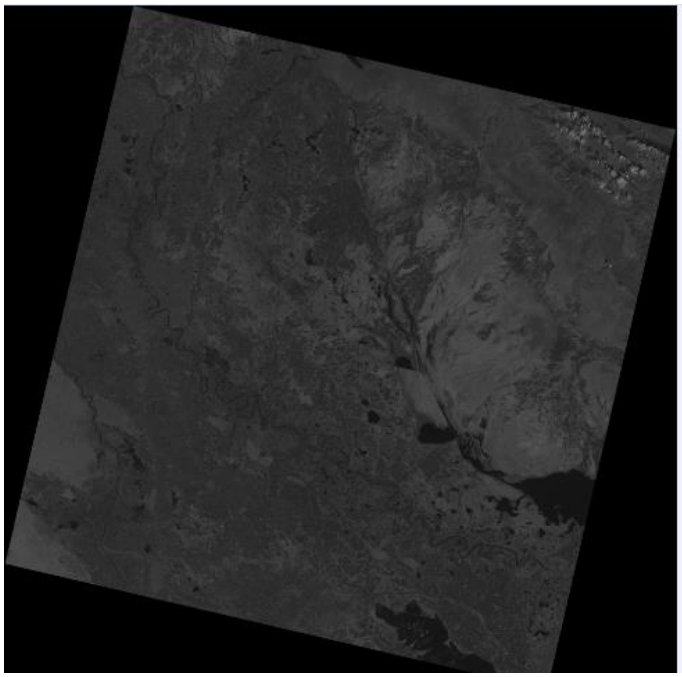

Figure (3 - 7): The B6 for Landsat 8 Row 37 Path 168 5/3/2019.

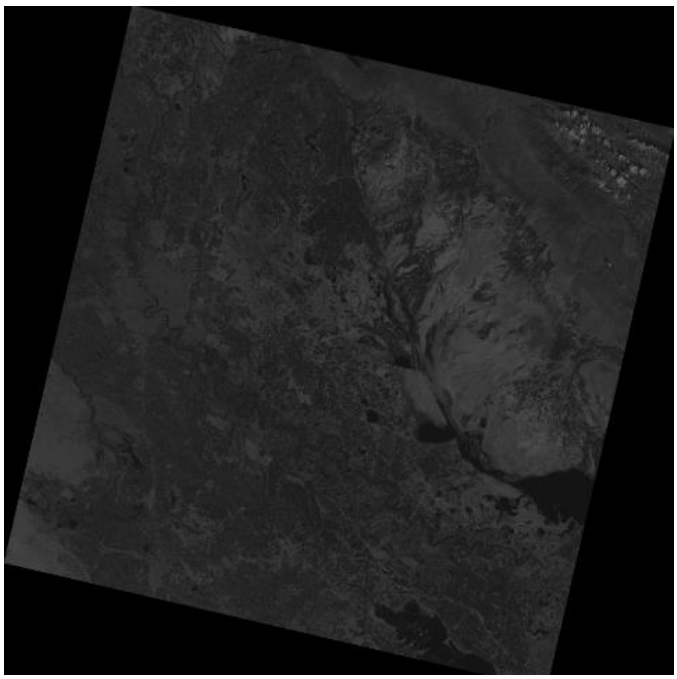

Figure (3 - 8): The B7 for Landsat 8 Row 37 Path 168 5/3/2019.

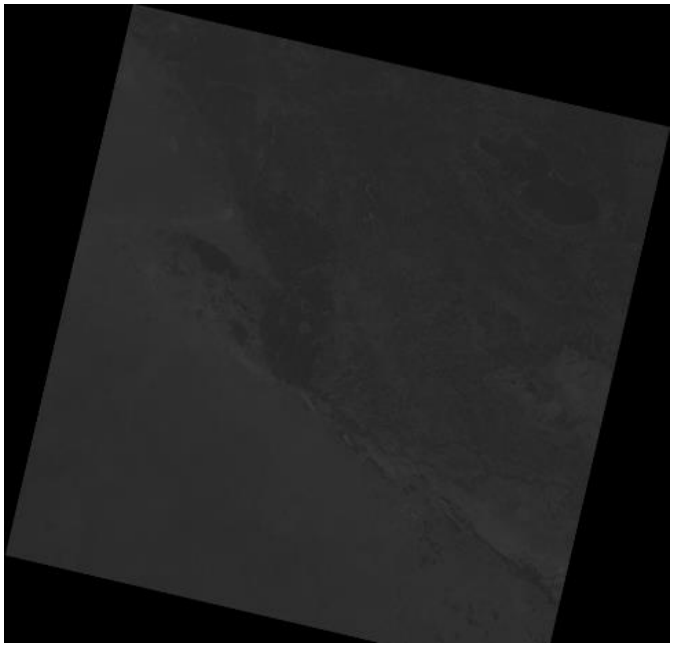

Figure (3 - 9): The B1 for Landsat 8 Row 38 Path 168 5/3/2019.

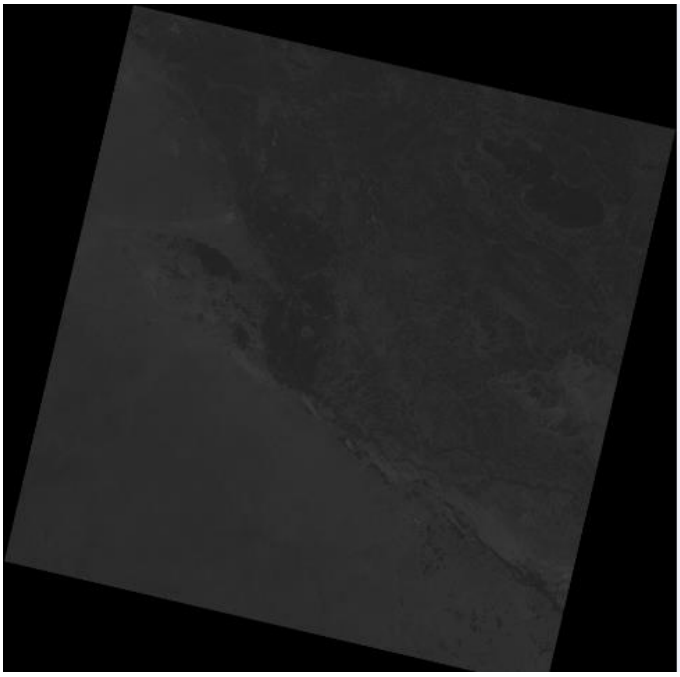

Figure (3 - 10): The B2 for Landsat 8 Row 38 Path 168 5/3/2019.

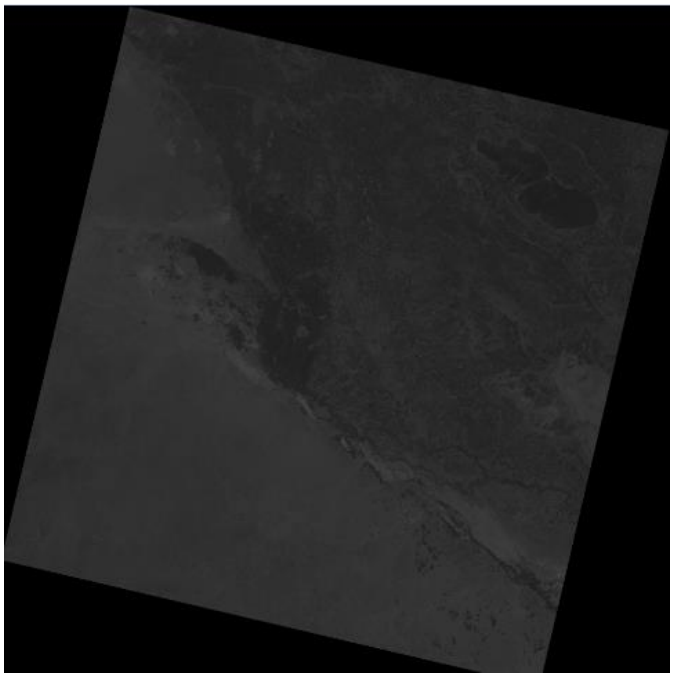

Figure (3 - 11): The B3 for Landsat 8 Row 38 Path 168 5/3/2019.

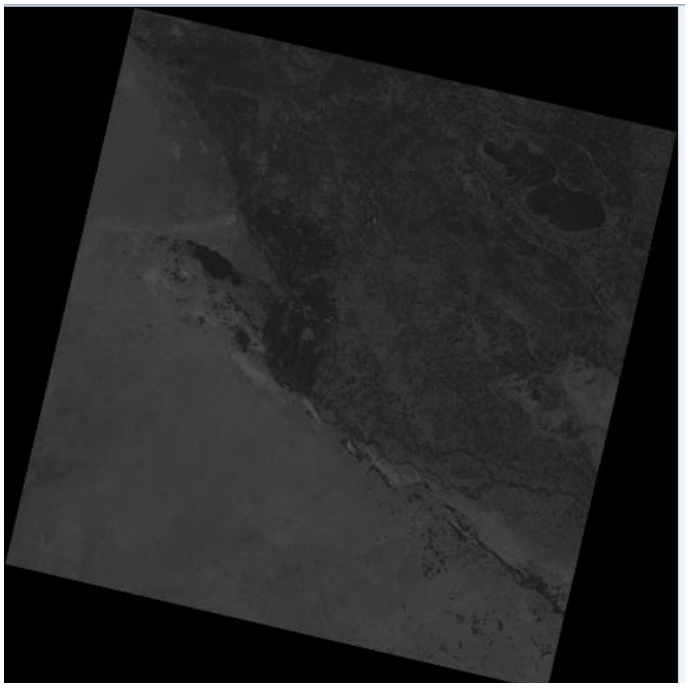

Figure (3 - 12): The B4 for Landsat 8 Row 38 Path 168 5/3/2019.

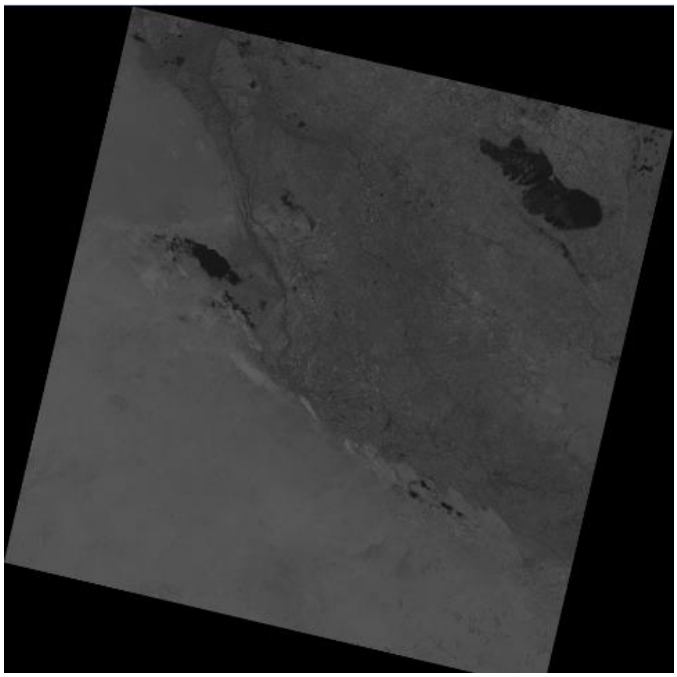

Figure (3 - 13): The B5 for Landsat 8 Row 38 Path 168 5/3/2019.

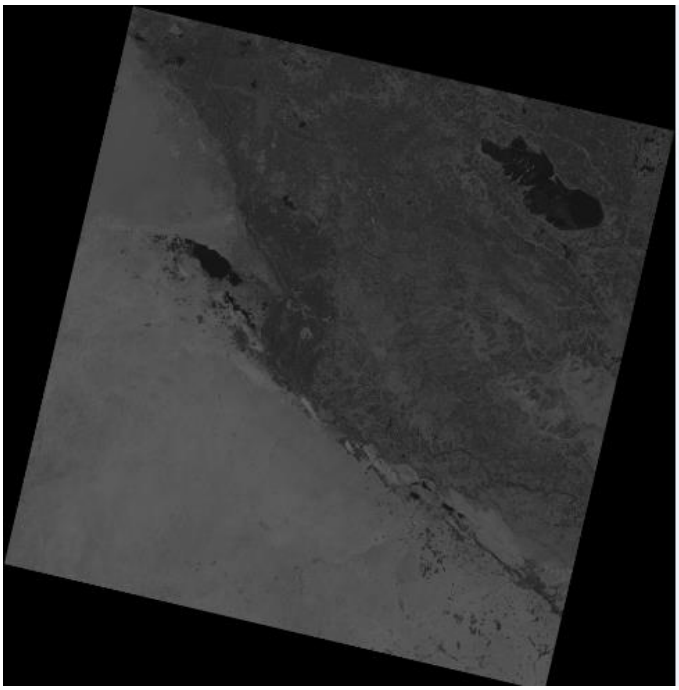

Figure (3 - 14): The B6 for Landsat 8 Row 38 Path 168 5/3/2019.

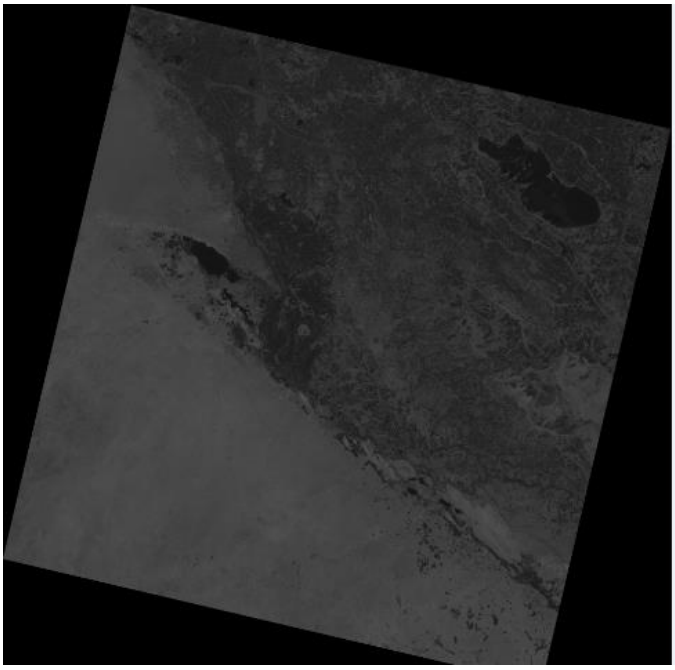

Figure (3 - 15): The B7 for Landsat 8 Row 38 Path 168 5/3/2019.

Note : that no scenes for Landsat 5 were remembered, due to the clarity of the idea through the satellite Landsat8 because of the large number of results offered.

3.4 Clipping for the Imageries

After downloading images by Landsat 5 and Landsat 8, with two scenes for each year of the study duration (2001, 2019), the clipping process was applied for each individually band. Each clip represents the one of the two part of the Babylon Governorate . This process is regarded one of the Pre-processing on the download band, the following section (3.4.1, 3.4.2) and figures show results that produced from the later process.

3.4.1 A Scene 1 Landsat 5

The following figuers represenred the clipping of Babylon bondaries from download bands for landsat 5 scene1:

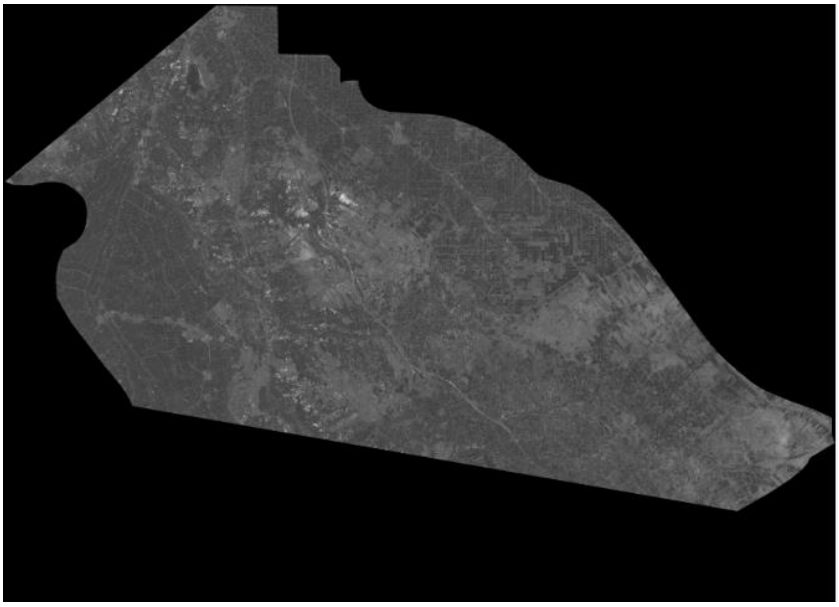

Figure (3 - 16): The B1 for Landsat 5 Row 37 Path 168 for the upper part of Babylon Governorate 19/3/2001.

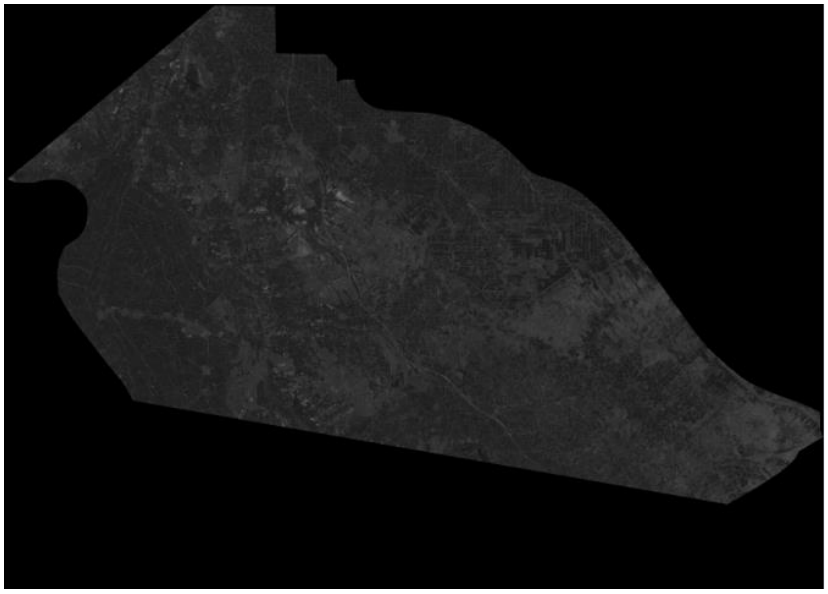

Figure (3 - 17): The B2 for Landsat 5 Row 37 Path 168 for the upper part of Babylon Governorate 19/3/2001.

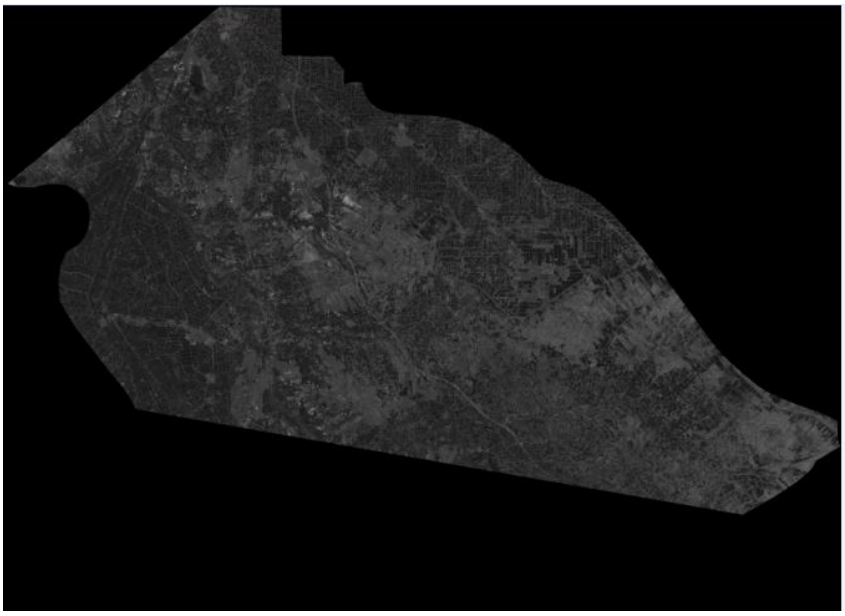

Figure (3 - 18): The B3 for Landsat 5 Row 37 Path 168 for the upper part of Babylon Governorate 19/3/2001.

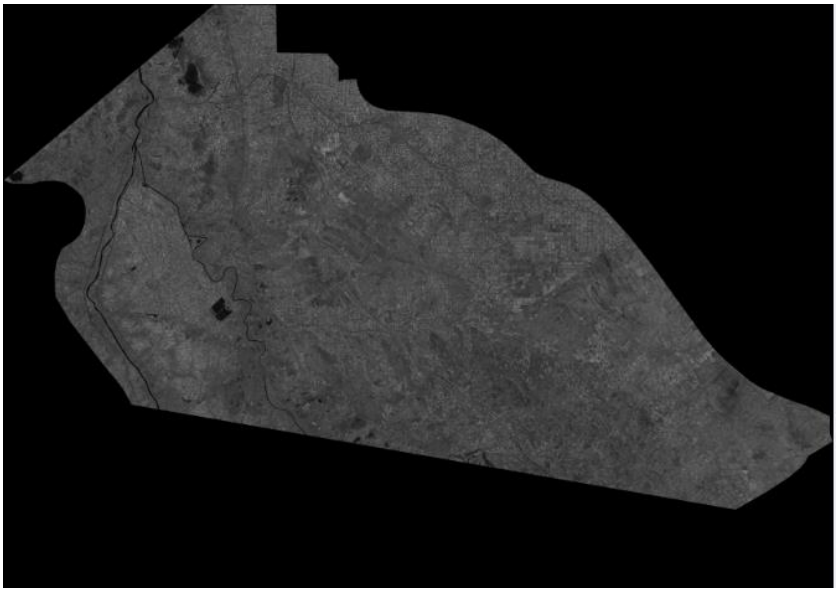

Figure (3 - 19): The B4 for Landsat 5 Row 37 Path 168 for the upper part of Babylon Governorate 19/3/2001.

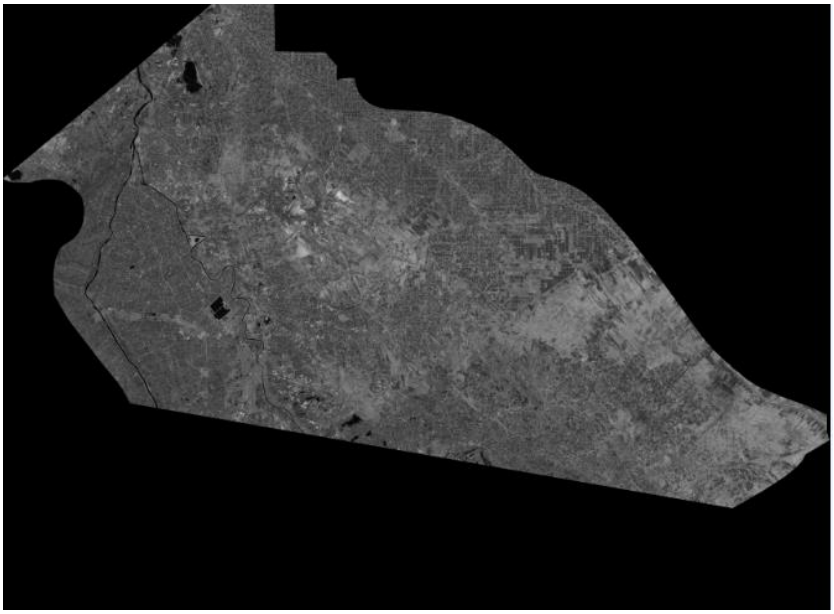

Figure (3 - 20): The B5 for Landsat 5 Row 37 Path 168 for the upper part of Babylon Governorate 19/3/2001.

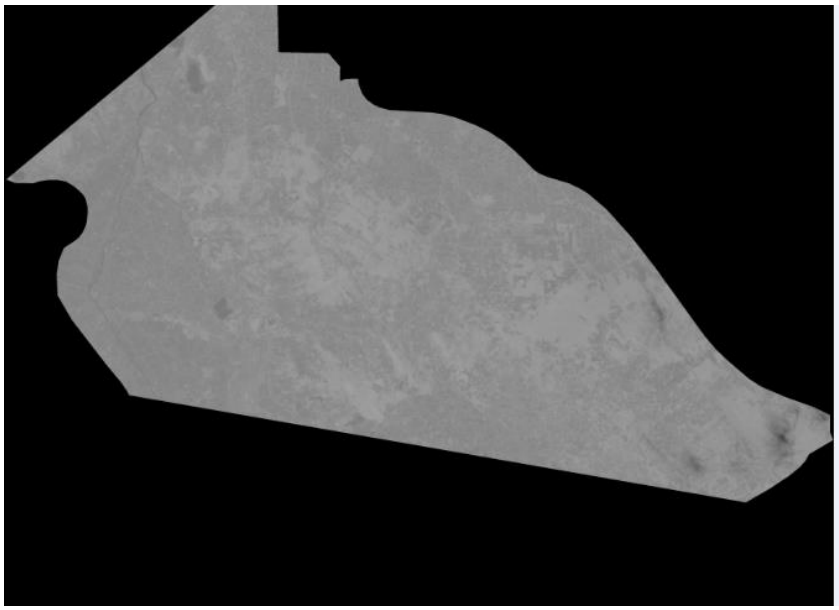

Figure (3 - 21): The B6 for Landsat 5 Row 37 Path 168 for the upper part of Babylon Governorate 19/3/2001.

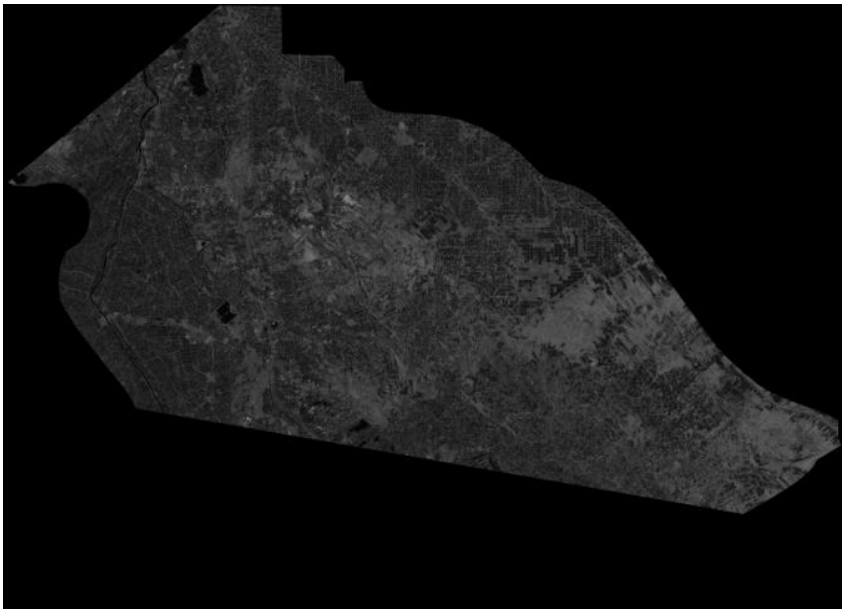

Figure (3 - 22): The B7 for Landsat 5 Row 37 Path 168 for the upper part of Babylon Governorate 19/3/2001.

3.4.2 A Scene 2 Landsat 5

The following figuers represented the clipping Babylon's bondaries from download bands of landsat 5 scene 2.

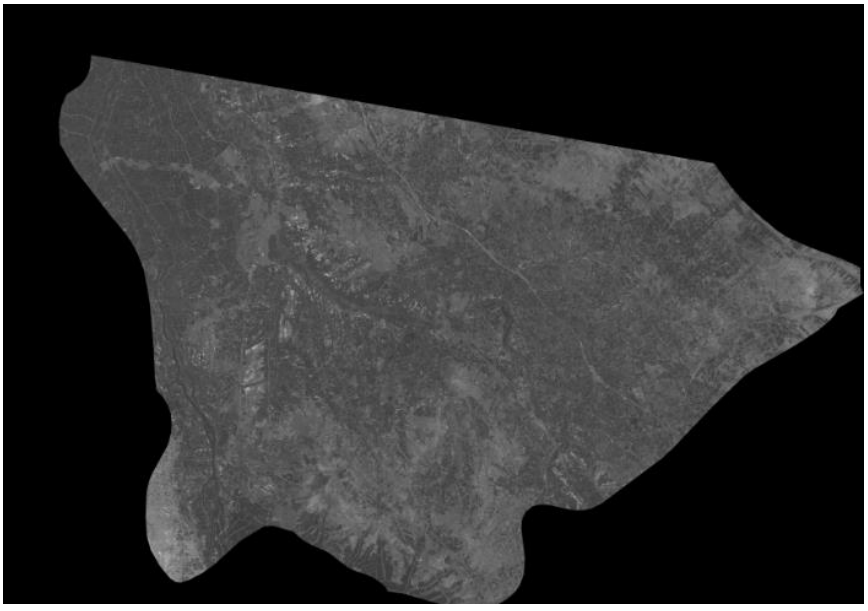

Figure (3 - 23): The B1 for Landsat 5 Row 38 Path 168 for the lower part of Babylon Governorate 19/3/2001.

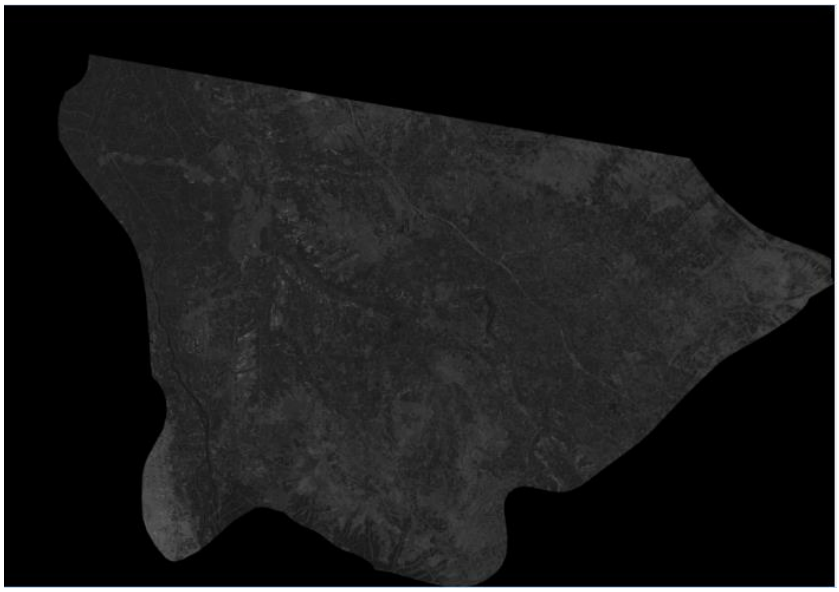

Figure (3 - 24): The B2 for Landsat 5 Row 38 Path 168 for the lower part of Babylon Governorate 19/3/2001.

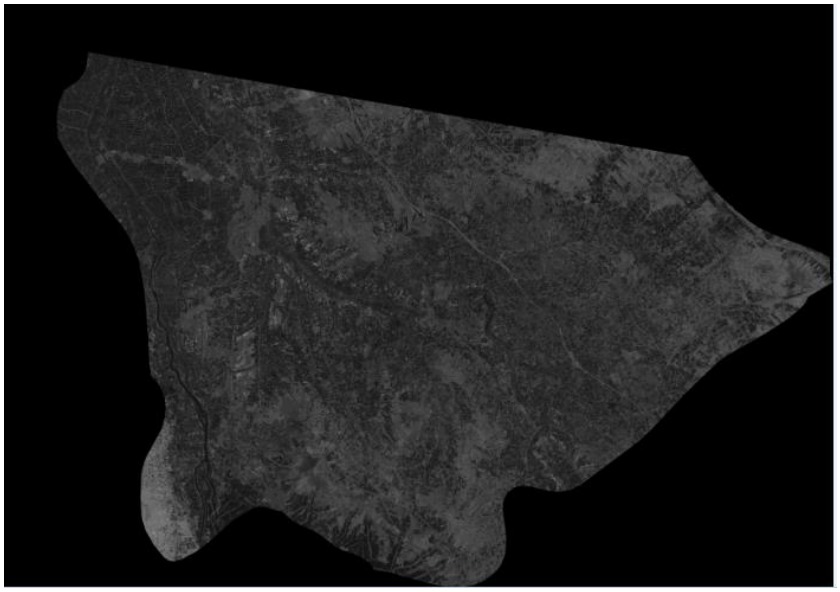

Figure (3 - 25): The B3 for Landsat 5 Row 38 Path 168 for the lower part of Babylon Governorate 19/3/2001.

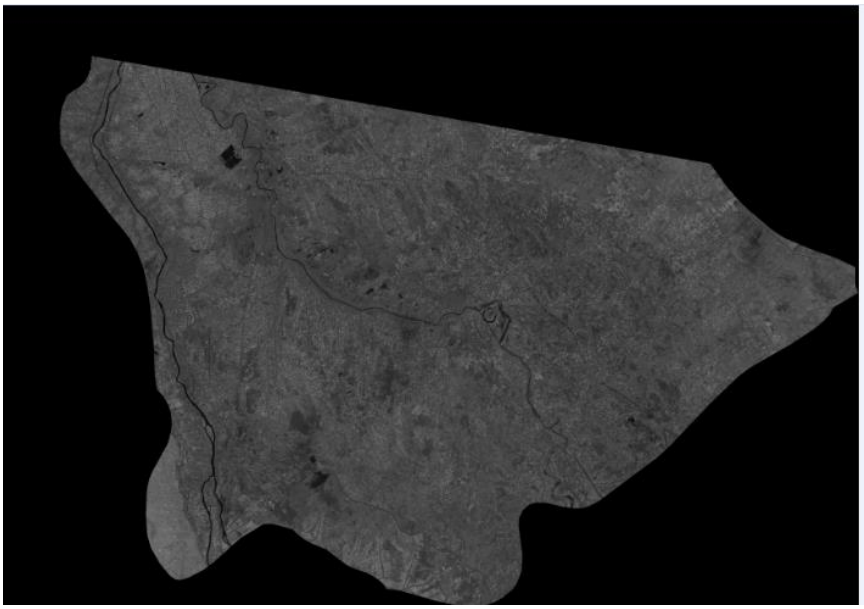

Figure (3 - 26): The B4 for Landsat 5 Row 38 Path 168 for the lower part of Babylon Governorate 19/3/2001.

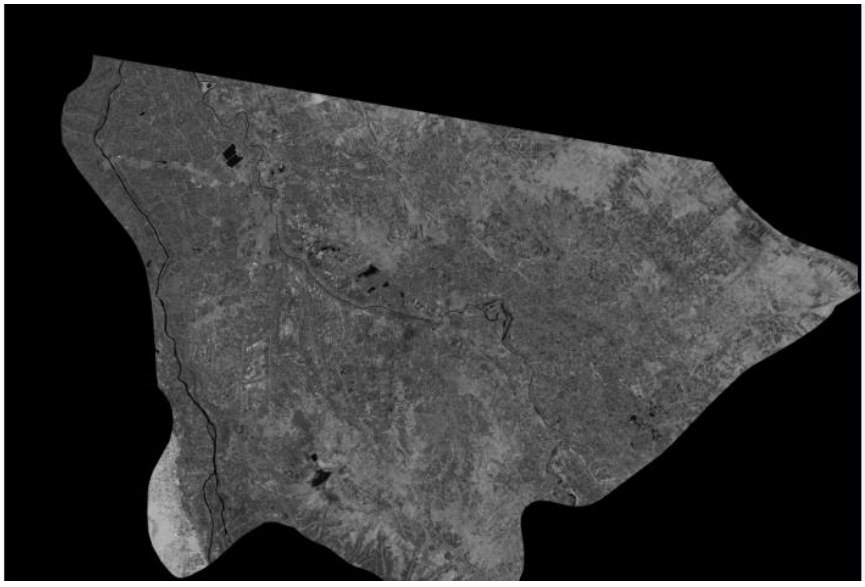

Figure (3 - 27): The B5 for Landsat 5 Row 38 Path 168 for the lower part of Babylon Governorate 19/3/2001.

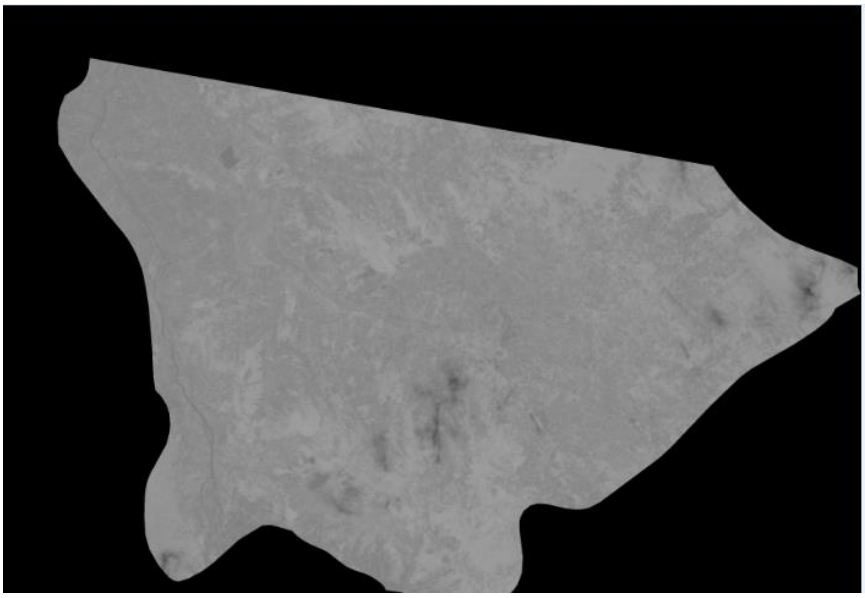

Figure (3 - 28): The B6 for Landsat 5 Row 38 Path 168 for the lower part of Babylon Governorate 19/3/2001.

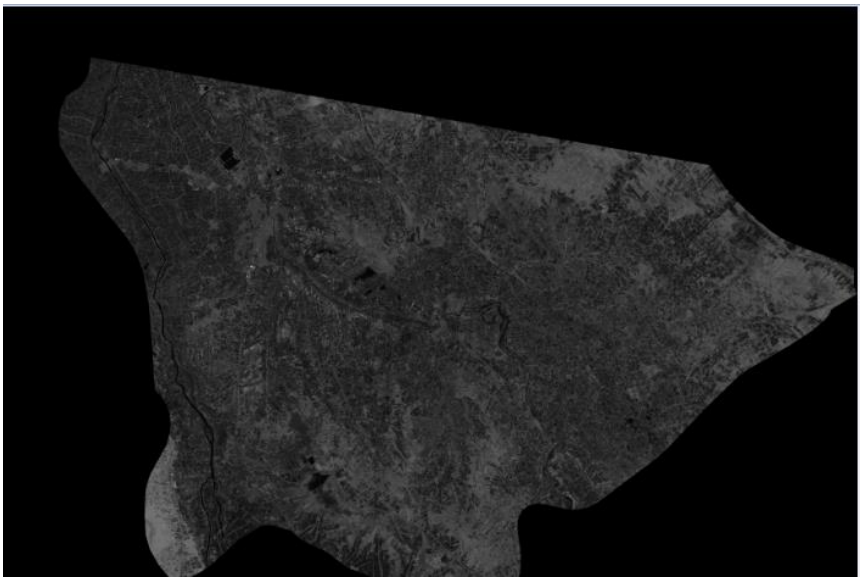

Figure (3 - 29): The B7 for Landsat 5 Row 38 Path 168 for the lower part of Babylon Governorate 19/3/2001.

The others scenes: scenes 1 and 2 from the Landsat8 were not mentioned here because the huge numbers of images. All the later images were analyzed in the same procedure that used to analyzed scene 1 and 2 from Landsat 5 (Figure (3 - 16) - Figure (3 -29)).

3.5 Mosaic for the Imageries

After downloading images by Landsat 5 and Landsat 8, with two scenes for each year of the study duration (2001, 2019), the mosaic process was applied for each couple of imageries in each year, in order to get a real scene of the study area for the Babylon Governorate.

3.5.1 Mosaic for the Band Landsat 5

The following figures represented the Mosaic process of two part clipping of band to Babylon Governorate for the Landsat 5.

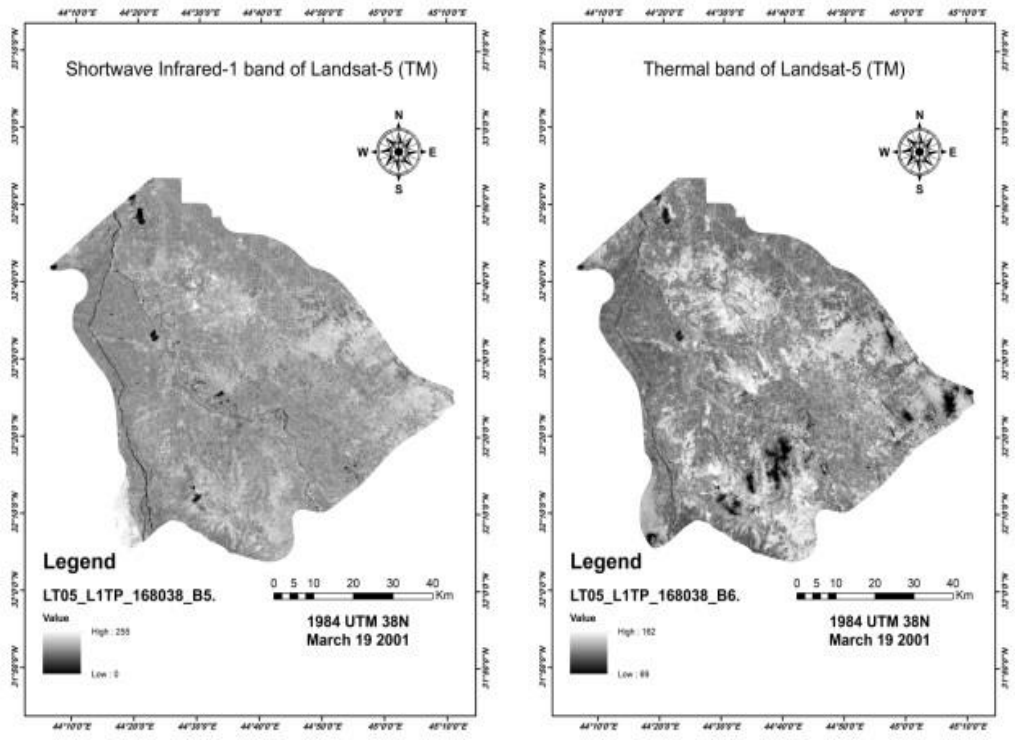

(a) **(b)**

Figure (3 - 30): The Mosaic process of two part clipping of the bands: (a) shows shortwave infrared-1 band. (b) represents thermal band. Both for the Babylon Governorate of the Landsat 5 in 2001.

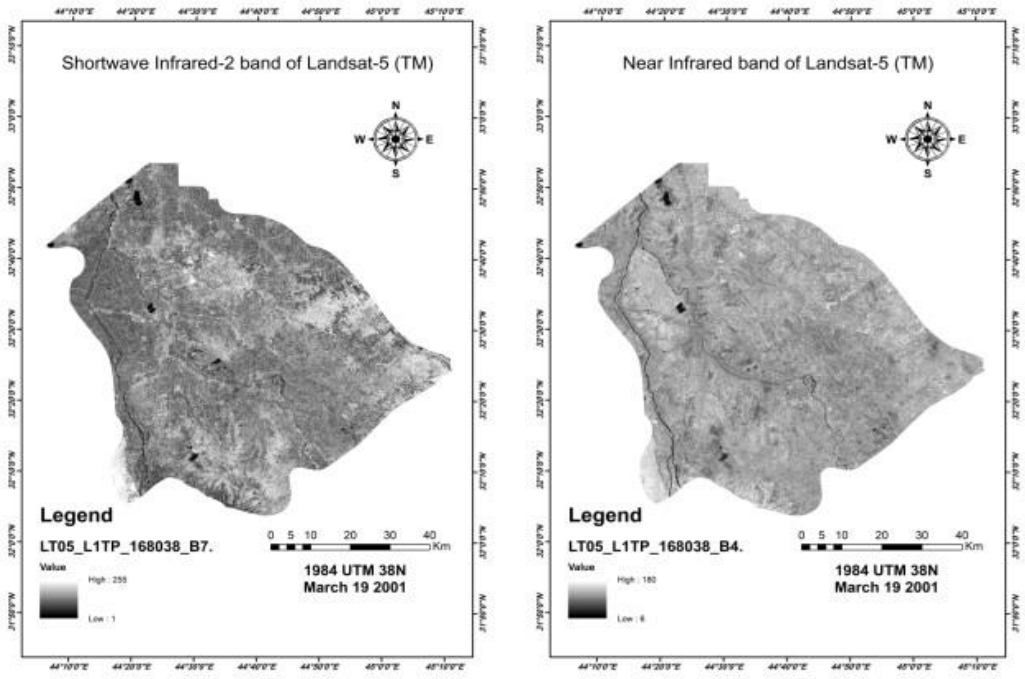

(a) **(b)**

Figure (3 - 31): The Mosaic process of two part clipping of the bands: (a) shows shortwave infrared-2 band. (b) represents Near infrared band. Both for the Babylon Governorate of the Landsat 5 in 2001.

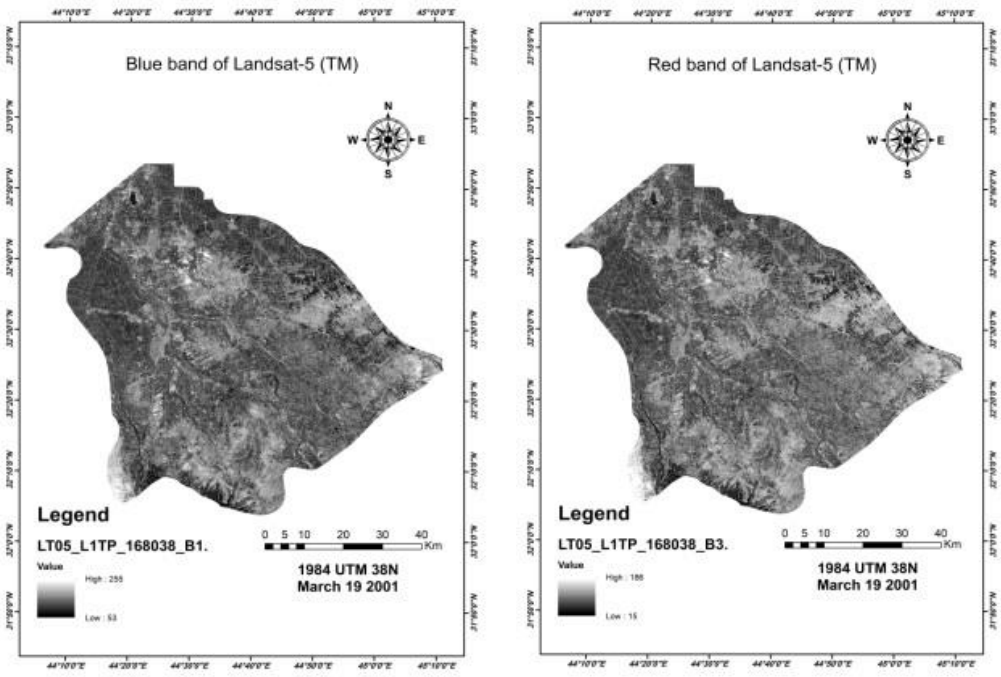

(a) **(b)**

Figure (3 - 32): The Mosaic process of two part clipping of the bands: (a) shows Blue band. (b) represents Red band. Both for the Babylon Governorate of the Landsat 5 in 2001.

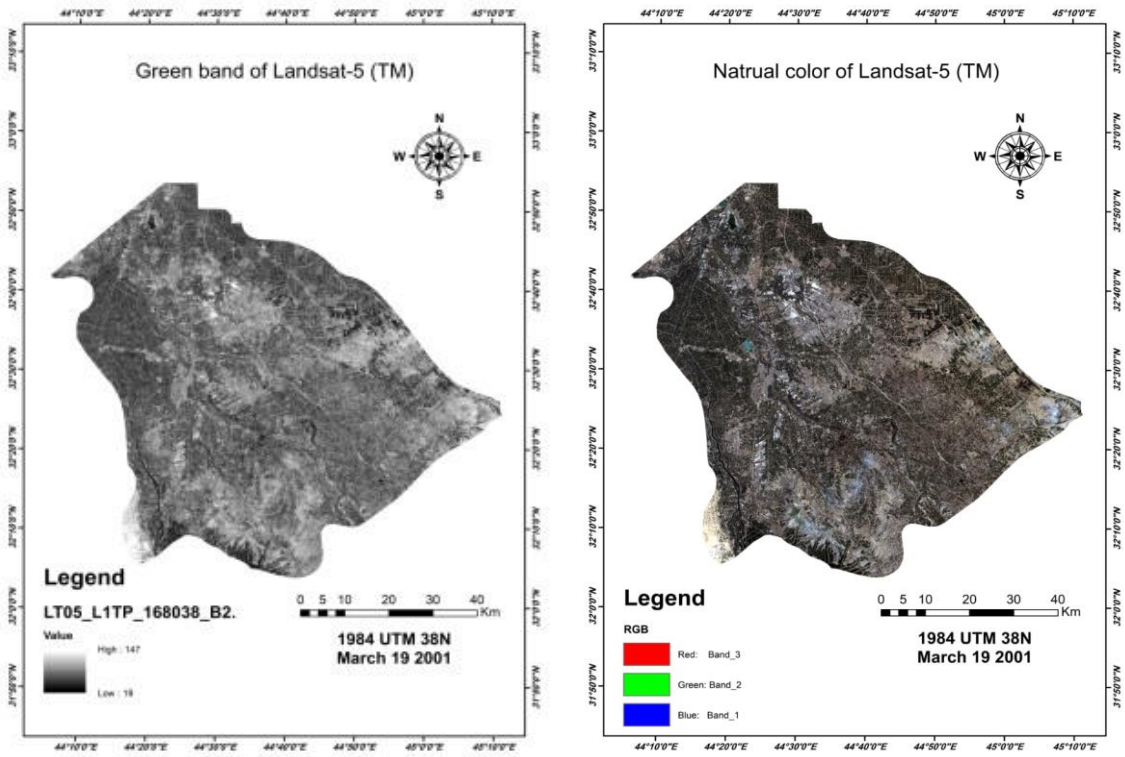

(a) **(b)**

Figure (3 - 33): The Mosaic process of two part clipping of the bands: (a) shows Green band. (b) represents Natural color. Both for the Babylon Governorate of the Landsat 5 in 2001.

3.5.2 Mosaic for the Band Landsat 8

The following figures represented the Mosaic process of two part clipping of band to the Babylon Governorate for the Landsat 8.

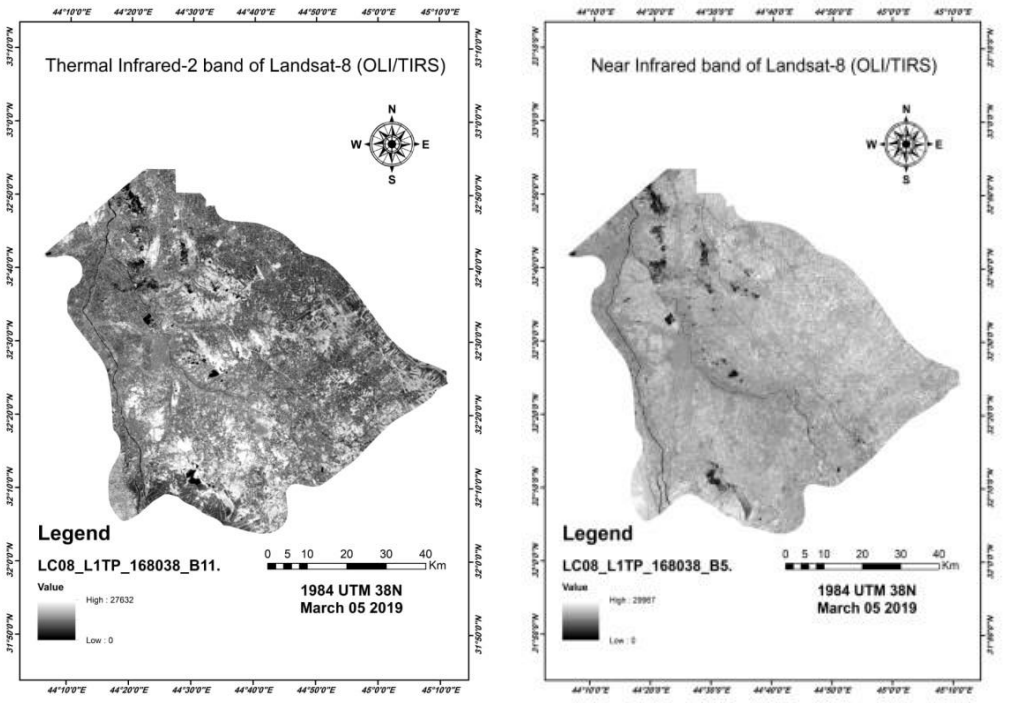

(a) **(b)**

Figure (3 - 34): The Mosaic process of two part clipping of the bands: (a) shows thermal infrared-2 band. (b) represents near infrared band. Both for the Babylon Governorate of the Landsat 8 in 2019.

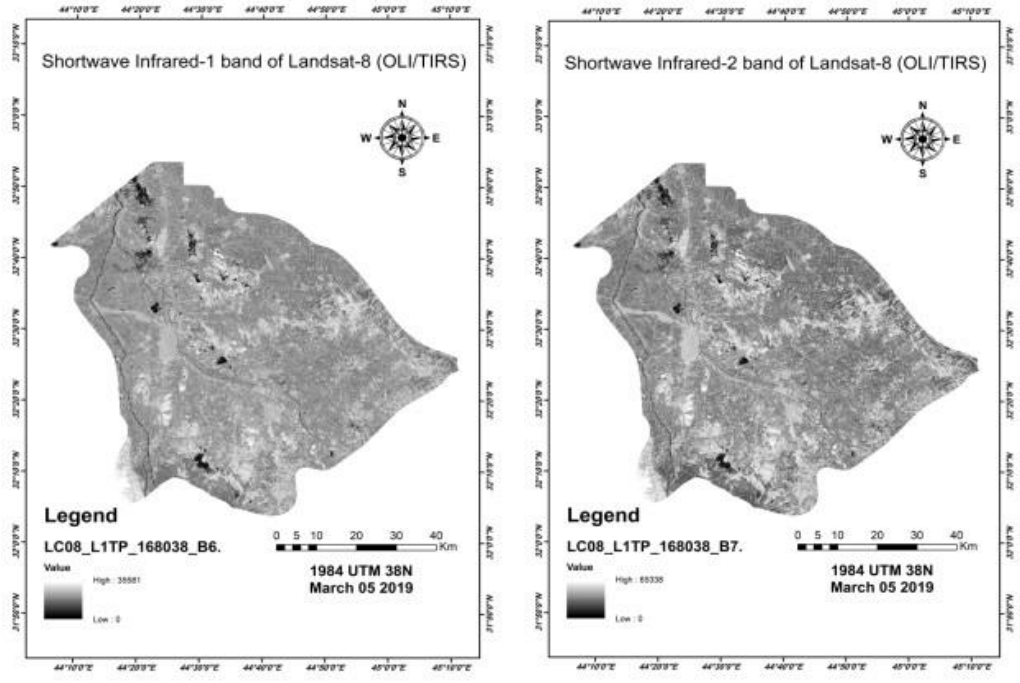

(a) **(b)**

Figure (3 - 35): The Mosaic process of two part clipping of the bands: (a) shows the shortwave infrared-1 band. (b) represents the shortwave infrared-2 band. Both for the Babylon Governorate of the Landsat 8 in 2019.

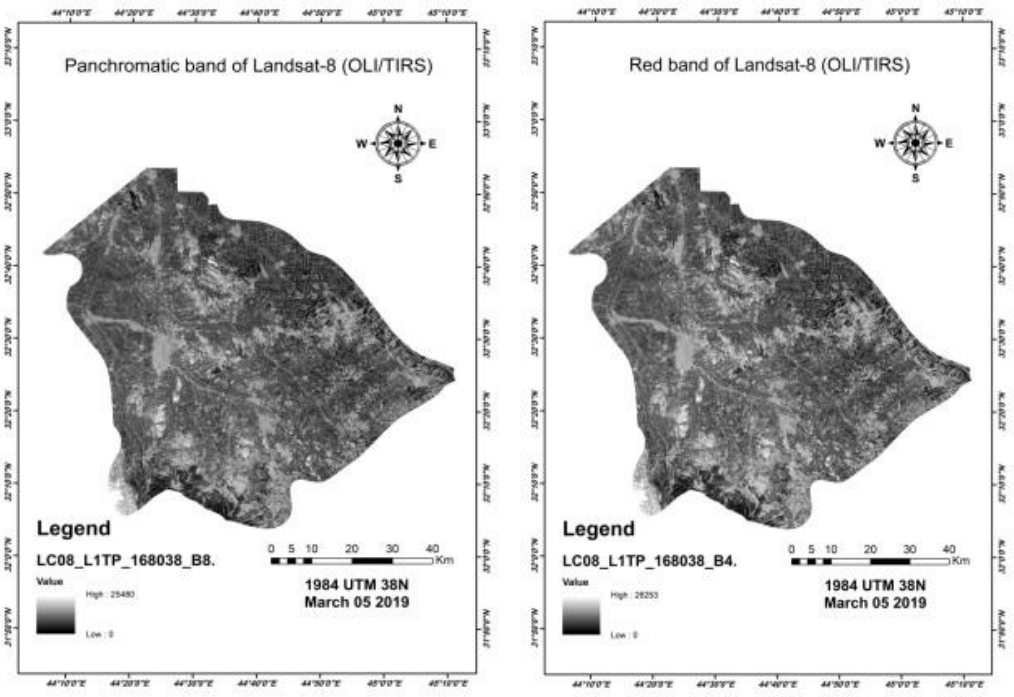

(a) **(b)**

Figure (3 - 36): The Mosaic process of two part clipping of the bands: (a) shows the panchromatic band. (b) represents the red band. Both for the Babylon Governorate of the Landsat 8 in 2019.

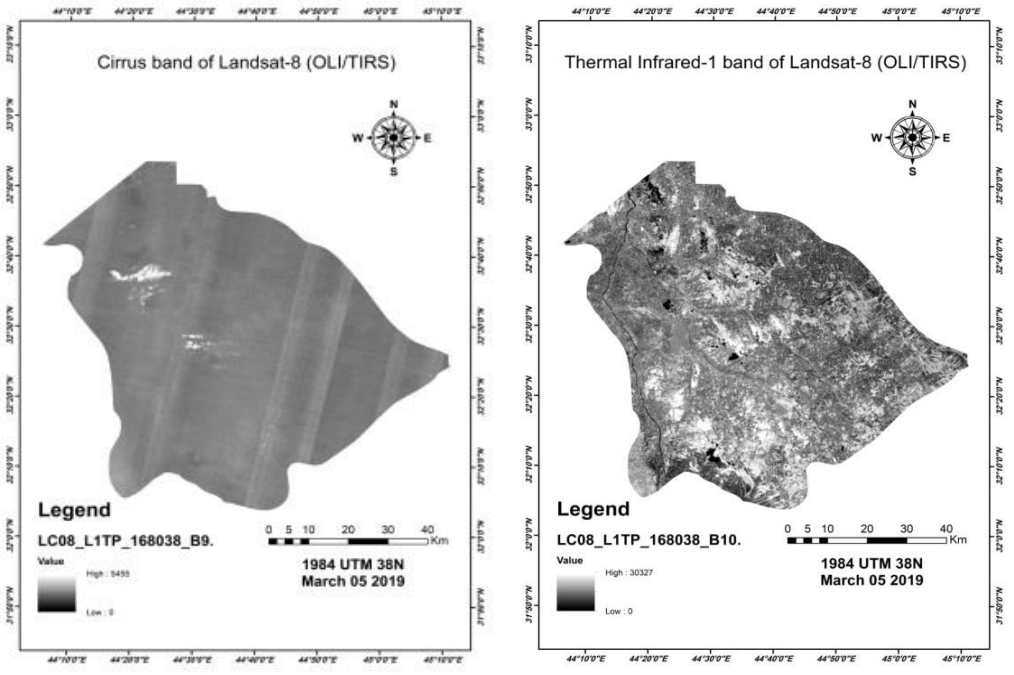

(a) **(b)**

Figure (3 - 37): The Mosaic process of two part clipping of the bands: (a) shows the cirrus band. (b) represents the thermal infrared-1 band. Both for the Babylon Governorate of the Landsat 8 in 2019.

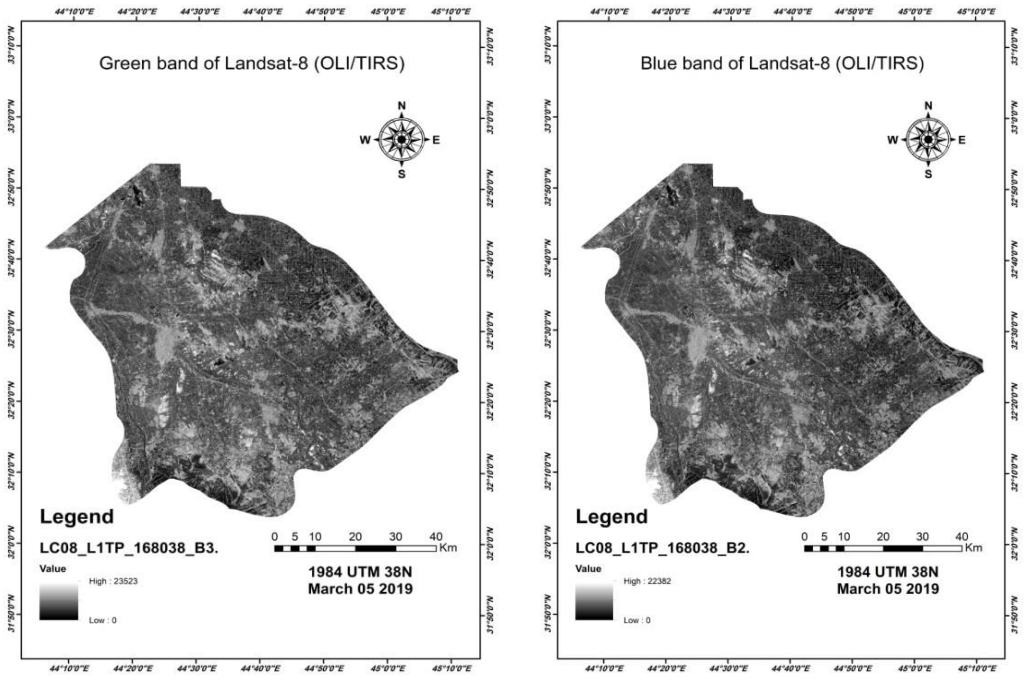

(a) **(b)**

Figure (3 - 38): The Mosaic process of two part clipping of the bands: (a) shows the green band. (b) represents the blue band. Both for the Babylon Governorate of the Landsat 8 in 2019.

3.6 Calculation of the NDVI for the Studied Area from Landsat 5

The results of the NDVI values for the Babylon Governorate were estimated by using the downloaded data of the Landsat 5 satellite for the first date (19/3/2001). After the mosaic process was done for each year scenes, the values of the NDVI was calculated by applying the equation (2) in chapter 2 in the Arc GIS program.

Figures (3 - 39) and (3 - 40) contain a classification of the NDVI values from Landsat 5 satellite. The NDVI values were extracted for each date imagery, where the extracted values represent the density of the vegetation cover. For Landsat 5 satellite, the red and NIR bands represented by numbers (3) and (4) respectively. From the special equation to calculate the NDVI. From figure (3 - 40 - b), the green

regions indicate the regions that covered with vegetation, and with a suitable condition for agriculture, while the white regions indicate the areas with no vegetation and with poor agriculture conditions.

Table (3-1) states the statistical analysis of the supervised classification technique for study area of Babylon, and the change was measured using the NDVI indicator for year 2001. The area of vegetation cover for year 2001 is 192191310 m^2 which is 36 % of the total area, and the area without vegetation cover is estimated at 335856960 m^2 with a percentage of 64 % of total area.

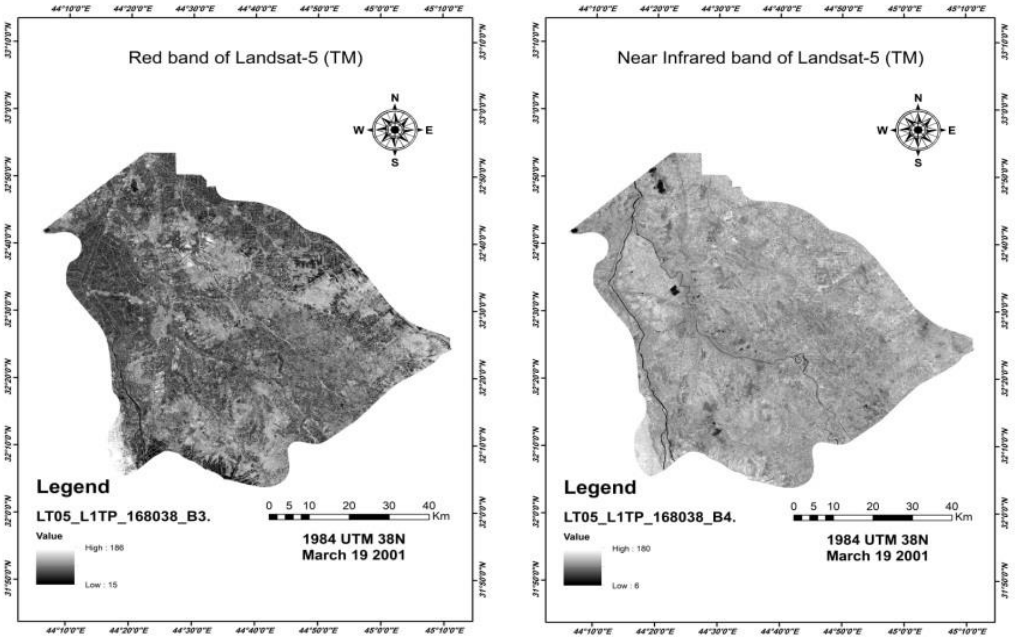

(a) **(b)**

Figure (3 - 39): The Red band (a) and Near infrared band (b) for Babylon Governorate by Landsat5 : March 2001.

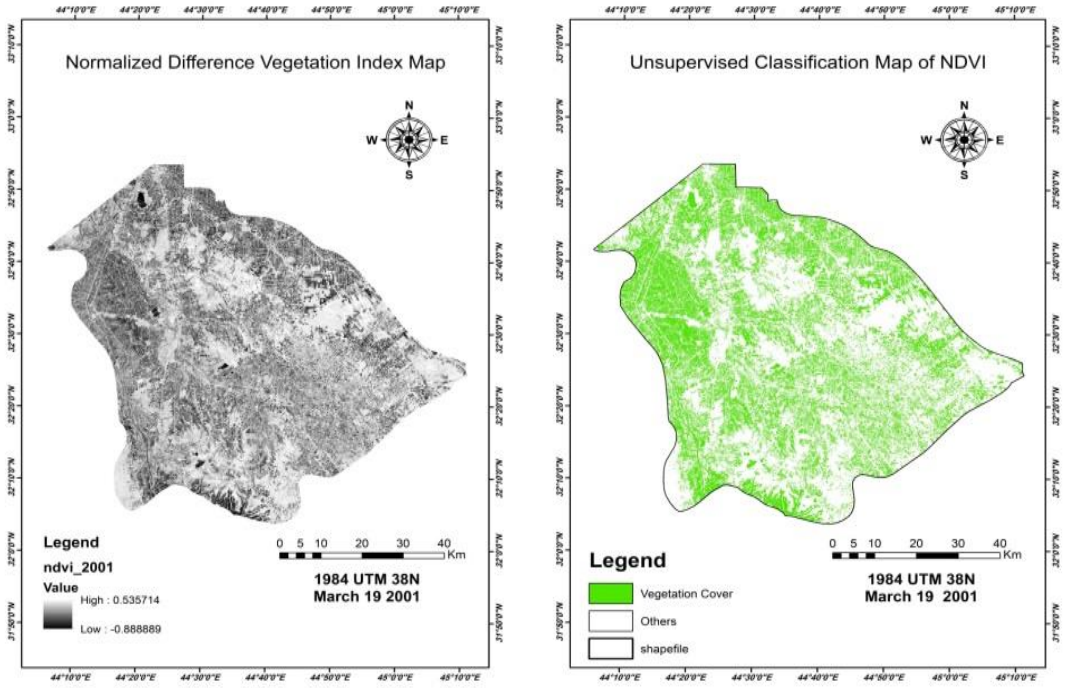

(a) **(b)**

Figure (3 - 40): (a) The results of the NDVI in 2001 and (b) shows the results of unsupervised classification of results the NDVI 2001 image.

Table (3 - 1): The statistical analysis that determined by applied the NDVI for Babylon Governorate (19/3/2001).

Date	Type	Count	Area (m^2)	MIN	MAX	Range	Mean	STD
2001/3/19	Vegetation	2135459	192191310	- 0.88888	- 0.69	0.947712	- 0.09472	±0.107445
	Non-vegetation	3731744	335856960	0.05936	- 0.8	0.476354	0.18947	±0.059172

Where:

$$\text{Mean} = \text{Arithmetic mean} = \frac{sum\ of\ values}{number\ of\ values} \quad (11)$$

$$\text{STD} = \text{Standard deviation} = \sqrt{\frac{sum\ (values - mean)^2}{number\ of\ values}} \quad (12)$$

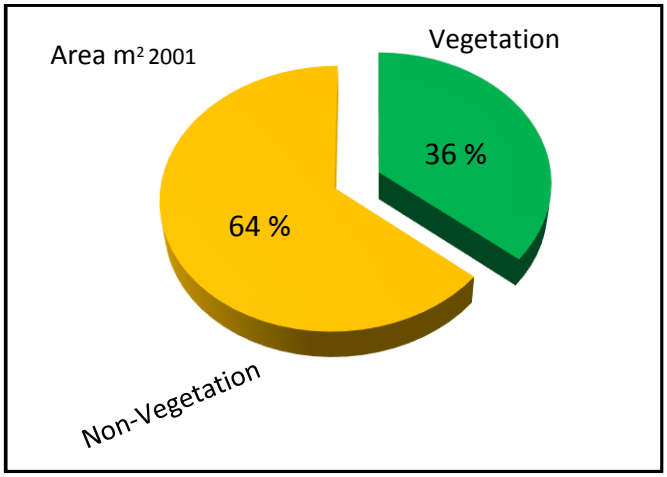

Figure (3 - 41): The greenness ratio for the year 2001.

3.7 Calculation of the NDVI for the Studied Area from Landsat 8

In order to calculate the NDVI values for the date (3/5/2019), the Landsat 8 was applied to extract year 2019 imagery with two scenes. After the mosaic process is done for each year scenes, the values of the NDVI was calculated by applying equation (3) in chapter 2 in the Arc GIS program.

Figures (3 - 42) and (3 - 43) contain a classification of the NDVI values from Landsat 8 satellite. The extracted NDVI values represent the density of the vegetation cover. For Landsat 8 satellite, the red and NIR bands represented by numbers (4) and (5) respectively. As well, in figure (3 - 43 - b), the green regions indicate the regions that covered with vegetation, and with a suitable condition for agriculture, while the white regions represent the areas with no vegetation and with poor agriculture.

Table (3 - 2) states the statistical analysis of the supervised classification technique for study area of Babylon, and the change was measured using the NDVI indicator for year 2019. The area of

vegetation cover for year 2019 is 216833220 m^2 which is about 41 % of the total area, and the area without vegetation cover is estimated ≈ 311228370 m^2 with a percentage of 59 % from the total area. These results lead to the fact that a clear increase in the area of vegetation, which is highest recorded in the controlled classification process for the study area. This shows that the NDVI process is accurate.

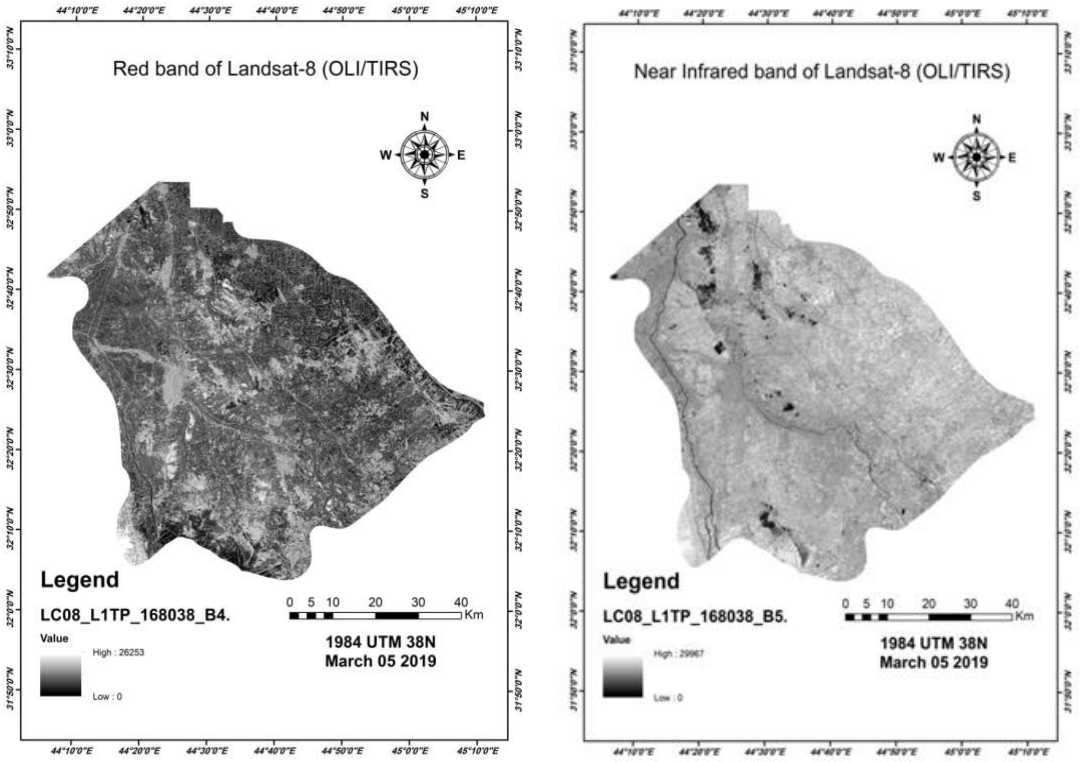

(a) **(b)**

Figure (3 - 42): The Red band (a) and Near infrared band (b) for Babylon Governorate by Landsat8 in March 2019.

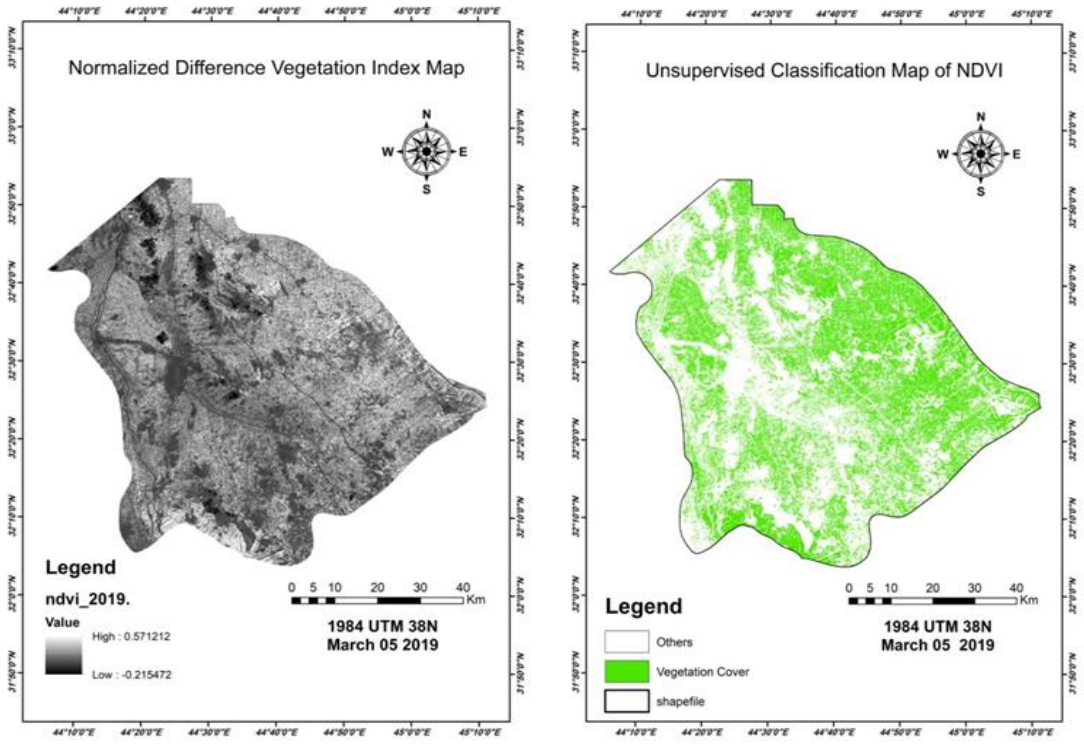

(a) **(b)**

Figure (3 - 43): (a) The results of the NDVI (2019) and (b) the results of unsupervised classification of results the NDVI (2019) image.

Table (3 - 2): The statistical analysis by applied the NDVI for Babylon Governorate (5/3/2019).

Date	Type	Count	Area (m^2)	MIN	MAX	Range	Mean	STD
2019/3/5	**Vegetation**	2409258	216833220	0.23610	- 1.03	0.335112	0.34501	±0.072648
	Non-vegetation	3458093	311228370	- 0.21547	- 0.73	0.451573	0.13230	±0.059376

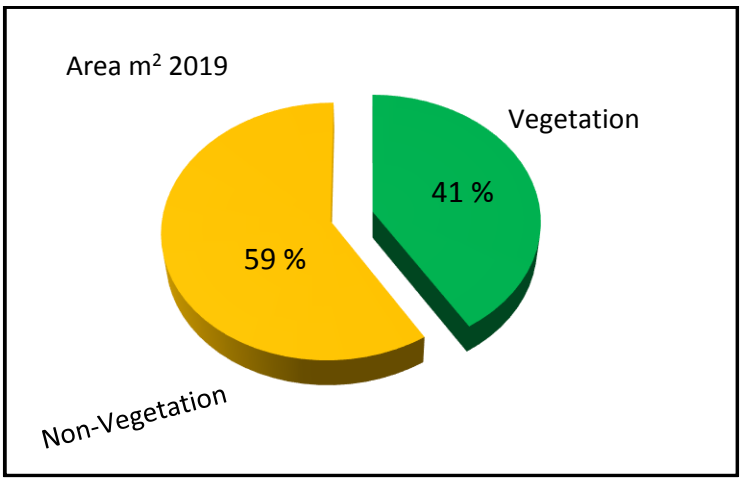

Figure (3 - 44): The greenness ratio for the year 2019.

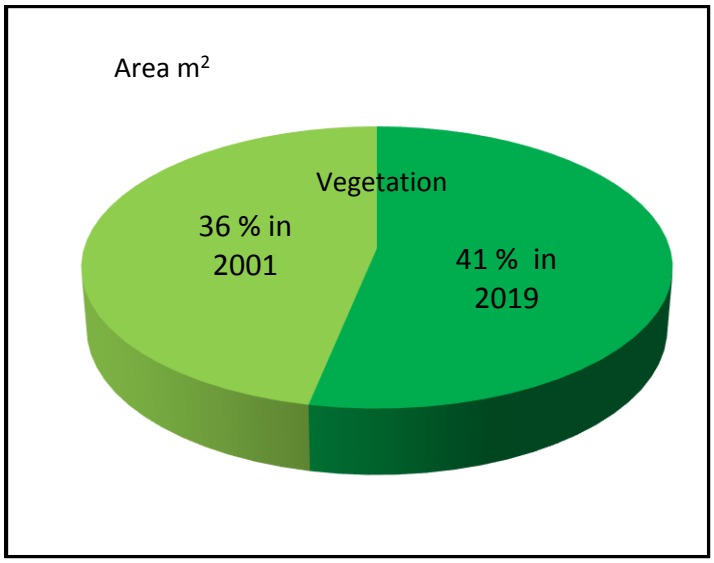

Figure (3 - 45): The difference for acreage cropped between 2001 and 2019.

3.8 Calculation of the NDWI for the Studied Area

By using Landsat 5 for the year 2001 and Landsat 8 for the year 2019, it was possible to estimate the normal difference water indices (NDWI), by applying the equation (4) in chapter 2 in the program of Arc GIS.

The NDWI value was extracted for each year. Where the extracted values represent availability of the density of the water body, as shown in figures (3 - 46 - b), and (3 - 48 - b) respectively, the blue color represents

the water content, while the white color represents the areas without water.

The water content area was illustrated in table (3 - 3) and (3 - 4), the NDWI value for the year 2001 is 46802700 m² which is about 8 % of the total area, and the area Non-water is 523368000 m^2 with a percentage of 92 % from the total area, and the NDWI value for the year 2019 is 123406200 m² which is about 19 % of the total area, and the area Non-water is 515720970 m^2 with a percentage of 81 % from the total area. These results lead to the fact that a clear increase in the area of water.

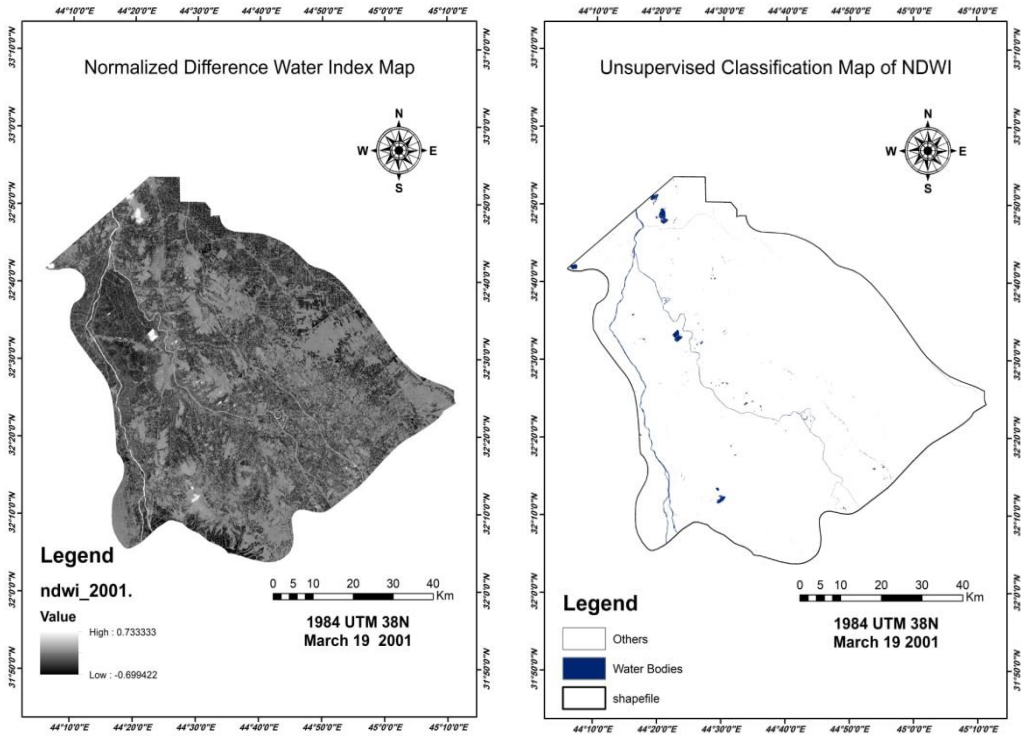

(a) **(b)**

Figure (3 - 46): (a) The results of Normalized different water index (NDWI) map, and (b) the results of unsupervised classification of results (NDWI) image (19/3/2001).

Table (3 - 3): The statistical analysis that determined by applied the NDWI for Babylon Governorate (19/3/2001).

Data	Type	COUNT	AREA (m^2)	MIN	MAX	RANGE	MEAN	STD
2001/3/19	Water	52003	46802700	0.074074	0.733333	0.659259	0.312042	±0.141879
	Non-water	5815200	523368000	- 0.69942	0.073684	0.773106	- 0.25721	±0.141955

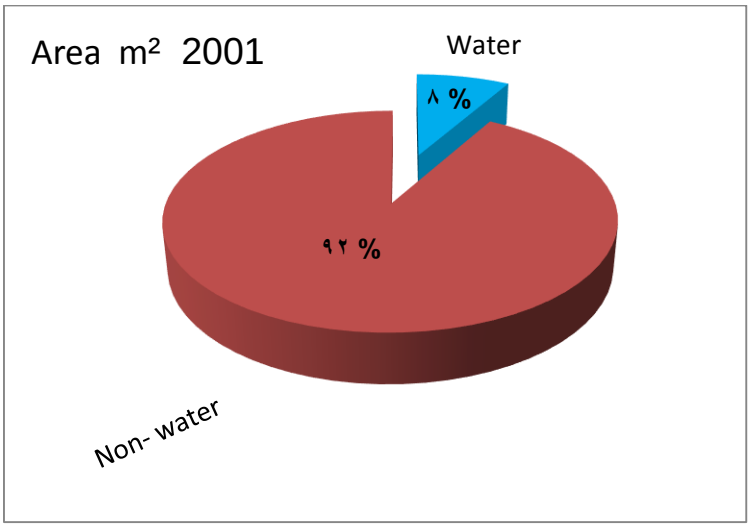

Figure (3 - 47): The waters ratio for the year 2001.

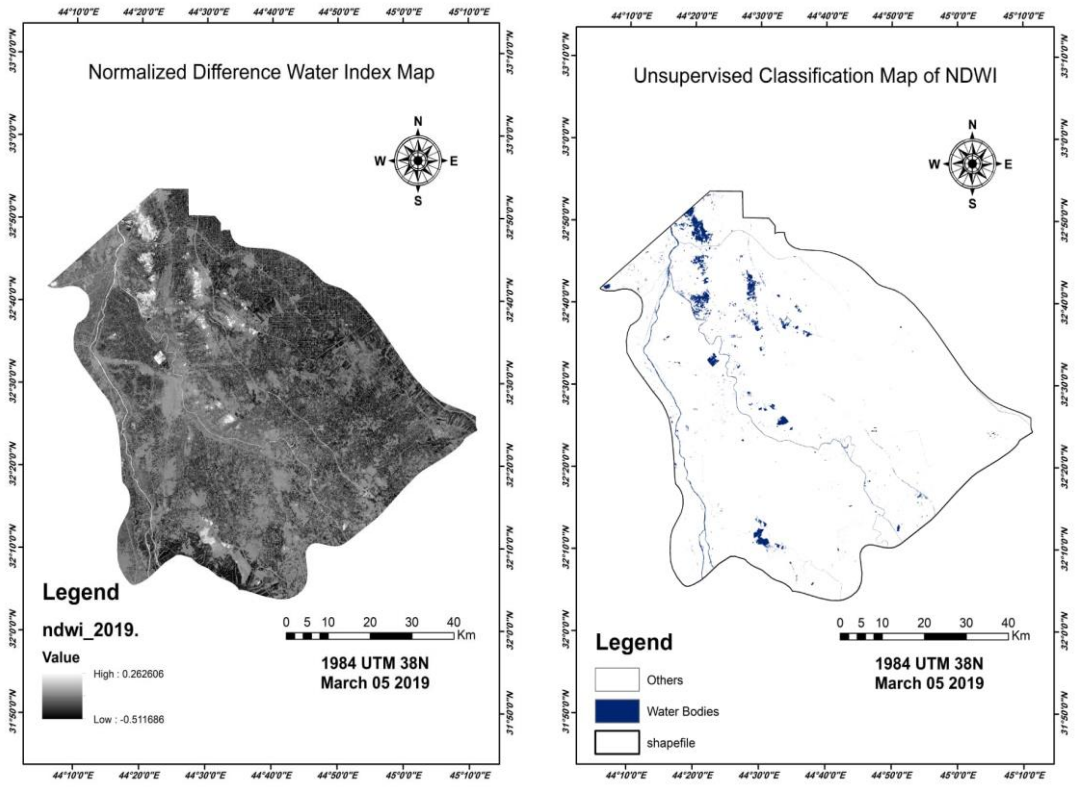

(a) **(b)**

Figure (3 - 48): (a) The results of Normalized different water index (NDWI) map, and (b) the results of unsupervised classification of results the NDWI image (5/3/2019).

Table (3 - 4): The statistical analysis that determined by applied the NDWI for Babylon Governorate (5/3/2019).

Data	Type	COUNT	AREA (m^2)	MIN	MAX	RANGE	MEAN	STD
2019/3/5	Water	137118	123406200	- 0.05799	0.249849	0.307848	0.053369	±0.078109
	Non-water	5730233	515720970	- 0.51168	0.262606	0.774292	- 0.22473	±0.090429

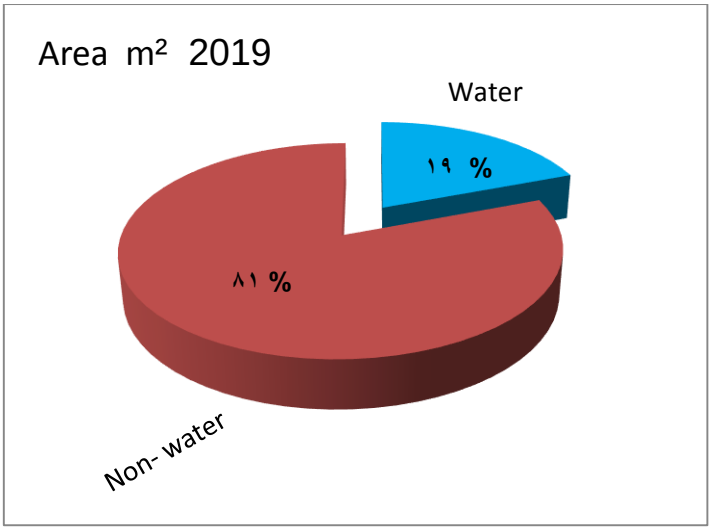

Figure (3 - 49): The waters ratio for the year 2019.

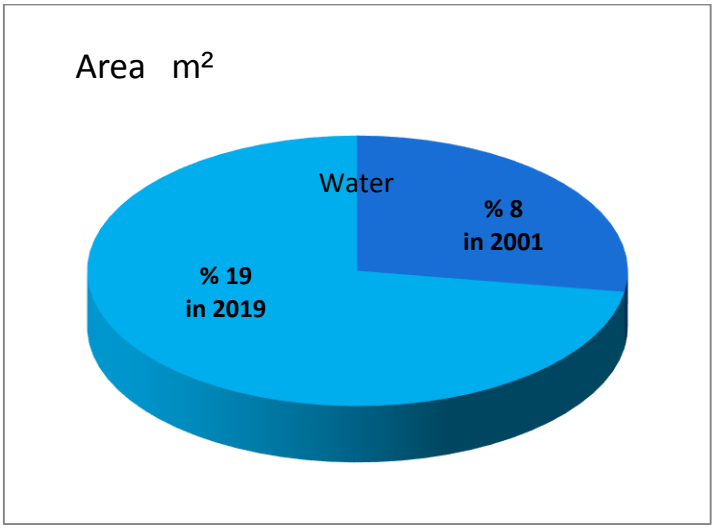

Figure (3 - 50): The difference areas for waters between 2001 and 2019.

3.9 Supervised Classification Results

The supervised classification for the Babylon Governorate was conducted on (19/3/2001) by using Landsat 5, while on (5/3/2019) was conducted by using Landsat 8. By using the Erdas program the study area was classified according to the land condition for six classes, the brown color indicates the arable land, the yellow color indicated the Mixed barren land, the light green color indicates the permanently irrigated land, dark green indicates the heterogeneous agriculture, pinky indicates

the Soil salination and the blue color indicates the rivers and canals content, as shown in figures (3 - 52) and (3 - 54). The result show that there is an increase in the area of Permantly irrigated lands from 636644700 m² ≈ 12 % in 2001 to 748221300 m² ≈ 14 % in 2019 with increasing ratio of 2 %. The Soil salination showed decreasing from 38811600 m² ≈ 1 % in 2001 to 24218100 ≈ 0 % in 2019 with an decreasing ratio of 1 %. The area of Heterogeneous agricultural showed the same trends, which was 1788619500 m² ≈ 34 % in 2001 while in 2019 was 1509721200 m² ≈ 29 % with a decreasing ratio of 5 %. The area of Water body raised from 42505200 m² ≈ 1 % in 2001 to 77653800 m² ≈ 2 % in 2019. The area of Arable land was 863890200 m² ≈ 16 % in 2001 and increased to 1607128200 m² ≈ 30 % in 2019, while the area of Mixed barren lands decreased from 1910011500 m² ≈ 36 % in 2001 to 1312110900 m² ≈ 25 % in 2019, the decreasing ratio ≈ 11 % from the total studied areas.

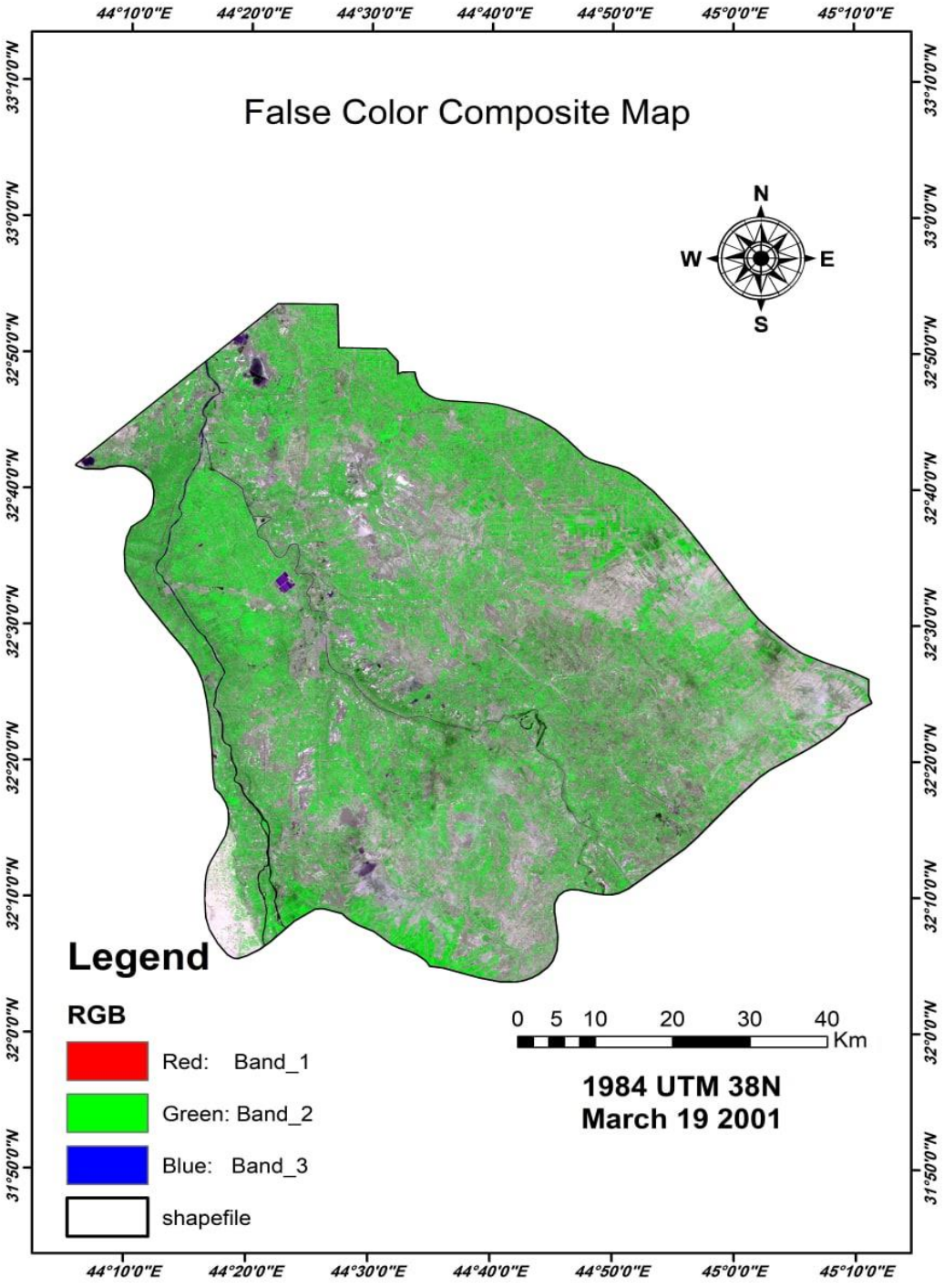

Figure (3 - 51): The False color composed map of the Babylon Governorate of (19/3/2001).

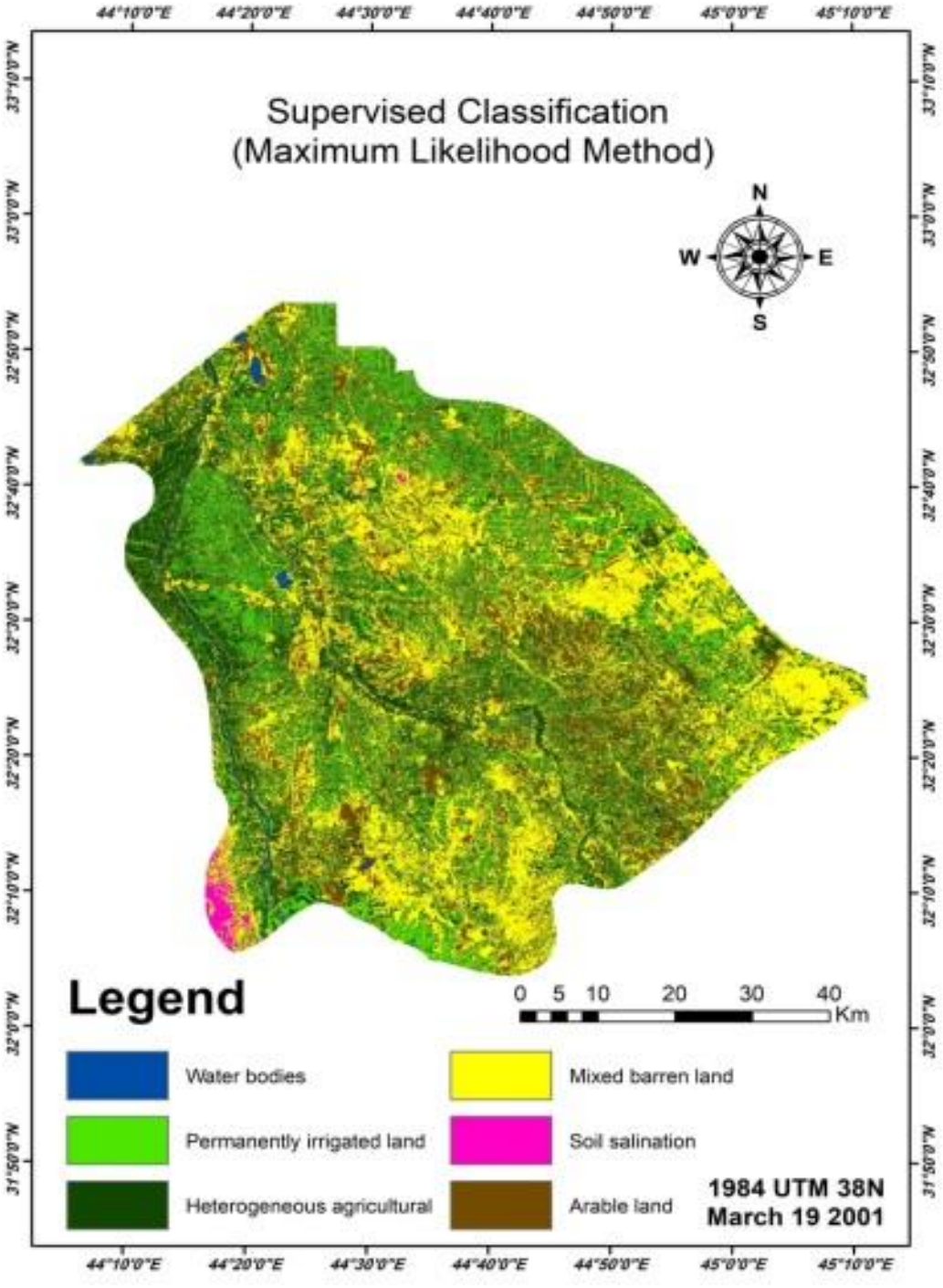

Figure (3 - 52): The supervised classification of the Babylon Governorate of (19/3/2001).

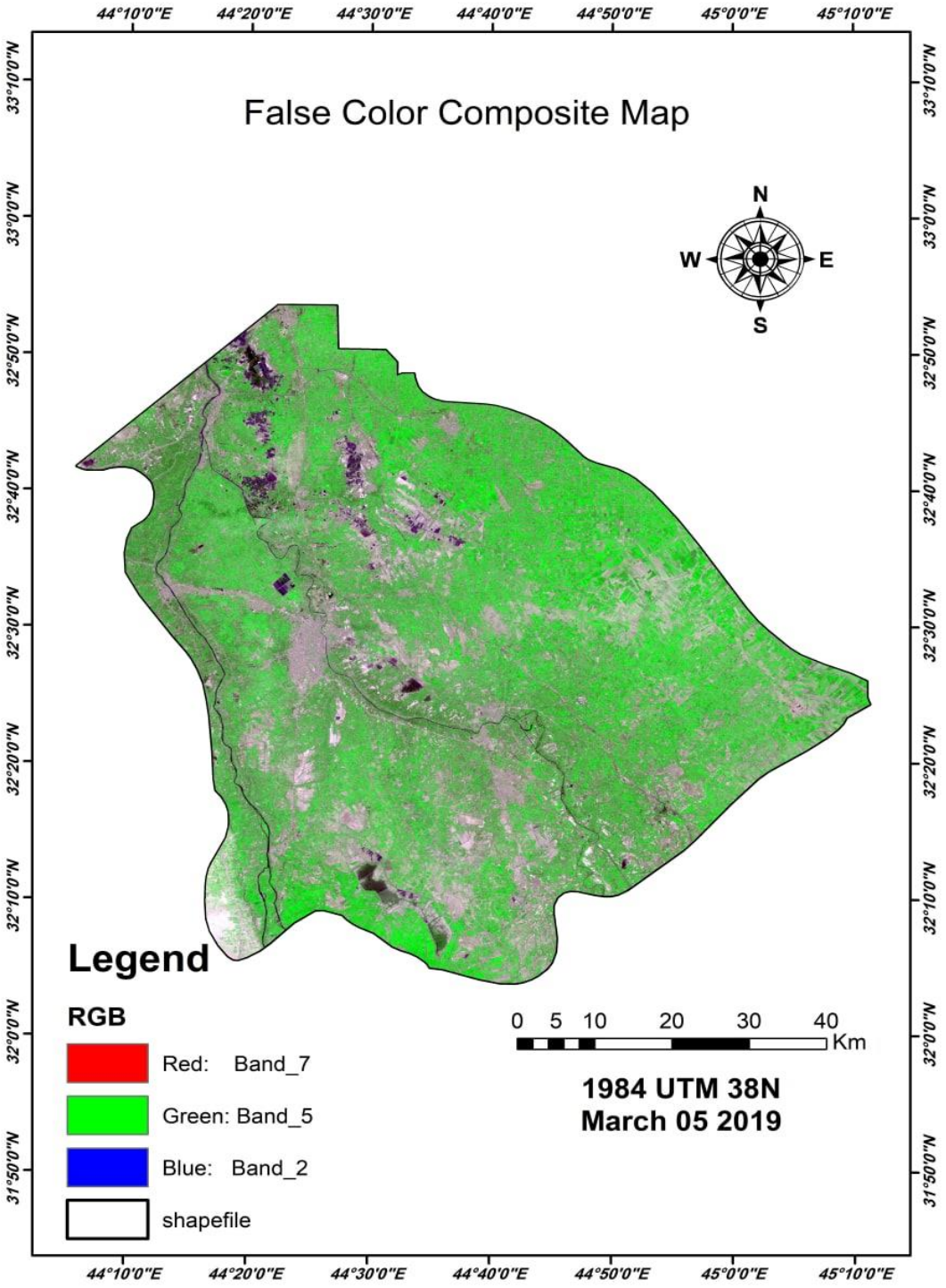

Figure (3 - 53): The False color composed map of the Babylon Governorate of (5/3/2019).

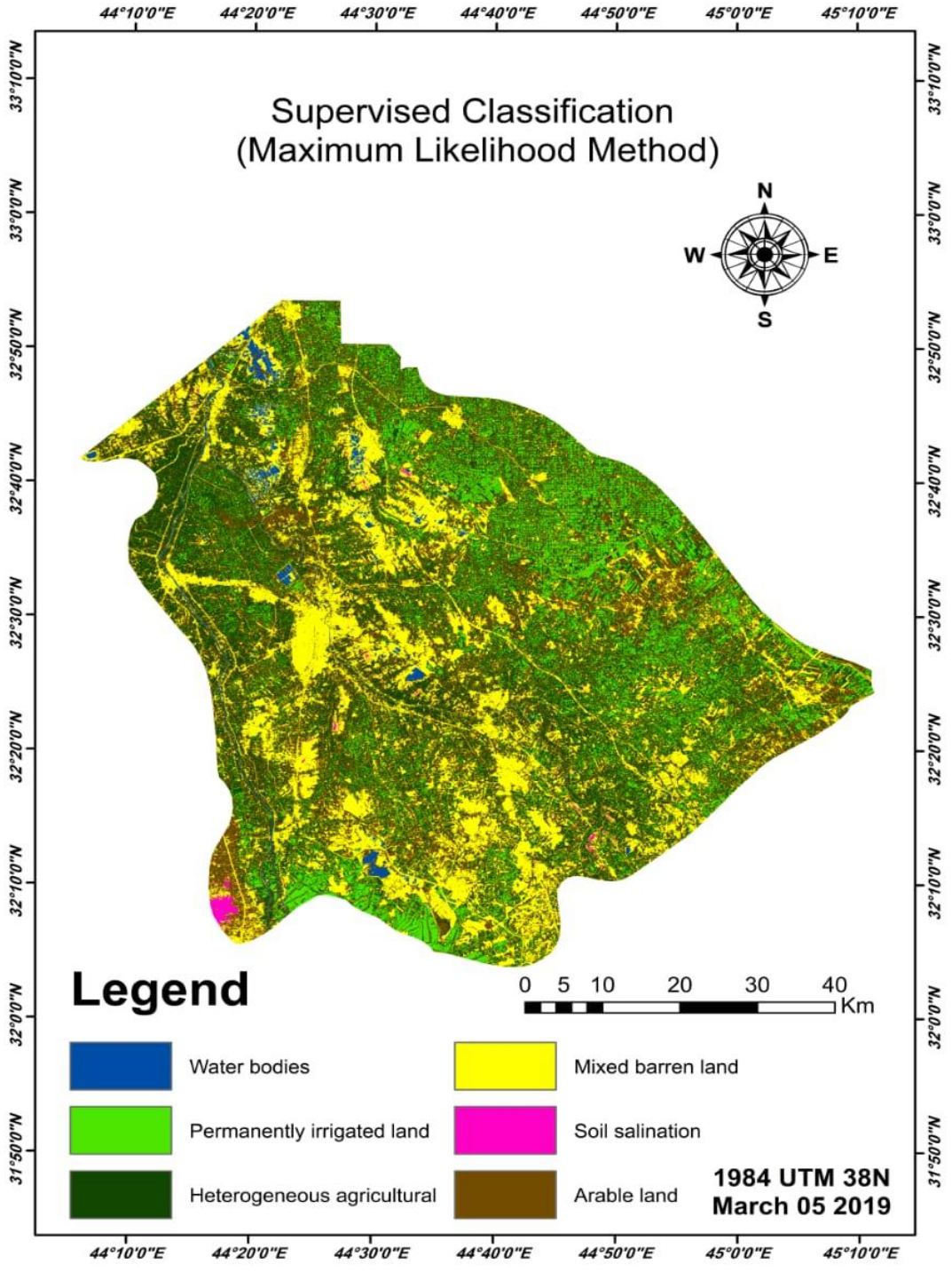

Figure (3 - 54): The supervised classification of Babylon Governorate of (5/3/2019).

Table (3 - 5): The statistical analysis for supervised of the Babylon Governorate in (19/3/2001).

Data	Type	COUNT	AREA (m^2)	MIN	MAX	RANGE	MEAN	STD
19/03/2001	Water bodies	47228	42505200	6	86	80	17.7832	±5.464591
	Permanently irrigated land	707383	636644700	66	152	86	97.03335	±9.49294
	Heterogeneous agricultural	1987355	1788619500	27	122	95	74.24811	±9.662974
	Mixed barren Land	2122235	1910011500	29	178	149	71.67539	±7.673255
	Soil salination	43124	38811600	80	180	100	105.556	±6.743075
	Arable land	959878	863890200	29	87	58	55.91365	±5.580086

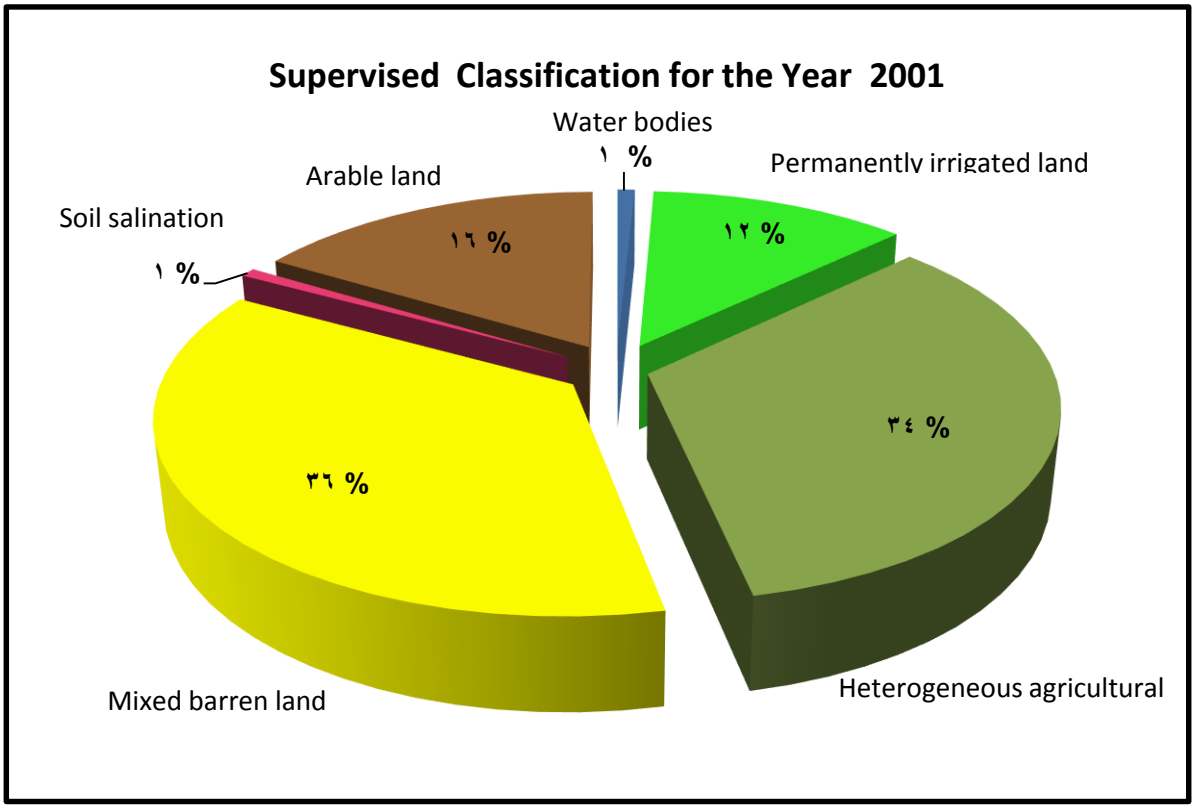

Figure (3 - 55): The supervised classification techniques for the year 2001.

Table (3 - 6): The statistical analysis for supervised of the Babylon Governorate in (5/3/2019).

Data	Type	COUNT	AREA (m²)	MIN	MAX	RANGE	MEAN	STD
05/03/2019	Water bodies	86282	77653800	0.2	10446	10446	7481.49425	±793.18928
	Permanently irrigated Land	831357	748221300	14837	26136	11299	18967.69371	±1426.93309
	Heterogeneous Agricultural	1677468	1509721200	9806	25291	15485	15750.32195	±1645.56985
	Mixed barren Land	1457901	1312110900	8863	22171	13308	14447.43109	±1492.84426
	Soil salination	26909	24218100	15012	29967	14955	19966.09491	±1403.32868
	Arable land	1785698	1607128200	8153	27418	19265	14807.29832	±1593.77274

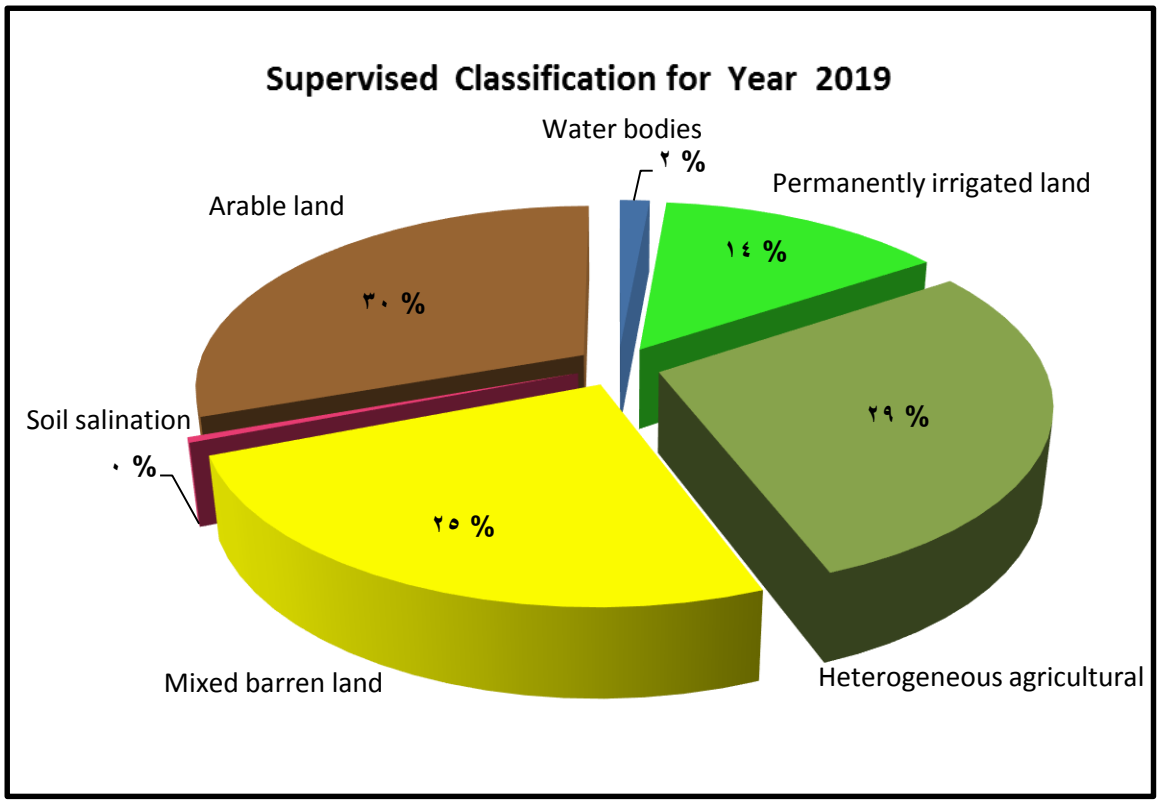

Figure (3 - 56): The supervised classification techniques for the year 2019.

Chapter Four

Field Data

4.1 Introduction

In order to compare the results of the NDVI index that have been determined in Chapter 3 with the field results from the ground, the agricultural data were obtained from the Babylon Agricultural Directorate for the period from 2009 to 2019. These data cover a wide range of information about agricultural production such as, number of trees (fag, palm, citrus (oranges, grapes, and pomegranates)) and cultivated areas for grain crop (wheat and yellow corn) for different districts into Babylon Governorate. Some information are not complete to cover the study period (2009 - 2019) which are missed in a few years, therefore they are ignored and focused on completed data as follows:

4.2 Figs Trees

The number of areas in the Babylon Governorate is (16) districts distributed as follows: Iiskandaria, Jurf al nasr, Al musayb and Sada al hindiya in the north of Babel Governorate, as for the south of the governorate, the area of Mudhatia, Hashimia, Kifl, Qasim, Shuwmli, and Taliea. As for the Al mashrue, which occupies the largest area of the governorate in the east side and the rest of the areas in the center, it is the center (Al-Hillah), Al mahawil, Al amam, Al nayl and Abi gharaq in the center of the governorate. All of these areas that I mentioned had information about fig cultivation in them, except for the (Jurf al nasr and al musayb) areas, It was not enough information, as most of the information was lost, and agriculture was few. In particular, it controlled the area of Jurf al sakhr, which was renamed Jurf al nasr

after its liberation during the period (2014 - 2017), another reason is not obtaining the rights of sufficient rights for farmers to continue, support and increase agriculture in that period, the figure (4 - 1) shows the cultivation of figs in each region separately, due to not available of cultivated area, we have relied on the number of trees, so the drawing was between the numbers of fig trees and years for the period (2009-2018) in figures from (a) to (n), and through these figures, it is clear that the Kifl region is the most area where figs are found, and the cultivation increases more with the progress of the years.

To determine the total number of fig's trees in the governorate, the total number of trees for all the areas studied in this paragraph was collected and presented in figure (4 - 1- o), which shows an increase in the number of trees from (2009 - 2018), according to the results after making a calibration of the drawing to determine the final behavior of the augmentation, which is the red line in figure (4 -1- o), and follows equation (5):

$$y= 9271.8x - 2E + 07 \quad (13)$$

Where:

y = The number of trees

x = The years

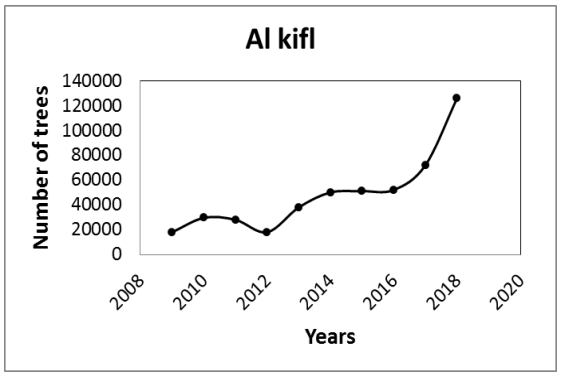
Al kifl
Number of trees
140000
120000
100000
80000
60000
40000
20000
0
2008
2010
2012
2014
2016
2018
2020
Years

(a)

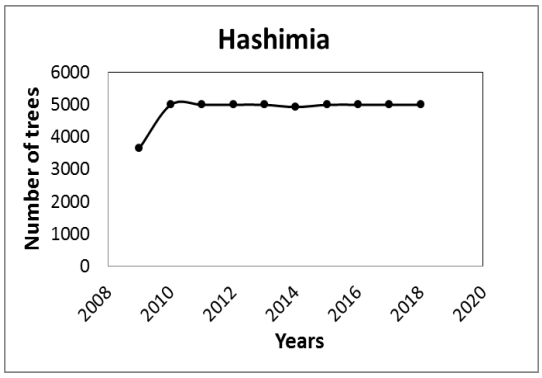
Hashimia
Number of trees
6000
5000
4000
3000
2000
1000
0
2008
2010
2012
2014
2016
2018
2020
Years

(b)

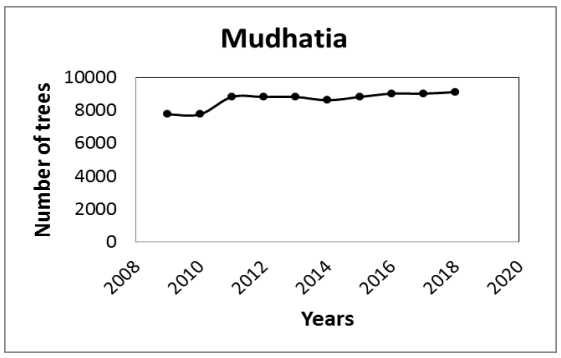
Mudhatia
Number of trees
10000
8000
6000
4000
2000
0
2008
2010
2012
2014
2016
2018
2020
Years

(c)

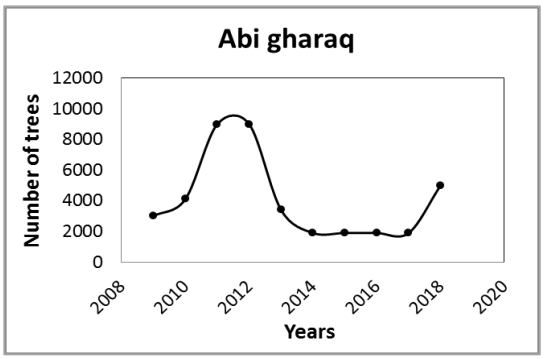
Abi gharaq
Number of trees
12000
10000
8000
6000
4000
2000
0
2008
2010
2012
2014
2016
2018
2020
Years

(d)

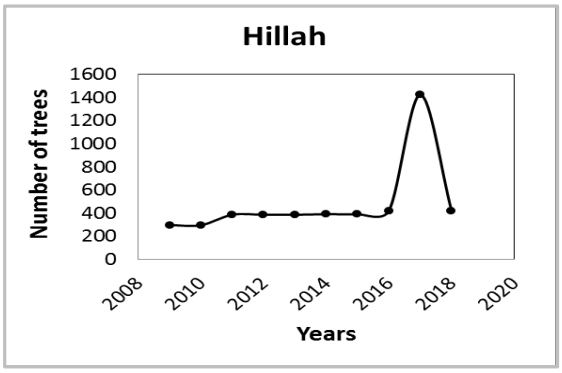
Hillah
Number of trees
1600
1400
1200
1000
800
600
400
200
0
2008
2010
2012
2014
2016
2018
2020
Years

(e)

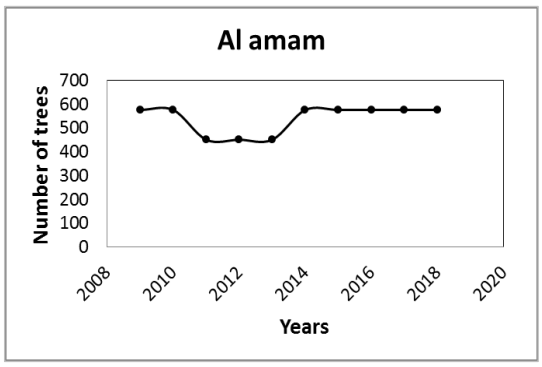
Al amam
Number of trees
700
600
500
400
300
200
100
0
2008
2010
2012
2014
2016
2018
2020
Years

(f)

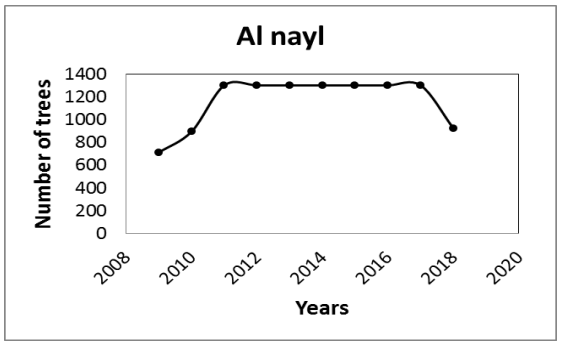
Al nayl
Number of trees
1400
1200
1000
800
600
400
200
0
2008
2010
2012
2014
2016
2018
2020
Years

(g)

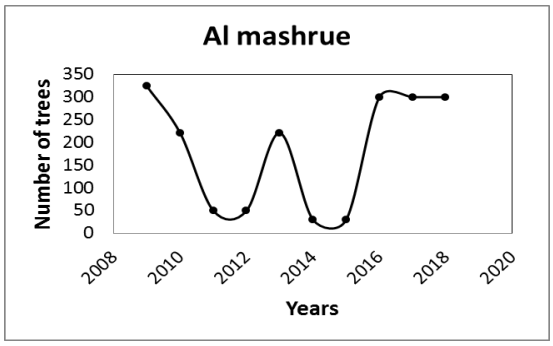
Al mashrue
Number of trees
350
300
250
200
150
100
50
0
2008
2010
2012
2014
2016
2018
2020
Years

(h)

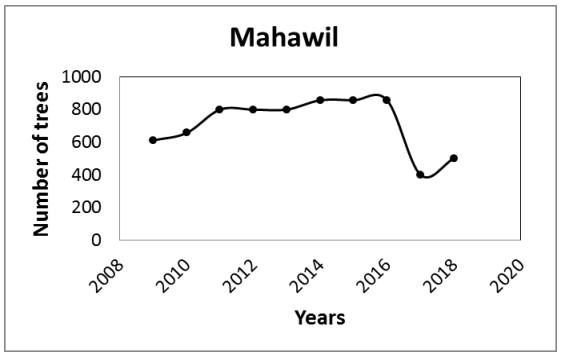
Mahawil
Number of trees
1000
800
600
400
200
0
2008
2010
2012
2014
2016
2018
2020
Years

(i)

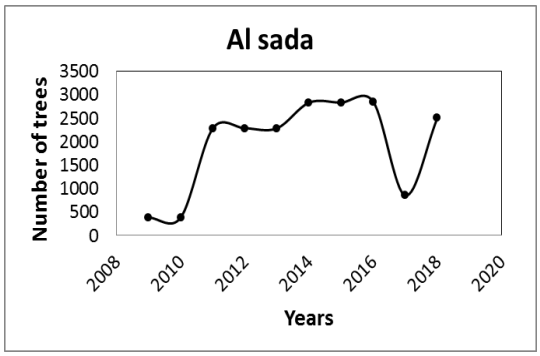
Al sada
Number of trees
3500
3000
2500
2000
1500
1000
500
0
2008
2010
2012
2014
2016
2018
2020
Years

(j)

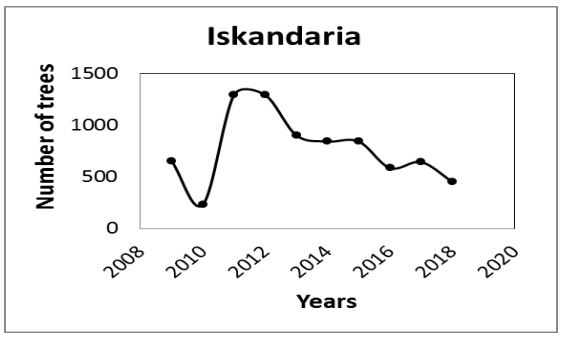
Iskandaria
Number of trees
1500
1000
500
0
2008
2010
2012
2014
2016
2018
2020
Years

(k)

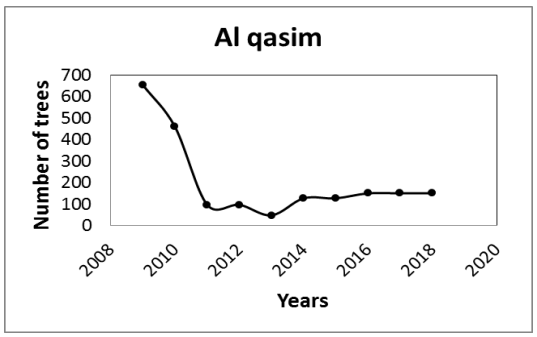
Al qasim
Number of trees
700
600
500
400
300
200
100
0
2008
2010
2012
2014
2016
2018
2020
Years

(l)

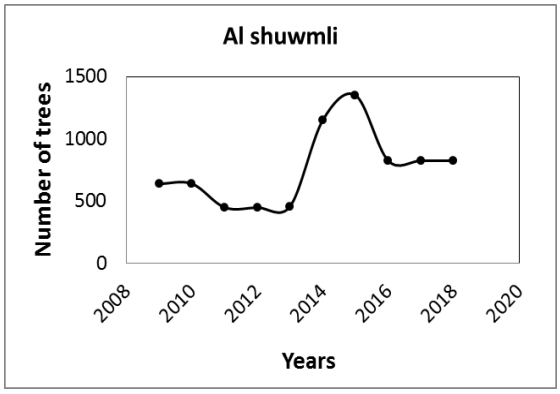

(m)

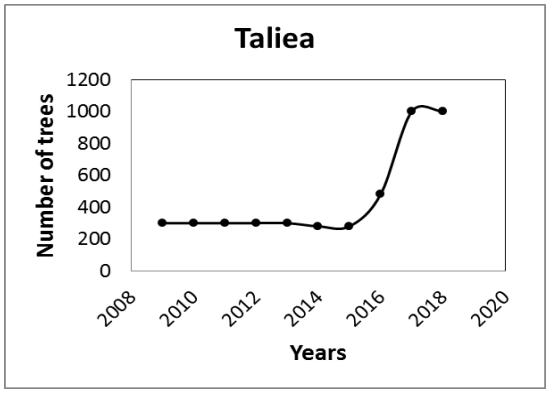

(n)

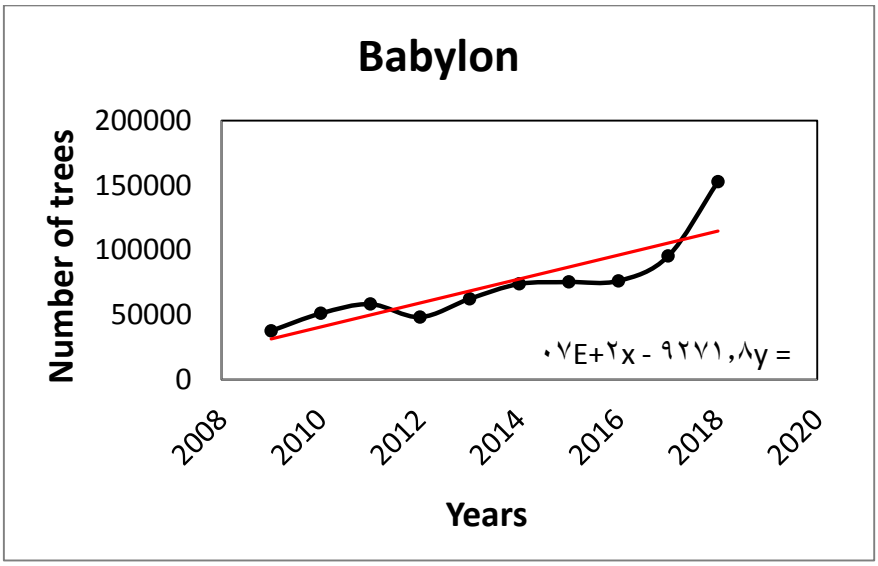

(o)

Figure (4 - 1): (a) to (n) The relationship between years and the number of fig trees for the period (2009 to 2018), (o) it generally shows the cultivation of figs in Babylon Governorate.

The increase is clear for this type of cultivation during the period between 2009 to 2018, and this supports the practical side in chapter 3, where we noticed that the vegetation cover and its density increased with the progress of the years until 2019.

4.3 Citrus Trees

For citrus cultivation I made a comparison between a year 2009 and 2019 of three types of fruits, namely, oranges, grapes, and

pomegranates in the regions of Hillah, Mahawil, Al sada and Hashimia. We note that some areas are almost conservative at the level of this cultivation and some of them have decreased. As shown in Figure (4 - 2).

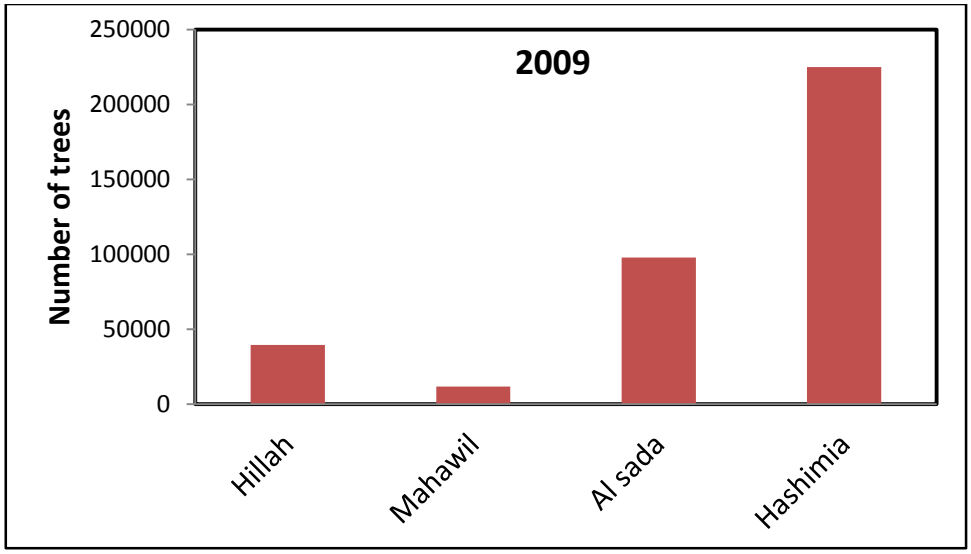

(a)

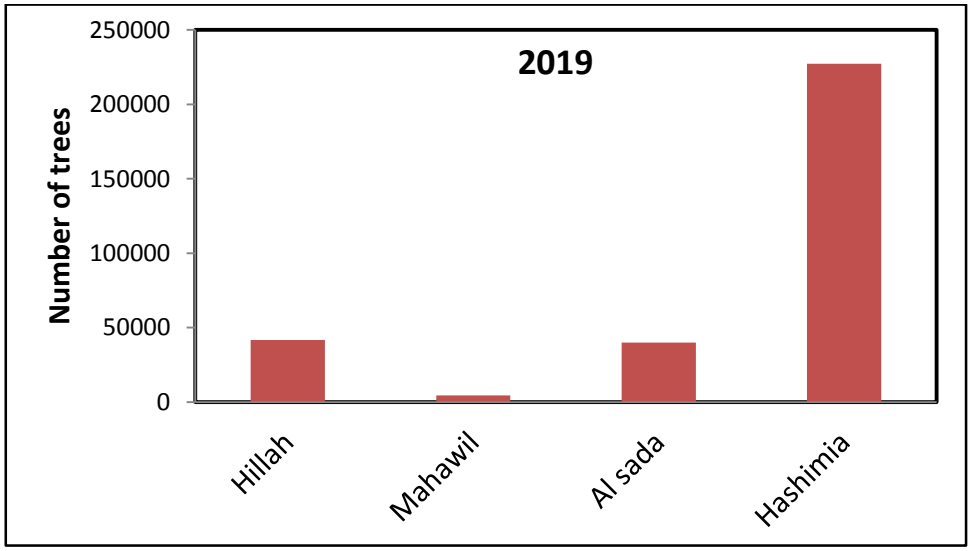

(b)

Figure (4 - 2): (a) The number of citrus trees in four regions of the Babylon Governorate for the year 2009, (b) It shows the cultivation of citrus fruits for the same areas for the year 2019.

The cultivation of this citrus was in large numbers in the Al hashimia region, and the least was in Al mahawil for yeare 2009, as for year

2019, this cultivation was almost stable in the Al hashimia and Hillah regions, and decreased in Al mahawil and Al sada.

4.4 Grain Crop

4 .4.1 The Wheat

It is known that the Babylon Governorate is famous for growing wheat, so it maintains its level during the previous ten years, and this can be known through the cultivated area until 2019, or increases by more in some years, as shown in Figure (4 - 3), after calibrating the drawing to determine the final behavior, it is shown in red line which follows equation (6):

$$y = -2084.7\,x + 4E + 06 \qquad (14)$$

Where:

y = The productive space

x = The years

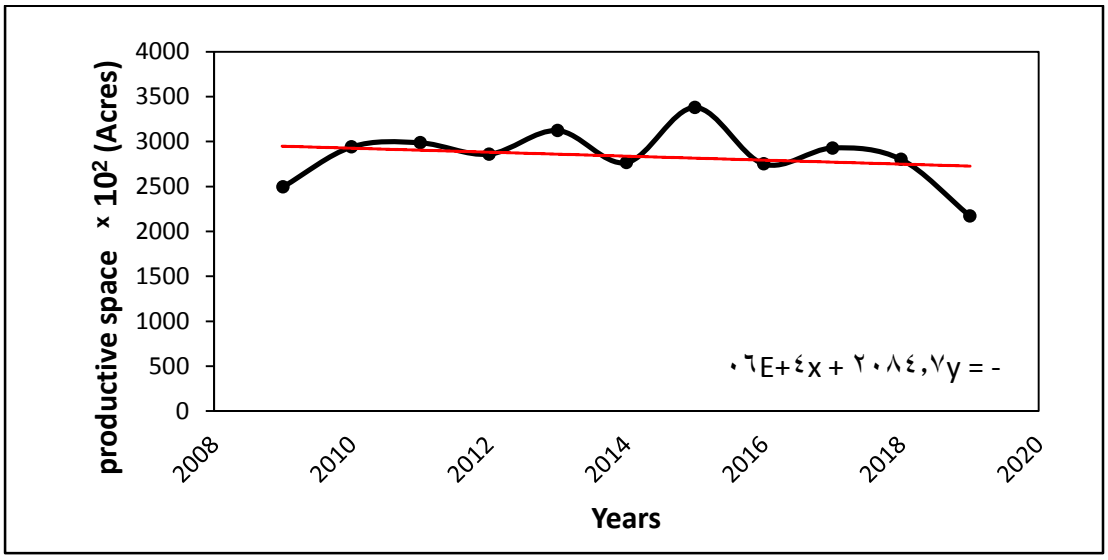

Figure (4 - 3): The area produced of wheat cultivation in the Babylon Governorate for the period (2009 - 2019).

4.4.2 The Yellow Corn

The yellow corn is one of the crops that the Babylon Governorate is well-known for its cultivation. I compared between 2009 and 2019 in the Al nayl, Kifl, Shuwmli, Al amam and Mudhatia regions, and the difference is clear as the production of this crop increased through the cultivated area, as shown in Figure (4 - 4).

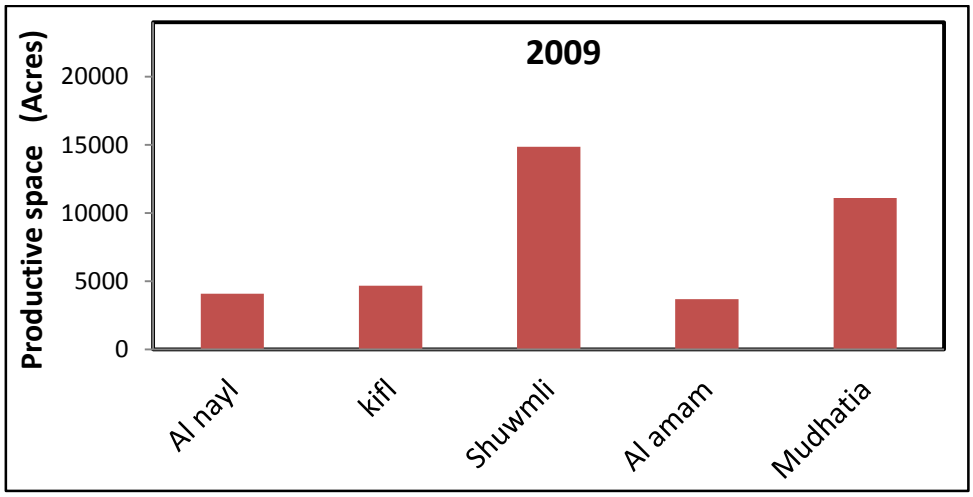

(a)

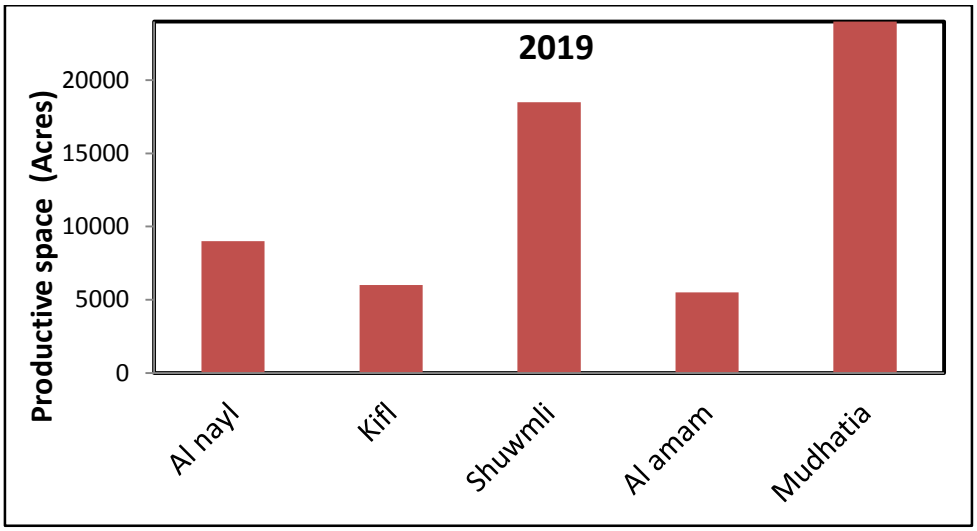

(b)

Figure (4 - 4): (a) The area produced for growing yellow corn in five regions of Babylon Governorate for the year 2009, (b) shows the increase in the area produced for growing yellow corn for the same regions for the year 2019.

The increase was due to the peasants interest in their lands, their exploitation of agriculture, and the increase in agricultural production with the availability of fertile land and water.

4.5 The Palm Trees

I obtained information about the number of palm trees, approximately 15 species, the most important of which is (Zahdi and Khestawi), which are the most famous types of palm trees in Iraq in general and in the Babylon Governorate in particular, where (Zahdi) constitute half of Iraq's production of dates, and the reason for this is due to the characteristics of the Zahdi palm, it is characterized by its high productivity as well as its tolerance to salinity, drought and frost and its speed of growth, and it is ability to be stored for long periods as well as one of the most used types in industries such as the manufacture of molasses, vinegar and other industries.

Figure (4 - 5), which shows the number of trees with years during the period (2009 - 2019), and after calibrating the drawing to determine the final behavior, it was shown in the red line according to the following equation:

$$y = - 200834\ x + 4E + 08 \qquad (15)$$

Where:

Y = The number of trees

X = The years

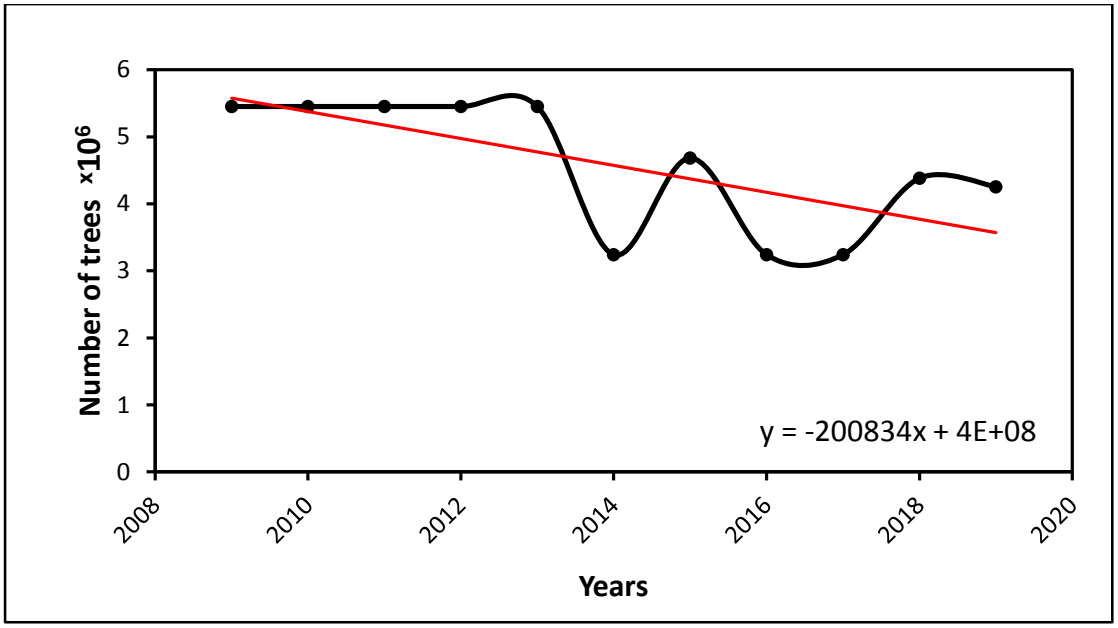

Figure (4 - 5): The number of palm's trees in Babylon Governorate for the period (2009 - 2019) for 15 species of palms.

Through the figure (4 - 5), it explained that the number of palm's trees lost its stability after 2013, and this instability is attributed to the reasons previously mentioned in addition to the high salinity in some areas where palm's trees grown.

Chapter Five

Conclusions, Recommendations, and Future Work

5.1 Conclusions

The use of Landsat 5 and Landsat 8 in diverse years duration can provide a perfect evaluation for land changes in the agriculture sector in the Babylon Governorate. This can give sufficient perceptions of the changes in the future. The results of this study show the state of the land changes by using the NDVI and NDWI indices values, which can be highly useful, due to the ability of providing accurate information about the vegetation condition and enable more precise and spatially. In addition to the consideration of society activities and climate fluctuations, it can be considered as a measure of future agricultural land degradation. The important results are listed in the following points:

1. The study gave a highlight on the needing of developing plans during short term and long term in order to address the state of the changes land.

2. The distribution of the NDVI for the period (2001 - 2019) showed a positive trends in the vegetation density.

3. The distribution of the NDWI values during the period (2001 - 2019) showed a positive change pattern in the surface area of the water of the survey area.

4. The findings of this study show an increase in the area of Permantly irrigated lands, the Soil salination showed decreasing, the area of Heterogeneous agricultural showed decreasing and the area of Water body increased. The area of Arable land increased, while the area of Mixed barren lands decreased.

5. The continuous waste of water resources due to uneconomic irrigation methods, failure of drainage projects, continuous burial of rivers and streams, frequent exceeding of water quotas and the high rate of migration to cities on one hand, and on the other hand the conversion of agricultural lands into housing areas, and some areas of the city exposed to terrorist and war operations during the period (2014 - 2017), this led to a decline in agriculture in some areas of Babylon Governorate,

6. After collecting data from the Babylon Agriculture Directorate the results were nearly identical to those of the NDVI measurements.

7. Manpower, as many workers with an agricultural background have resorted to other activities such as the police, the army, and other jobs in pursuit of a faster and higher financial return, such as establishing fish ponds, with the absence of the government oversight, which led to an increase of rivers and canals areas.

5.2 Recommendations

1. The research was conducted in the Babylon Governorate. It is necessary to conduct more studies of the region and compare it with different periods and other regions of Iraq.

2. Working on providing specialized centers for remote sensing in the areas of Babylon Governorate for the purpose of monitoring the conditions that pass over the region, which allows for the possibility of avoiding the factors that lead to their deterioration and treating them before their severity increases.

3. Working to communicating the results of studies to decision-makers in government institutions and ministries such as the Ministry of Environment, the Ministry Agriculture and the Ministry of Trade, so that the necessary measures are taken and appropriate solutions to the problems related to the deterioration and its effects.

4. Giving the opportunity to contribute to improving agricultural production and water availability, and to identify and solve problems through continuous monitoring during the coming years.

5.3 Future Work

1. An extensive remote sensing procedure of land changes can be undertaken with the availability of the necessary resources and time, as this study can be used as a starting point for further (RS) research in order assess all the states of the vegetation cover, in addition to field data for multiple years with climate factors, desertification factors and soil degradation.

2. Applying the research steps to other areas in Iraq, and for other periods of time.

Supervisors Certification

We Certify that this thesis titled (**Assessment the Land Vegetation Cover for Babylon Government by Using Remote Sensing and GIS Techniques**) was prepared by the student (**Zahraa Ali Naife Hamza**) under our supervision at the College of Sciences, University of Babylon in Partial Fulfillment of the requirements for the Degree of Master in Physics.

Signature:

Supervisor: Dr. Ameerah Ab. Al-Sadooni Khanjer

Title: Asst. Prof.

(Supervisor)

Data: / / 2021

Signature:

Supervisor : Dr. Ebtesam F.

Title: Prof.

(Supervisor)

Data: / / 2021

Head of the Department Certificate

In view of the available recommendation, I forward this thesis for debate by the examining committee.

Signature:

Name: Dr. Abdulazeez O. Mousa Al-Ogaili

Title: Prof.

(Head of the Physics Department, College of science, University of Babylon)

Data: / / 2021

Examining Committee Certificate

We certify that we have read this thesis entitled **(Assessment the Land Vegetation Cover for Babylon Government by Using Remote Sensing and GIS Techniques)** and, as an examining committee, examined the M.Sc. student **(Zahraa Ali Naife Hamza)** in its content and that, in our opinion it meets the standards of a thesis for the degree of Master of Science in Physics with (Excellent) degree.

Signature:

Name: **Dr. Mohsin Kadhim Muttaleb Al-Janaby**
Title: **Professor**
Address: **College of Science/ University of Babylon**
Data: / / **202١**
(Chairman)

Signature:

Name: **Dr. Nihad Abdulameer Salih**
Title: **Professor**
Address: **College of Science/ University of Babylon**
Data: / / **2021**
(Member)

Signature:

Name: **Dr. Sundus A. Abdullah**
Title: **Professor**
Address: **College of Sciences/ University of Baghdad**
Data: / / **2021**
(Member)

Signature:

Name: **Dr. Ameerah Ab. Al-Sadooni**
Title: **Professor**
Address: **College of Sciences/ University of Babylon**
Data: / / **2021**
(Member and Supervisor)

Signature:

Name: **Dr. Ebtesam F. Khanjer**
Title: **Professor**
Address: **College of Sciences/ University of Baghdad**
Data: / / **2021**
(Member and Supervisor)

Approved By the College Committee on Graduate Studies.

Signature:

Name: **Dr. Enas M. Al-Robayi**
Title: **Professor**
Address: **Dean of the College of Science/ University of Babylon**
Date: / / **2021**

Contents

List of Tables

List of Figures

List of Symbols

Symbol	Meaning
RS	Remote Sensing
GIS	Geographic Information System
PA	Precision Agriculture
NDVI	Normalized Difference Vegetation Index
NDWI	Normalized Difference Water Index
EO	Earth Observation
TM	Thematic Mapper
OLI	Operational Land Imager
TIRS	Thermal Infrared Sensor
USGS	United States Geological Situation
VIS	Visual
MSS	Multispectral Scanner
ETM	Enhanced Thematic Mapper
DEM	Digital Elevation Model
LULC	Land Use Land Cover
MNDWI	Modified Normalized Difference Water Index
NASA	National Aeronautics and Space Administration
ERTS	Earth Resources Technology Satellite
NIR	Near Infrared

Symbol	Meaning
SWIR	Short Wavelength Infrared
WRS	World Reference System
LTAP	Long Term Acquisition Plan
CIR	Color Infrared
GSD	Ground Sample Distance
DBMS	Database Management System
GUI	Graphical User Infrared
SAVI	Soil Adjusted Vegetation Index
EVI	Enhanced Vegetation Index
ML	Maximum Likelihood
MD	Minimum Distance
MH	Mahalanobis Distance
B1,B2,…..	Band 1, Band 2, …..
MIN	Minimum
MAX	Maximum
STD	Standard Deviation

CHAPTER ONE

General Introduction and Literature Review

CHAPTER TWO

Theoretical Concept

CHAPTER THREE

Results and Experimental Work

CHAPTER FOUR

FIELD DATA

CHAPTER FIVE

Conclusions, Recommendations and Future Work

REFERENCES

References

[1] D. W. Wong and M. Sun, "Handling Data Quality Information of Survey Data in GIS: A Case of Using the American Community Survey Data", (2013).

[2] D. beurs and Townsend, "Estimating the effect of gypsy moth defoliation using MODIS", Remote Sens Environ, p. 112, (2008).

[3] M. Arr, "Kerala Environment Congress 2012 Focal Theme at RGCB Auditorium, Thiruvananthapuram Organized by Centre for Environment and Development", (2015)

[4] P. Shanmugapriya, S. Rathika, T. Ramesh, and P. Janaki, "Application of Remote Sensing in Agriculture -A Review ", (2019).

[5] X. You, J. Meng, M. Zhang and T. Dong, " Remote Sensing Based Detection of Crop Phenology for Agricultural Zones in China Using a New Threshold Method", (2013).

[6] P. K. Kingra, D. Majumder and S. P. Singh, "Application of Remote Sensing And GIS in Agriculture and Natural Resource Management Under Changing Climatic Conditions", Agric Res J., 53 (3): 295-302, (2016).

[7] P. S. Thenkabail, E. A. Enclona, M.S. Ashton, and V. Der Meer, "Accuracy assessments of hyperspectral waveband performance for vegetation analysis applications", Remote Sensing of Environment, P. 91, (2004).

[8] Schowengerdt and A. Robert, "Remote sensing :models and methods for image processing", (2007).

[9] H. E. Adam and Zakaria, "Integration of Remote Sensing and GIS in Studying Vegetation Trends and Conditions in the Gum Arabic Belt in North Kordofan, Sudan", p. 146, (2010).

[10] I. Anwar and A. Thunoun, "Utilizing Remote Sensing tools for. Studying Mosul Dam lake Topography", University of Mosul, No. 2 vol. 17, p. 1, (2010).

[11] Z. Shao, N. S. Sumari, A. Portnov, F. Ujoh, W. Musakwa and P. J. Mandela, "Urban sprawl and its impact on sustainable urban development: a combination of remote sensing and social media data", p. 1, (2020).

[12] D. Culinovic, " Remote sensing data & Data Analysis in Tableau", (2021).

[13] L. Karthikeyan, I. Chawla, and A. K. Mishra, "A review of remote sensing applications in agriculture for food security: Crop growth and yield, irrigation, and crop losses", vol. 586, p. 124905, (2020).

[14] Waheed, R. B. Bonnell, S.O. Prasher and E. Paulet, " Measuring performance in precision agriculture: CART-A decision tree approach", Agric. Water Mgmt, (2006).

[15] S. Oza, S. Panigrahy and J. S. Parihar, " Concurrent use of active and passive microwave remote sensing sensing in the Yaqui Valley, Sonora, Mexico", Agric. data for monitoring of rice crop. Int. J. Applied Earth Obst. Geoinform., (2007).

[16] Remote sensing to deal with national strategic challenges: official, TEHRAN TIMES, (2018).

[17] M. Arr, "Remote sensing applications in agriculture and forestry", Centre for Environment and Development Thozhuvancode,

Vattiyoorkavu Thiruvananthapuram, Kerala, India-695013, p. 222, (2012).

[18] M. D. Nellis, K. P. Pricey and D. Rundquist, "Remote Sensing of Cropland Agriculture", (2009).

[19] E. F. Khanjer, B. AlRazaq, R. Ismail and Z. Rasheed, "Using spatial analysis techniques to Preparing maps for distribution of pollutant concentrations in Shatt al-Arab waters in November 2015" International journal of advanced biological Research. IJABR, p. **7,** (2017).

[20] M. Arr, "Kerala Environment Congress 2012 Focal Theme at RGCB Auditorium, Thiruvananthapuram Organised by Centre for Environment and Development", (2012).

[21] O. M. Chua and K. Yunus, "Metals Pollution in Tropical Wetlands", (2019).

[22] Ministry of Planning and Development Cooperation, Central Organization for Statistics and Information Technology Annual Statistical Abstract, Baghdad, p. 3, (2007).

[23] N. Al-Ansari and A. chabuk, "Soil Characteristics in Selected Landfill Sites in the Babylon Governorate, lraq", (2017).

[24] I. J. Muhsin, F. K. Mashee and R. J. Tawfeeq, "Monitoring the Vegetation and Water Content of AlHammar Marsh Using Remote Sensing Techniques", Baghdad Science Journal, vol. 8(2), p. 646, (2011).

[25] N. K. Ghazal1, A. H. Shaban and F. K. Mashee, "Change Detection Study Of Al Razaza Lake Region Utilizing Remote Sensing And GIS Technique", Iraqi Journal of Science, (2012).

[26] A. S. Muhaimeed and S. M. Al-Hedny, " Drought Monitoring for Northern Part of Iraq Using Temporal NDVI and Rainfall Indices", (2013).

[27] E. J. Knight and G. Kvaran, "Landsat-8 Operational Land Imager Design, Characterization and Performance", (2014).

[28] R. K. Assi and A. Al-Ajeali, "Study of The Risk of Flooding and Water Flowing of AL-Najaf Sea using GIS", (2015).

[29] A. Al Salam Mohammed, " Desertification Detected in the Udhaim River Basin, Iraq Based on Spectral Indices Derived from Remote Sensing Images", (2017).

[30] J. Cristóbal, J. C. Jiménez-Muñoz, A. Prakash, C. Mattar, D. Skoković and J. A. Sobrino, "An improved single-channel method to retrieve land surface temperature from the landsat-8 thermal band", No. 3, vol. 10, (2018).

[31] M. M. Abd, F. K. Mashee and F. M. Al-Mohammed, "Determination of the Possibility of Ground Water in the Holy Governorate of Karbala using the Thermal Classification of Satellite Images Using Remote Sensing", International Journal of Scientific & Engineering Research, vol. 9, p. 403, (2018).

[32] H. Xu, "Modification of Normalized Difference Water Index (NDWI) to Enhance Open Water Features in Remotely Sensed Imagery", (2019).

[33] N. A. AL Naqeeb, J. S. Al Hassany and F. K. Mashee, "Assessment of the water quality of Um El-Naaj Marshes by Diatoms", Eco. Env. & Cons., p. 26, (2020).

[34] T. A. Dhamin, E. F. Khanjer and F. K. Mashee, "Detection Agriculture Degradation for the South of Baghdad City Using Remote Sensing Data for Years 2010-2019", Iraqi Journal of Science, (2020).

[35] L. Karthikeyan, I. Chawla and A. K. Mishra, "A review of remote sensing applications in agriculture for food security: Crop growth and yield, irrigation, and crop losses", J. Hydrol., vol. 586, p. 124905, (2020).

[36] E. F. Khanjer, W. A. Hassan, B. S. Ismael and N. K. Gazal, "Radon Distribution in Baghdad Governorate by Using Remote sensing techniques", J. Phys. Conf. Ser., No.1, vol. 1530, (2020).

[37] L. Karthikeyan, I. Chawla and A. K. Mishra, "A review of remote sensing applications in agriculture for food security: Crop growth and yield, irrigation, and crop losses", J. Hydrol., vol. 586, p. 124905, (2020).

[38] I. J. Muhsin, "Change detection of remotely sensed image using NDVI subtractive and classification methods", Iraqi Journal of Physics, vol. 14, No.29, P. 125, (2016).

[39] A. Al Salam and M. Mail, "Desertification Detected in the Udhaim River Basin, Iraq Based on Spectral Indices Derived from Remote Sensing Images", Miscellanea geographical- regional studies on development, No. 3, vol. 21, (2017).

[40] J. Cristóbal, J. C. Jiménez-Muñoz, A. Prakash, C. Mattar, D.

Skoković and J. A. Sobrino, " An improved single-channel method to retrieve land surface temperature from the landsat-8 thermal band", Remote Sens., No. 3, vol. 10, (2018).

[41] H. S. Abbas and A. S. Mahdi, "Study of Desertification using Remote Sensing Imagery in South Iraq", Iraqi Journal of Science, No. 4, vol. 60, p. 904, (2019).

[42] A. Najeeb and F. H. Mahmood, "Effect of Land Degradation Degree on the Land Cover Type Using Gis Technology in the West of Baghdad / Iraq", No. 2, vol. 53, p. 444, (2012).

[43] E. F. Khanjer, "Create Maps For Temperature Distribution In Iraq Using Arc-Gis Create Maps For Temperature Distribution In Iraq Using Arc – Gis Techniques", (2019).

[44] M. Sharma , "What is Active and Passive Remote Sensing", (2019).

[45] M. A. Ridwan, N. A. M. Radzi, W. Siti, H. Munirah, W. Ahmad, and I. S. Mustafa, "Applications of Landsat-8 Data : a Survey Applications of Landsat-8 Data : a Survey", (2018).

[46] M. A. Wulder, M. A. Loveland and D. P. Crawford, "Current status of Landsat program, science, and applications", *Remote Sens. Environ.*, vol. 225, p. 127, (2019).

[47] H. Sheng, X. Chen, J. Su, R. Rajagopal, and A. Ng, "Effective data fusion with generalized vegetation index: Evidence from land cover segmentation in agriculture", (2020).

[48] O. Rozenstein, Z. Qin, Y. Derimian and A. Karnieli, "Derivation of Land Surface Temperature for Landsat-8 TIRS Using a Split Window Algorithm" p. 5768, (2014).

[49] E. J. Knight and G. Kvaran, "Landsat-8 operational land imager design, characterization and performance" *Remote Sens.*, No. 11, vol. 6, p. 10286, (2014).

[50] M. Montanaro, A. Lunsford, Z. Tesfaye, B. Wenny and D. Reuter, "Radiometric Calibration Methodology of the Landsat 8 Thermal Infrared Sensor", (2014).

[51] K. Yinghai, I. Jungho, L. Junghee, H. Gong and R. Young, "Characteristics of Landsat 8 OLI-derived NDVI by comparison with multiple satellite sensors and in-situ observations", Remote Sensing of Environment, vol. 164, p. 298, (2015).

[52] M. Moraca and A. Pepe, "Studio comparativo tra lo stato dei luoghi prima e dopo l'incendio del Vesuvio tramite analisi satellitare", (2017).

[53] C. Parente and R. Santamaria, "Synthetic Sensor of Landsat 7 ETM+ Imagery to Compare and Evaluate Pan-sharpening Methods", (2014).

[54] L. Rocchio, "Chronicling the Landsat Legacy", The Earth Observer, November – December, No. 6, vol. 23, p. 4, (2011).

[55] C. Loyd, "Putting Landsat 8's Bands to Work ", Map Box, June 14, (2013).

[56] T. D. Acharya and I. Yang, "Exploring Landsat 8″, International Journal of IT, Engineering and Applied Sciences Research, No. 4, vol.4, p. 4, (2015).

[57] E. O. Makinde and A. D. Obigha, "Comparison between Landsat 7 Enhanced Thematic Mapper Plus (ETM+) and Landsat 8

Operational Land Imager (OLI) Assessment of Vegetation Indices", *Niger. J. Environ. Sci. Technol.*, No. 2, vol. 1, p. 355, (2017).

[58] E. F. Khanjer, "Motoring the Environmental Changes in Al-Hawizeh Marsh using Remote Sensing Techniques", *Int. J. Sci. Res.*, No. 1, vol. 7, p. 476, (2018).

[59] A. A. Ezzat, "Investigation of Environmental Parameters Using Remote sensing Techniques", (2014).

[60] G. Rowan and M. Kalacska, "Remote sensing of submerged aquatic vegetation: an introduction and best practices review", p. 1, (2020).

[61] W. Yang, W. Qi and J. Zhou, "Decreased post-seismic landslides linked to vegetation recovery after the 2008 Wenchuan earthquake", *Ecol. Indic.*, vol. 89, p. 438, (2018).

[62] P. Wolf, S. Rößler, T. Schneider and A. Melzer, "Collecting in situ remote sensing reflectances of submersed macrophytes to build up a spectral library for lake monitoring", European Journal of Remote Sensing, (2013).

[63] N. Verda, G. Mallinis, M. Teakiri and C. Georgiadis, "Assessment of Radiometric Resolution Impact on Remote Sensing Data Classification Accuracy", (2018).

[64] M. R. Heffels and J. Vanschoren, "Aerial Imagery Pixel-level Segmentation", p. 1, (2020).

[65] J. Kim, S. Kang, B. Seo, A. Narantsetseg, and Y. Han, "Estimating fractional green vegetation cover of Mongolian grasslands using digital camera images and MODIS satellite vegetation indices", *GIS science Remote Sens.*, No. 1, vol. 57, p. 49, (2020).

[66] H. García-Martínez, H. Flores-Magdaleno, R. Ascencio-Hernández , A. Gardezi , L. Tijerina-Chávez , O. R. Mancilla-Villa and M. A. Vázquez-Peña, "Corn grain yield estimation from vegetation indices, canopy cover, plant density, and a neural network using multispectral and rgb images acquired with unmanned aerial vehicles", No. 7, vol. 10, p. 1, (2020).

[67] M. F. Goodchild, "Twenty years of progress: GIS science in 2010", Journal of Spatial Information Science (1), (2010).

[68] United Nations Publications, Handbook on geographic information systems and digital mapping, No. 79, vol. 1, (2000).

[69] A. P. Hunter and A. Bishop, "Introduction to GIS Definition of GIS", *Introd. to GIS*, p. 2, (2013).

[70] D. Grantor, "optimalne lokacije novih studentskih domova u Gradu Zagrebu Primjena GIS-a u prostornom planiranju – određivanje optimalne lokacije novih studentskih domova u Gradu Zagrebu Diplomski rad", (2021).

[71] E. V. Koroleva and Y. Y. Nikitin, "U-max-statistics and limit theorems for perimeters and areas of random polygons", *J. Multivar. Anal.*, vol. 127, p. 98, (2014).

[72] E. Ali, "Geographic Information System (GIS): Definition, Development , Applications & Components", (2020).

[73] B. Gorain and S. Paul, "Hardware and Software Components of a Geographic Informaion System (GIS)", *AGROBIOS Newsl.*, (2017).

[74] V. N. Sambrani, "Business graphics a new approach to decision making", (2007).

[75] R. P. Sishodia, R. L. Ray and S. K. Singh, "Applications of remote sensing in precision agriculture: A review", *Remote Sens.*, No. 19, vol. 12, p. 1, (2020).

[76] T. B. Kshetri, "NDVI, NDBI & NDWI Calculation Using Landsat 7, 8", Tribhuvan University, (2018).

[77] I. J. Muhsin, "Assessment of vegetal cover changes using Normalized Difference Vegetation Assessment of vegetal cover changes using Normalized Difference Vegetation Index (NDVI) and subtractive (NDVI) time-series , Karbala province , Iraq", (2017).

[78] M. Ali, F.K. Mashee and A. B. Ali, "Evaluation of impact of vegetation decrease on precipitation rates in Baghdad City using remote sensing technique", *Biotechnol. Environ. Sci. Eco. Env. Cons*, vol. 25, p. 44, (2019).

[79] S. E. Profile, "A Business Model Monitoring Using Autonomous Drones in Smart Agriculture", *A Bus. Model Monit. Using Auton. Drones Smart Agric.*, No. January, p. 7, (2021).

[80] S. K. McFeeters, "Using the normalized difference water index (ndwi) within a geographic information system to detect swimming pools for mosquito abatement: A practical approach", *Remote Sens.*, No. 7, vol. 5, p.3544, (2013).

[81] V. K. Gautam, P. K. Gaurav, P. Murugan, and M. Annadurai, "Assessment of Surface Water Dynamicsin Bangalore Using WRI, NDWI, MNDWI, Supervised Classification and K-T Transformation", *Aquat. Procedia*, vol. 4, p. 739, (2015).

[82] A. Fisher and T. Danaher, "A water index for SPOT5 HRG satellite

imagery, New South Wales, Australia, determined by linear discriminant analysis", *Remote Sens.*, No. 11, vol. 5, p. 5907, (2013).

[83] E. S. Han and A. goleman, "Determining The Best Path Of Oil Pipeline Linking The Oil Wells Of Down Iraq And The Strategic Oil Line By Geographic Information Systems And Remote Sensing Techniques", No. 9, vol. 53, (2019).

[84] I. Pôças, A. Calera, I. Campos and M. Cunha, "Remote sensing for estimating and mapping single and basal crop coefficientes: A review on spectral vegetation indices approaches", *Agric. Water Manag.*, vol. 233, p. 106081, (2020).

[85] E. Farg, S. M. Arafat, M. S. Abd El-Wahed and A. M. El-Gindy, "Estimation of Evapotranspiration ETc and Crop Coefficient K c of Wheat, in south Nile Delta of Egypt Using integrated FAO-56 approach and remote sensing data", *Egypt. J. Remote Sens. Sp. Sci.*, No. 1, vol. 15, p. 83, (2012).

[86] P. Lourenço, "Ecosystem functioning of protected area networks. A remote sensing assessment across social-ecosystem contexts", (2015).

[87] M. Clark and N. Kilham, "Mapping of land cover in northern California with simulated hyperspectral satellite imagery", ISPRS J Photogramm Remote Sens, (2016).

[88] D. Guidici and M.L. Clark, "One-dimensional convolutional neural network land-cover classification of multi-seasonal hyperspectral imagery in the San Francisco Bay Area", California, Remote Sens, (2017).

[89] H. B. Wakode, K. Baier, R. Jha and R. Azzam, "Analysis of urban growth using Landsat TM/ETM data and GIS-a case study of Hyderabad, India", Arab. J. Geosci., No. 1, vol. 7, p. 109, (2014).

[90] R. Mc Govern, C. Kostick, L. Farrelly, and F. Ludlow, "Reconstructing the climate of Ancient Babylonia", *Eur. Geosci. Union Gen. Assem.*, (2020).

[91] A. H. Khaled and S. J. Kazem " The impact of climate on the production and distribution of grain crops in Babil Governorate" , Mustansiriya University, Faculty of Basic Education, vol. 22, No. 93, (2016).